POLITECNICO DI TORINO

Corso di Laurea in Ingegneria biomedica

Tesi di laurea magistrale

Design and fabrication of highly flexible tactile sensors based on green hydrogel

Relatori
PROF. Stassi Stefano
DOTT.SSA Chiappone Annalisa

Candidato
Mogli Giorgio

Anno accademico 2020-21

Abstract

The current technological development requires new ways of interfacing between humans and machines. Soft tissues typical of human body actually need to be linked to the rigid electronics and mechanical components of machineries thanks to devices which reproduce the features of both realms. Drawing inspiration from the human skin, tactile or smart sensors are devices able to sense external stimuli, such as deformations, temperature, moisture and light. These devices find applications in a wide range of fields like world of wearables, soft robotics, prosthetic and e-skin. In particular, the reproduction of haptic sensation is a challenge which still yielded no applicable results, despite its considerable importance in biomedicine. Herein, a sandwich-like tactile sensor composed of a cellulose based hydrogel encapsulated by a flexible substrate, is presented. A methacrylated carboxymethylcellulose (M-CMC) hydrogel endowed of ionic conductibility by sodium chloride (NaCl) was used as sensitive part. Both the sensible layer, electrodes and shells were investigated to find the best setup. Finally, sensors with different M-CMC concentrations were subjected to stretching and bending stimuli and their electrical properties variations were measured through an LCR meter. Devices shows a very high sensitivity to external deformation and an extreme stretchability up to 600%. After the selection of the best configuration, sensors were used to monitor different human body signals. The results demonstrated that the performances of these sensors could be a promising starting point for the development of transparent, low-cost, eco-friendly and easy manufacturable devices.

Contents

List of Tables

List of Figures

Chapter 1

Introduction

In recent years the need to interface the human world with the electronic one has drastically growth. One one side, living tissues are characterized by softness, multi-sensing capacity, self-heal ability and adaptability. On the other side, robots and machines are generally stiff and unable to auto-repair. Therefore, devices with intermediate properties are necessary to link the two realms. Drawing inspiration from the human skin, which is the largest sensor tissue of living beings, tactile or smart sensors, which are devices able to sense external stimuli, such as deformations, temperature, moisture and light, could represent an optimal solution. The main difference from the traditional sensors is that they are built exploiting flexible materials, in order to be more compliant to the irregular surfaces of soft tissues and robots. This feature makes tactile sensors applicable in a wide range of fields like world of wearables, soft robotics, prosthetic and e-skin. As a consequence, thanks to the progress in these fields, the global market of soft tactile sensors has incredibly growth in the last years. In particular, the reproduction of haptic sensation is a challenge which still yielded no applicable results, despite its considerable importance in biomedicine: flexible strain sensors are ideal candidates to overcome this issue.

Herein, a sandwich-like strain sensor made of soft hydrogel encapsulated by an elastic substrate is investigated. A derivative of cellulose (mathacrylated carboxymethylcellulose), the most available natural polymer, is used to form the UV curable hydrogel, which constitute the sensitive part of the sensor. In fact, electrical conductivity is given by the ions derived from a salt (NaCl) dissolving in the water solution used to form the hydrogel. The cellulose hydrogel is then encased between two shells of a flexible and transparent material; two electrodes constitute the link between the sensitive part of the device and the external circuitry. In this way a transparent, low cost and easy manufacturable device which mainly exploit piezoresistance transduction mode, is produced.

In this research, an overview on the state of the art of flexible sensors is provided at first: it includes a summary of the transduction methods and the principal types of tactile sensor and their possible applications. Then a survey on the cellulose hydrogel and the materials selected for encapsulation is given in the materials and methods chapter. Moreover, the key investigation techniques, employed in the characterization of the sensors, and their settings are briefly explained. In the results section, before all, the reactivity of the hydrogel is assessed through the photoreologies by varying the molarity of salt and the cellulose content. Then, the findings about the mechanical properties and features of the three materials (polydimethylsiloxane, TRAD 2800 and VHB bi-adhesive tape) chosen for the encapsulation shells are explored. Electrochemical impedance spectroscopy analyses data are subsequently taken into account for the choice of the electrodes material that ensures the best performances. Furthermore, sensors with different cellulose contents, subjected to stretching and bending stimuli, are tested through the LCR meter to find the concentration that offers the best balance among sensitivity to external deformations, repeatability of measures and durability. Thanks to these examinations, the best setup, concerning the materials of encapsulation and electrodes and the cellulose content, is selected. Then, temperature sensitivity was also demonstrated. After that, several applications related to the monitoring of human body signals, such as arterial pulse wave, joints motion and vocal chord vibrations, were performed. The outcomes shows that these sensors could represent ideal candidates for the development of transparent, low-cost, eco-friendly and easy manufacturable devices. Finally, benefits and limitations in association with possible further developments are presented at the end of this research.

Chapter 2

Flexible tactile sensors

Humans receive informations from the external environment through the five senses. Among them, sight is the best developed one due to the largest brain part dedicated to the image processing. Nevertheless, it was demonstrated that human brain integrates visual and haptic perceptions, to obtain more reliable informations [1][2]. Therefore, touch is crucial for gathering feedbacks from tasks performed in the external world: skin is the largest sensor system of our bodies [3]. It can be divided into three principal layers: epidermis, dermis, hypodermis. The sensitive organelles, called mechanoreceptor, which are submerged

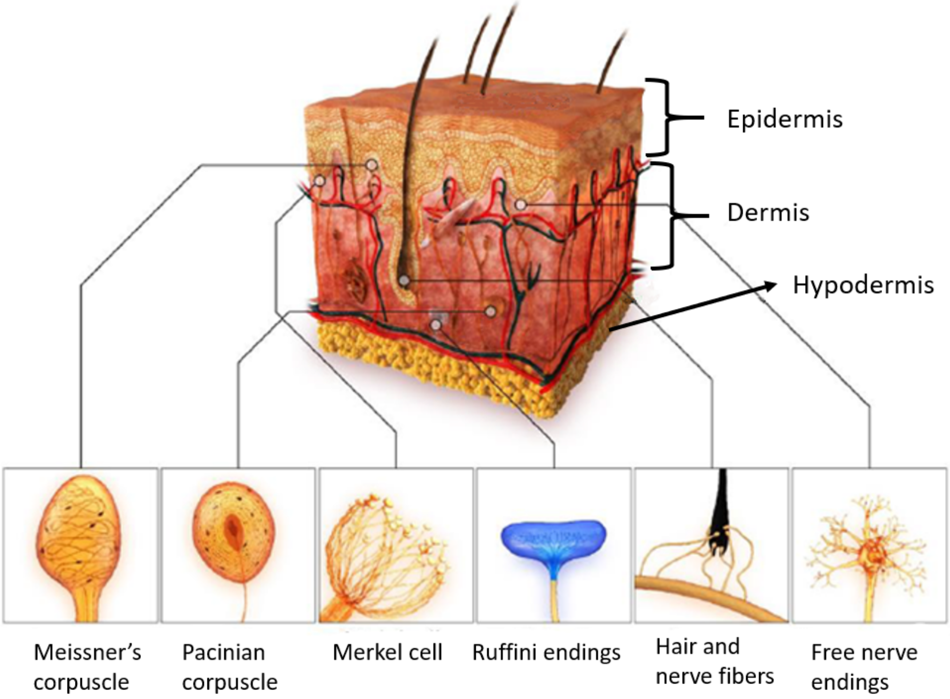

Figure 2.1: Human skin structure and various kinds of mechanoreceptors [3]

at different depths in the skin, are classified into four principal categories: Meissner and Pacinian corpuscles, Ruffini endings and Merkel cells (Figure 2.1). Each kind of receptor is specialized to sense a specific stimulus, and holds distinct adaption rate to it. These mechanoreceptors convert mechanical deformations coming from outside, to an electrical signal composed by a train of pulses (frequency of which is proportional to the stimuli magnitude), that arrives, through nerves, to the central nervous system, and provide it with a tactile feedback of what has been touched [4].

In the past three decades, the need to make more comfortable everyday life, through digitalization and automation, widely enhanced the interest towards artificial intelligence, internet of things and human-computer interfaces. In addition, taking inspiration from the human tactile system, smart sensors, have gradually gained relevance due to the high number of potential applications, such as healthcare, smart vehicles and robotic technology. In fact, market forecasts say that global business of these sensors will grow from USD 36.6 billion in 2020, to USD 87.6 billion in 2025 [5]. Furthermore, the number of researches, regarding smart sensors, developed in the last years demonstrates this rising trend (Figure 2.2).

According to Suresh et al., tactile sensors, known also as pressure sensors, smart sensors or e-skin (electronic skin), are transducers able to sense different properties of an object, such as shape, hardness, texture, pressure, moisture content, temperature [5].

Recently, researchers focus on the exploration of new materials that can mimic both mechanical and electrical properties of human skin. Therefore, tactile sensors shall be flexible and stretchable to ensure an optimal integration with human body, prosthesis and wearable applications [6]. Hydrogels, elastomers and polymers represent optimal solutions for avoiding discrepancy of mechanical features with human tissues. For instance, Lei et al. presented a hydrogel pressure sensor based on interpenetrated networks of alginate chains

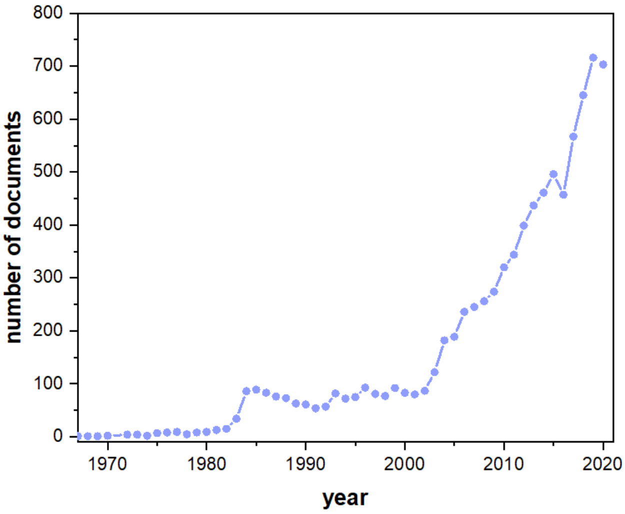

Figure 2.2: Scopus papers containing the key words "Tactile sensors" published by years

and polyacrilic acid (PAA), in which small amorphous carbonate calcium particles were crosslinked. A commercial transparent tape was used as dielectric between two hydrogel layers, to create a flexible capacitive sensor [7].
Sensitivity is an important parameter of any type of measuring systems, defined as the ratio of variation in magnitude of the output to the variation in magnitude of the measurand (input), as it is shown in equation 2.1. Hence, graphically, it is represented by the slope of transfer curves depicted in figure 2.3a.

$$S = \frac{d(output)}{d(input)} \approx \frac{\Delta(output)}{\Delta(input)} \tag{2.1}$$

An higher sensitivity provides better signal to noise ratio and greater resolutions (resolution is described as the smallest input change that can be resolved). Ensuring an adequate value of this parameter is often an intriguing challenge. The usage of 3D micro or nano patterns represents a solution: for example, Pang et al. enhanced the sensitivity of their pressure sensor throughout an interlocking structure between metal-coated nanofibers, which guarantees a greater number of contacts among the conductive structures [8]. An easier sensor's calibration is supplied by a linear transfer curve, namely a linear relationship between output and input. Non linear sensors own non constant sensitivity along their measuring range (Figure 2.3a). Therefore, devices with a transfer curve close to the ideal linear one are preferable. Moreover, if at a null input corresponds non-zero output, an offset, known also as zero error, is present.
Hysteresis is a common phenomenon that could affect the device. It consists of a different output reading for the same input value depending on whether the measurand was increased or decreased prior the current measurement (Figure 2.3b).
A small responsive time is another important feature that the device should own if it is used to sense a measurand which varies rapidly. In fact, responsiveness means the time that sensor's output takes to reach a percentage (usually 95%) of its final settled value [5].

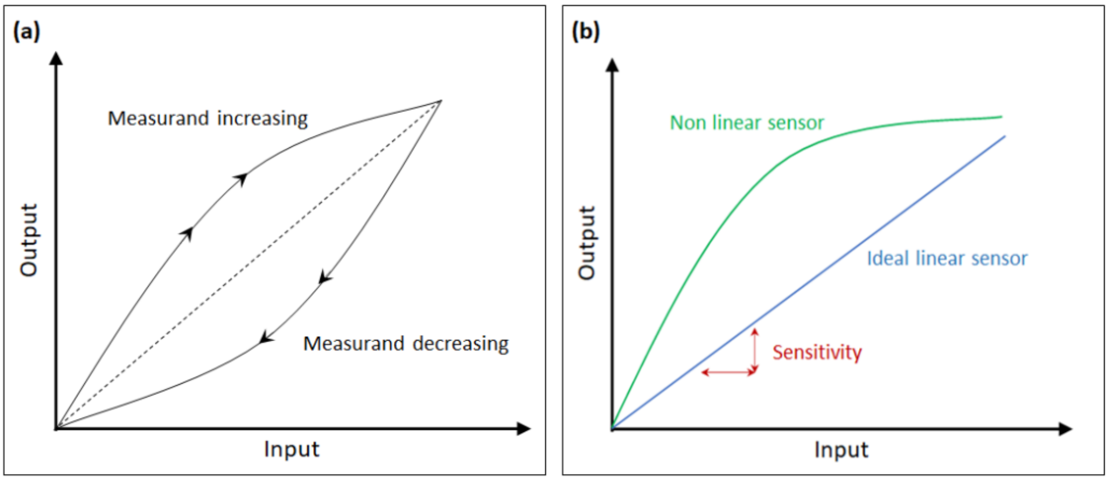

Figure 2.3: Examples of sensors transfer curves: (a) Linear and non linear sensors (b) Hysteresis loop

Recovery time, on the other hand, is the period spent for coming back to the initial value of the output, after a stimulus. For tactile sensors, it is also desirable a tiny recovery time. Other important characteristics of tactile sensors are reproducibility and stability. The former means that the same value of measurand should trigger same value of output in various measurements carried out under equal conditions. The latter is essential to maintain sensor operating characteristics constant over the time. This property includes also the stability of the output value when a constant input is applied in a single measurement. Another important aspect is the power supply: sensors with simple conditioning circuit and low power consumption are excellent for the previously mentioned applications. At present, there is the tendency to explore self-powered devices for avoiding the use of heavy and cumbersome batteries. Wang et al. proposed a gelatin hydrogel sensor doped with silver nanowires to guarantee electrical conductibility; the device was then assembled between two different electrodes (a zinc layer and a air electrode) to obtain a galvanic cell [9]. In this way, the chemical energy obtained from ions motion across the hydrogel network ensured self-powering.

If the device is used in contact with human skin or for implantable purposes, biocompatibility must be taken into account, too [10]. Hence, biomaterials should be used to build the device. In sensors applications, materials must be inert with respect to human tissues: this is the first definition of the word "biomaterial" coined in the sixth “Annual International Biomaterial Symposium” in Clemson, South Carolina [11]. Moreover biodegradability could be a relevant feature if the device need to be implanted.

Finally, skin compatibility is not to be neglected: in addition to conformability with human skin, it would be better if the device was air/sweat permeable, to prevent any possible allergic reaction in wearable applications [5].

These are the principal features that a tactile sensors should own. Nevertheless, many others appealing properties are present in literature. Transparency ensures a good aesthetic result for daily activities and it is essential in case of applications in see-through surgical operation, for instance [12] [13]. Self-healing is a crucial property to increase durability and lifetime of the device [14]. Moreover, devices with intrinsic adhesiveness are preferable for an optimal integration with human skin, without the usage of additional tape [6]. Tactile sensors design and building must finally take into account the exploitation of eco-friendly and low cost materials for competitive devices and a large-scale production.

2.1 Transduction mechanisms

A first classification of smart sensors can be made according to the transduction mechanism. Magnetic tactile sensors exploit Hall effect: a transverse difference of potential, called "Hall potential", is measured when a conductor is crossed longitudinally by a current and is caused by electrons deflection due to a magnetic field perpendicular to the current, as shown in figure 2.4. Therefore, it is possible to quantify magnetic field magnitude, measuring Hall potential. For instance, Jones et al. introduced a magnet submerged in a elastomer used for sensing forces applied in thumb immobilisation splints: when an external force was employed, elastomer was deformed and magnet moved causing a variation of magnetic field [15].

Optical sensors can be also use to gather tactile informations exploiting several approaches.

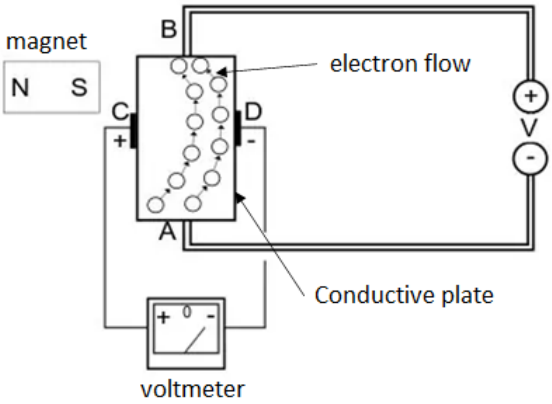

Figure 2.4: Hall effect in a conductive plate

Among them, optical fibers and pattern-recognition methods are widely investigated. For instance, TacTip family devices, developed by Bristol Robotics Laboratory, are robust customizable and versatile opto-force sensors. Inspired by ridges in human fingertips, TacTip sensor presented by Ward-Cherrier et al., exhibited a cylindrical shape with a convex tip. At tip end, there was a soft dome equipped with a pattern, composed of white pins, internally. This geometry was acquired by a camera mounted on a rigid 3D printed support at the other end of the sensor. Device configuration is shown in figure 2.5. Pattern became deformed when an external force was applied on the dome; image of deformed pattern was compared to the image of the not deformed one and several informations, such as object shape, contact and shear forces, were derived [16]. Conversely, Konstantinova et al.

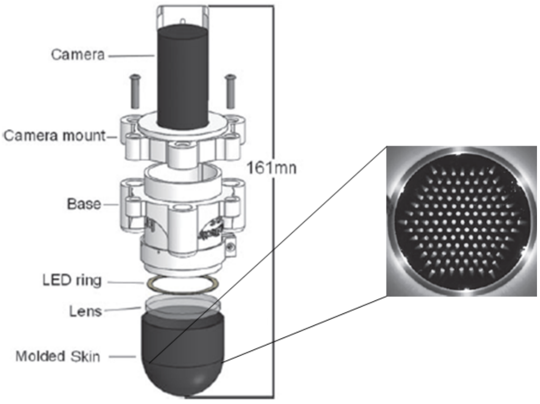

Figure 2.5: TacTip sensor configuration [16]: the white pattern is shown in the inset

presented an optical fiber based tactile sensor. Operating system consisted in a sending fibre which transmitted light to a reflective surface and a receiving fibre which collected reflected rays, as shown in figure 2.6a. The intensity of reflected light varied when the

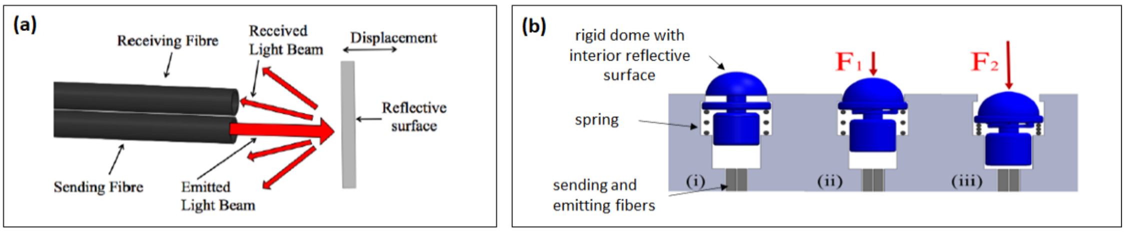

Figure 2.6: (a) Optical fiber working principle (b) Optical fiber fingertip sensor: different forces applied on the sensor [17]

distance between sending fibre and reflective surface changed. The device was composed of a rigid dome, which acted as interface with external environment, placed on a spring in a hollow of the support. A couple of optical fibers were placed below the "tactile" part 2.6b. Inner base of the dome was reflective: thus, exploiting the working principle before mentioned, it was possible to detect the force applied through the light intensity measured by the receiving fiber [17]. Array of these sensors could be easily assembled, too.

Another approach involves ultrasounds, namely sound waves with frequency higher than 20 kHz. Ultrasound are generated by applying a sinusoidal potential to piezoelectric materials. The same piezoelectric material serves as receiver, producing a sinusoidal potential as output. Piezoelectric working principle will be explained in detail in section 2.1.3. Chuang et al. created a ultrasound force sensor by overlaying different layers, as shown in figure 2.7. Sheets of polyvinylidene fluoride (PVDF), a piezoelectric polymer, were used both as ultrasound transducer and receiver. A TFT (Thin-Film Transistor) was necessary to drive the transducer film and to detect the voltage generated by receiver sheet. An outer elastomer layer served as interface with external objects; it was micro-structured to improve force concentration. Working principle was the same of ultrasound pulse-echo in medical imaging: an AC voltage was applied to the first PVDF layer, generating a "pulse" of ultrasound which propagated until they were reflected from contacting surface and were collected by the other PVDF layer. Change in contact area was directly linked with time of flight of ultrasounds. In this way, contact force, which was related to contact area, was estimated [18].

Nevertheless, electric transduction mechanism is the most used. Tactile stimuli are converted into electrical signals in this case. Literature is plenty of electric strain sensors since output signals are easy to process, conditioning circuit are usually simpler and devices are cheaper to build and more adaptable. Furthermore, they are the closest sensors to human tactile perception which is based on electrical pulses generated by mechanoreceptor after an exterior stimulus, as previously explained. A force input applied on a conductor alters several electrical quantities such as resistance and capacitance. Hence, these tactile sensors are still divided into four sub-classes, according to which quantity is analysed. Piezoresistance, piezocapacitive, piezoelectric and triboelectric sensors will be illustrated more extensively in the following sections.

2.1.1 Piezoresistance sensors

Piezoresistance effect consists in a variation of electrical resistance as a result of an external stimulus (Figure 2.8). Resistance represents how a conductive material is opposed to current flow and depends on both material resistivity and object geometry. Resistivity is an intrinsic parameter of materials and in S.I it is measured in $[\Omega \cdot m]$. In products data sheets, conductibility, indicated with σ, is often given instead of resistivity. It is basically the inverse of resistivity and its measurement unit is $[S/m]$. Resistance mathematical formula for an ideal conducting wire, also known as second Ohm's law, is given by:

$$R = \rho \frac{L}{A} \tag{2.2}$$

where ρ indicates the material resistivity, L and A are the length and the cross sectional area of the conductor, respectively. Additionally, this equation can be extended to a general conductor.

It is useful to make the logarithm of both side of the equation 2.2, for relating the resistance with the mechanical stimulus applied:

$$\ln R = \ln \rho + \ln L - \ln A \tag{2.3}$$

Knowing that $\frac{\mathrm{d}(\ln X)}{\mathrm{d}X} = \frac{1}{X}$, where X is a generic quantity, the equation 2.3 differentiated can be written:

$$\frac{\mathrm{d}R}{R} = \frac{\mathrm{d}\rho}{\rho} + \frac{\mathrm{d}L}{L} - \frac{\mathrm{d}A}{A} \tag{2.4}$$

From this formula, it is easy to note, that an increase of resistivity and/or length brings to higher value of resistance; instead, if cross sectional area grows, resistance will reduce. The term $\frac{\mathrm{d}L}{L}$ is called axial strain and is usually marked by ϵ_{ax}. In a cylindrical shape conductor, cross sectional area can be found as $A = \pi D^2/4$, where D is the diameter; thus, differentiating the logarithm of this equation, $dA/A \approx 2dD/D$ is obtained. In such case,

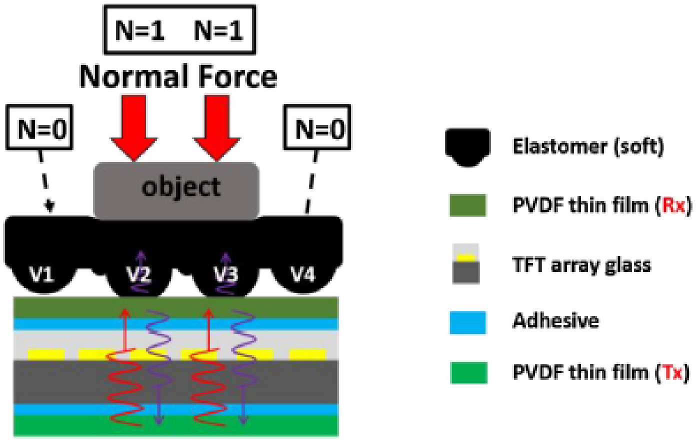

Figure 2.7: Ultrasound sensor configuration [18]

dD/D is also known as transverse strain, indicated as ϵ_t. Hence,

$$\frac{\mathrm{d}R}{R} = \frac{\mathrm{d}\rho}{\rho} + \epsilon_{ax} - 2\epsilon_t \tag{2.5}$$

can be written from 2.4. Moreover, axial and transverse strains are linked through Poisson's coefficient, ν, according to structural mechanic. In particular, if an axial compression is present, the object will expand transversally and vice versa. Thus, the relationship between the two deformations is:

$$\epsilon_{ax} = -\nu\epsilon_t \tag{2.6}$$

Rearranging eq. 2.5 and eq. 2.6, one finally obtains:

$$\frac{\mathrm{d}R}{R} \approx \frac{\Delta R}{R} = \frac{\mathrm{d}\rho}{\rho} + \epsilon_{ax}(1 + 2\nu) \tag{2.7}$$

The relative variation in resistivity ($\mathrm{d}\rho/\rho$) represents the "piezoresistive effect". Conversely, the second term of the equation is referred to the extrinsic geometric effect [5]. Therefore, piezoresistance effect depends on both piezoresistivity and variations in geometry. In such case, sensitivity, known also as "gauge factor" (GF) if a strain is applied, is the ratio of relative resistance change to external stimulus :

$$S = \frac{\frac{\mathrm{d}R}{R_0}}{\Delta X} \approx \frac{\frac{\Delta R}{R_0}}{\Delta X} = \frac{\frac{(R-R_0)}{R_0}}{\Delta X} \tag{2.8}$$

where R is the current resistance measured, R_0 is the resistance measured when no stimulus is present, and ΔX is the variation of external stimulus, like a strain, a pressure and so on.
Doped semiconductor and metallic sensors mainly exploit resistivity change: these devices are usually very sensitive but their stretchability and flexibility is very poor [19]. Therefore, they are unappropriated for wearable applications. Elastomers are generally used

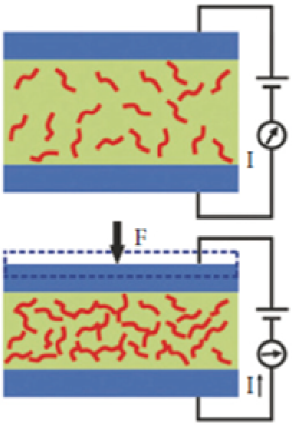

Figure 2.8: Piezoresistance effect in a matrix with conductive fillers: an external force produces a resistance variation and hence the current passing through the conductor changes

to compensate for this lack. Nevertheless, due to their poor conductibility, conductive fillers like metal particles, nanowires, need to be inserted in the elastic matrices. It is important that the fillers are homogeneously dispersed and well adhered to the matrix, to prevent alteration of the sensing characteristics [20]. These types of sensors exploit geometry change as main contributor for resistance variation. For instance, Roh et al. produced a sandwich-like patch (Figure 2.9a) formed by a hybrid film of single-wall carbon nanotubes (SWCNTs) and a conductive elastomeric composite of polyurethane (PU) poly(3,4-ethylenedioxythiophene) polystyrenesulfonate (PEDOT:PSS), deposited on a thin layer of polydimethylsiloxane (PDMS). In this case, electric conductibility was due to the presence of both carbon nanotubes and PEDOT:PSS. This patch, attached to the forehead of a subject, was then used as piezoresistance sensor for detecting facial expression like laughing or crying (Figure 2.9a), proving an high reproducibility. Actually, the high gauge factor for little strains made it suitable for small muscles activity detection [12]. Another approach consists of using soft and stretchable hydrogel doped with moving ions (investigated in detail in section 1.2.2). In work of Shao et al., a ionic gel composed of tannic acid coated cellulose nanocrystal (TA-CNCs), polyacrilic-acid (PAA) and aluminium ions (Al^{3+}), needed for current conduction, was used as strain sensor. Its piezoresistance effect was demonstrated connecting the device with a light-emitting-diode (LED): when the sensor was stretched, and so the resistance increased, led darkened because less ionic current flowed through the device (Figure 2.9b). At greater strain applied (2000 %) the device showed an high sensitivity (7.8). At lower strain (100 %) sensitivity was slightly lower (5.5), on the contrary. This ionic sensor was basically suitable for both large deformations (e.g joint motions) and subtle strains (e.g pulse), thanks to its good sensibility and ultra-stretchability [21].

Piezoresistance tactile sensors are the most commonly employed thanks to their flexibility, low cost and simple read-out mechanism [20] [22]. Moreover, they are capable to sense static loads [23]. The principal drawbacks of piezoresistance sensors are the temperature influence that could lead to resistance variations [24], and hysteresis due to the viscoelasticity of most of stretchable substrates employed [25]. Finally, design of low consumption devices is essential, because this kind of sensors need an external power supply to monitor resistance change.

2.1.2 Piezocapacitive sensors

Capacitance is an electrical quantity that describes the ability of a certain object to store a charge. Its SI unit of measure is the Farad (F). A traditional capacitor is composed by an intermediate dielectric layer between two conductive films called armature plates (Figure 2.10a): the dielectric, which is an electrical insulator with high polarizability, becomes polarized when a difference of potential, that generates an electrical field, is applied between the two armature plates through a DC power supply. Thus, negative and positive charges accumulate on plates surfaces as long as regime conditions are reached. Then, current stops flowing in the external circuit, capacitor stops charging and potential across it becomes equal to that of power supply. If the capacitor is disconnected from the power supply, the stored energy will remain on its plates. However, when the capacitor is short circuited, a current, of opposite direction compared to the previous, flows across the circuit as a result

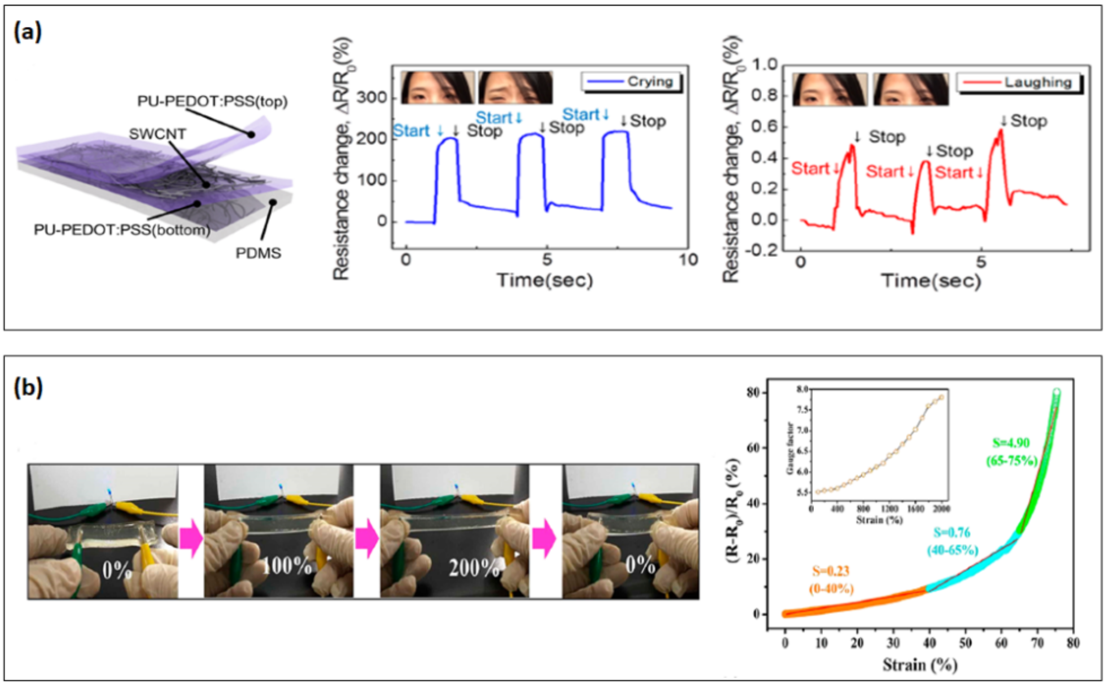

Figure 2.9: Examples of piezoresistance sensors configurations: (a) On the left, the sensor made of a composite of PU and PEDOT:PSS with carbon nanotubes. On the right, resistance variation when the device is attached to the forehead during crying and laughing [12] (b) On the left, the transparent ionic gel is connected to the LED and stretched. On the right the curve $\Delta R/R$ vs ϵ is given; in the inset gauge factors at different strain value [21]

of stored charge releasing and potential between armature plates will decay to zero. Consequently, capacitance depends on dielectric permittivity, namely how the material opposes to the electric field applied (thus, how easily it polarizes), and geometry of capacitor. For a parallel plates capacitor just described, capacitance can be computed by this formula:

$$C = \epsilon \frac{A}{d} \tag{2.9}$$

where ϵ is the dielectric permittivity, A is the overlapped area of the armatures and d is the distance between them. Moreover, permittivity is computable as $\epsilon = \epsilon_0 \epsilon_r$, wherein ϵ_0 means the vacuum dielectric constant ($\epsilon_0 = 8{,}854\,187\,817\,62 \cdot 10^{-12}$ F/m) and ϵ_r is the relative permittivity, known also as dielectric constant, that depends on the chosen material.

Piezocapacitive effect means a transduction of mechanical stimuli in capacitance variations. Capacitor geometry actually varies when a deformation is applied on it: according to eq. 2.9, if plates surface increases and/or distance between them decreases, then capacitance becomes higher (Figure 2.10b), and vice versa. Distance variation is usually used to sense normal forces [26], on the other hand, area variation acts primarily when shear forces are applied [27]. Both distance and area vary when a tensile strain is measured. Sensors based on relative permittivity (ϵ_r) are not very popular due to the low number of materials

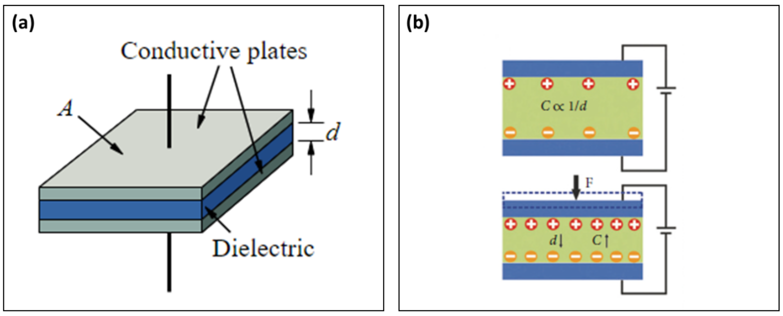

Figure 2.10: (a) Parallel plate capacitor (b) Piezocapacitive effect: an external force produce a capacitance variation and hence the current passing through the conductor changes

usable [20].

As previously seen for sensors based on piezoresistance effect, sensitivity of a piezocapacitive sensor can be computed with:

$$S = \frac{\frac{\mathrm{d}C}{C_0}}{\Delta X} \approx \frac{\frac{\Delta C}{C_0}}{\Delta X} = \frac{\frac{(C-C_0)}{C_0}}{\Delta X} \tag{2.10}$$

where C is the capacitance measured under a certain stimulus, C_0 is the capacitance with no deformation applied and ΔX is the variation of external stimulus.

Performances of these sensors can be improved using deformable dielectrics in order to ensure higher variation of area and distance between electrodes and to improve stretchability of the device. Therefore, several studies on piezocapacitive smart sensors involving elastomers and hydrogel are present in literature. For instance, Lipomi et al. produced a capacitive transparent sensors by coupling two different elastomers, polydimethylsiloxane (PDMS) and Ecoflex silicone. Single-wall carbon nanotubes (SWNTCs) in a solution of N-methylpyrrolidone were spray-coated on PDMS surface, which was before activated through oxygen plasma: two flexible electrodes were built, in this way. Carbon nanotubes ensured both optical transparency and electrical conductibility, plus their film contiguity was not interrupted after a strain. Ecoflex silicone elastomer was employed as dielectric between two PDMS-SWNTCs layers thanks to its higher deformability compared to PDMS. A matrix made of these sensors was easily created thanks to the application of a mask during spray coating (Figure 2.11a). Strain and pressure stimuli could be distinguished, because the former involved all the sensors along the axis of deformation, the latter only affected the sensors in the load neighbourhood [26]. Instead, a polyacrilamide hydrogel containing sodium chloride (NaCl) was used in the work of Sun et al., for mimicking human skin. A sheet of VHB tape (3M), a transparent, bi-adhesive elastomer, was inserted between two films of hydrogel. Therefore a capacitive sensor was built: VHB tape acted as dielectric, whereas the layers of hydrogel, thanks to ionic conductibility given by NaCl ions, behaved like armatures of a capacitor. This device was encapsulated through other VHB tape to prevent water evaporation (Figure 2.11b). It was demonstrated that this "ionic skin" could be employed both as strain and pressure sensor. However, performances for sensing pressure stimuli were limited due to the viscoelastic behaviour of VHB tape: the device, when stimulated by loading and unloading cycles, showed a hysteresis loop (Figure 2.11b), actually [28]. Air gaps are usually used as dielectric to increase compressibility of

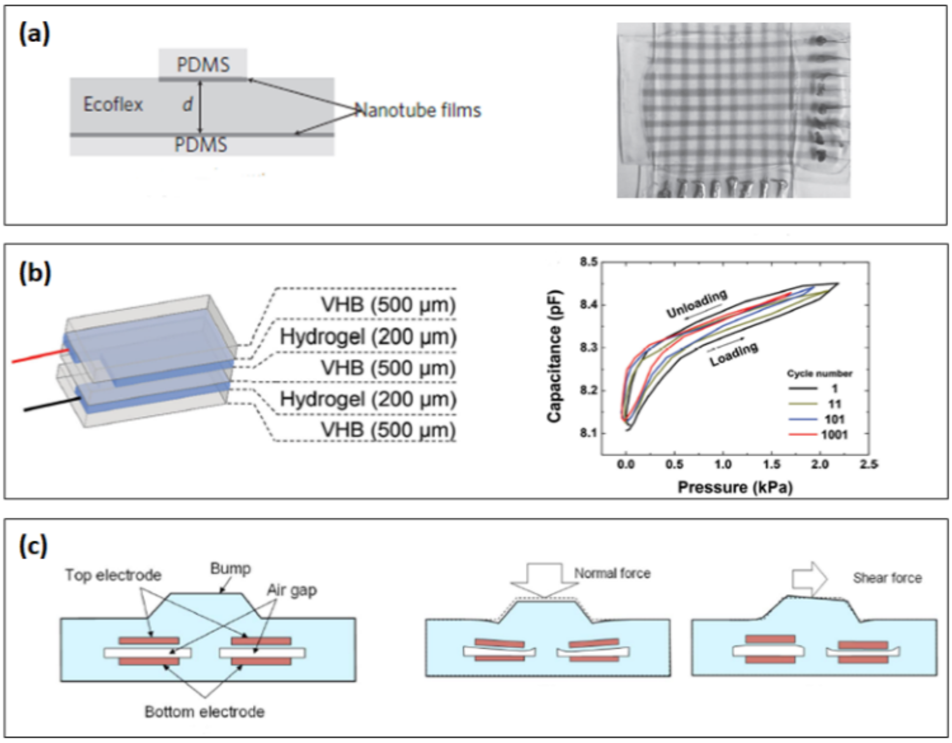

Figure 2.11: Examples of piezocapacitive sensors configurations: (a) On the left PDMS-Ecoflex-NTCs based sensor. On the right a matrix of these sensors [26] (b) Ionic skin structure and hysteresis loop after pressure stimuli (at different loading/unloading cycle) [28] (c) Air gaps tactile sensor structure and its responses to normal and shear stimuli [24]

sensors. Lee et al. managed to separate shear and normal forces through tactile sensor made up of four capacitors with air gaps as dielectrics, submerged in a PDMS structure. A PDMS bump acted as force booster. As can be seen in figure 2.11c, a different mechanical stimulus produced various deformation of air gaps, thus capacitances increased or decreased as appropriate [24]. Nevertheless, air owns small value of relative permittivity, thus sensors capacitances are little and also signal to noise ratio is low consequently [20]. Piezocapacitive sensors generally demonstrate high sensitivity, ability to measure static forces [23], and low power consumption [29]. On the other side, they are very susceptible to electromagnetic interferences from external source [30]. Furthermore, miniaturizing the sensor results in a reduction of the armatures area A; in this way, capacitance reduces (eq. 2.9) and hence signal to noise ratio also diminishes. Additionally, piezocapacitive sensors require an external power source like piezoresistance devices.

2.1.3 Piezoelectric sensors

Piezoelectric effect was discovered in 1880 by Pierre and Jacques Curie, which noted that when some materials like ceramics, quartz, tourmaline, perovskite, were pressed, a voltage difference was generated at their ends. At rest, these crystals own an electrically neutral structure without a centre of symmetry [31]; when they are stretched or compressed in a certain direction, oriented electric dipoles move in the lattice and thus one side of the crystal and the opposite become negatively and positively charged, respectively. A voltage difference, measurable with a voltmeter, is consequently created. This is called "direct piezoelectric effect" (Figure 2.13a). Moreover, compression and stretching generate voltages of opposite signs. For istance, quartz (SiO_2) owns a piezoelectric behaviour due to its organization of crystalline lattice. In figure 2.12 non centre-symmetric quartz cell is represented: when it is subjected to a strain, balance between oxigen atoms (charged negatively and silicon atoms (charged positively) is upset, thus the system is no longer electrically neutral. This effect is completely reversible: actually, when a voltage difference is applied to two opposite face of the crystal, a mechanical deformation of the lattice is generated. The type of deformation depends on the sign of the potential employed. In this case, it is known as "converse piezoelectric effect" or it is also named "Lippman effect" after its discoverer (Figure 2.13b). Piezoelectric materials find a wide range of applications like ultrasound probes for medical imaging, microphones, sonar arrays, as ignition source for cigarette lighters and transducers.

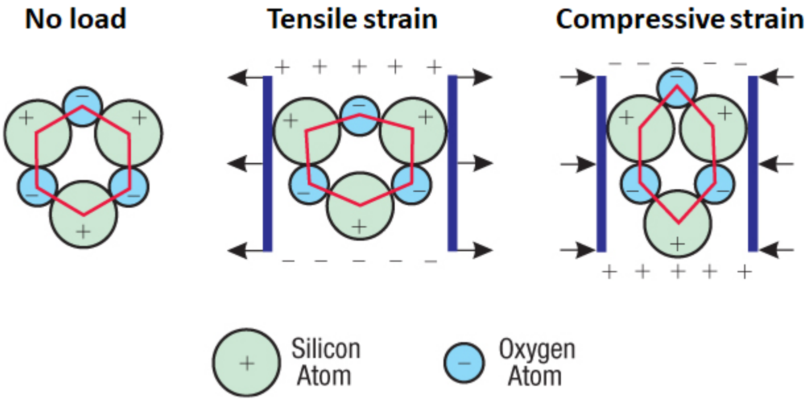

Figure 2.12: Quartz structure at rest, under tension and compression

Tactile sensors exploit direct piezoelectric effect, converting mechanical stimuli into voltage differences directly. A linear relationship exists between the stress applied (X_{jk}) and the charge density along the ith direction (D_i), which can be written as:

$$D_i = d_{ijk} X_{jk} \tag{2.11}$$

The term d_{ijk} (C N^{-1}) is the piezoelectric coefficients tensor of a certain material [32]. Crystals and ceramic materials generally have high d_{ijk}, thus they are very efficient, but possess low flexibility. To exceed this limit, Park et al. proposed a flexible piezoelectric nano-generator, namely a device which harvests energy from environmental sources, by depositing a thin layer of perovskite (PZT) on a polyethylene terephthalate (PET) substrate (Figure 2.14a). PZT thin layer was transferred from a sapphire substrate to PET flexible film through a process called laser lift-off (LLO) [33]. Gold electrodes were then deposited on PZT and the device was encapsulated with epoxy resin (Figure 2.14a). In this way,

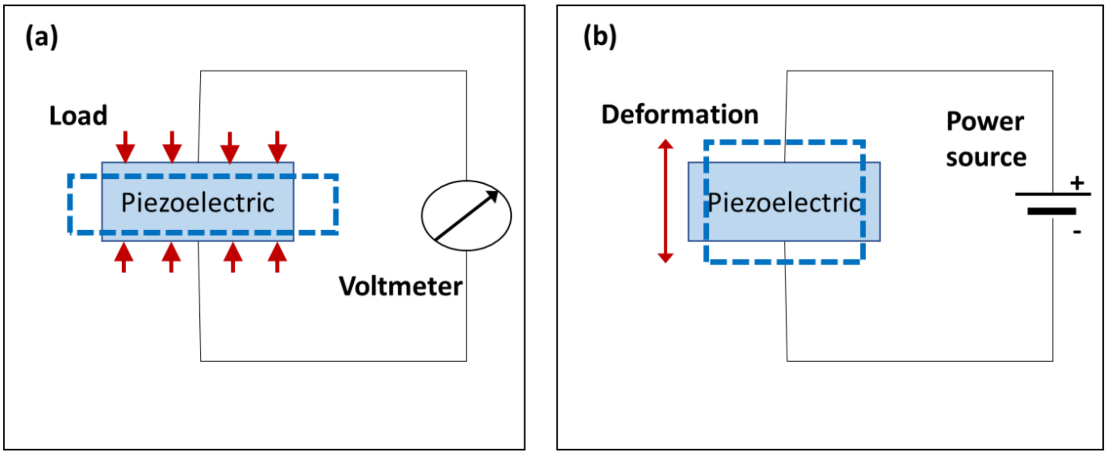

Figure 2.13: (a) Direct piezoelectric effect (b) Converse piezorelectric effect

they obtained an high efficiency, lightweight and flexible piezoelectric nano-generator [34]. Piezoelectric polymers, such as poly(vinylidene fluoride) (PVDF) and its copolymers, represent another solution to flexibility issue: they are widely use due to their softness and low cost, despite having lower conversion efficiency with respect to rigid ceramics. However, these polymers usually do not exhibit piezoelectric behaviour in their raw form: actually, they shall undergo "poling" process through the application of an electrical field to orient dipoles in a single direction [35]. A novel technique was presented by C. Chang et al.: they used electrospinning to print PVDF fibers (Figure 2.14b) with dipoles directly aligned thanks to the strong electrical field and mechanical stretching generated by this production technique. Therefore "poling" process was no longer needed. The electro-spun fibers were used to built a piezoelectric nano-generator which showed optimal repeatability under different strain cycles (Figure 2.14b) and high energy conversion efficiency [36]. To increase sensing performance and reliability, Park et al. used ZnO (zinc oxide, a piezoelectric inorganic compound) to fabricate vertical-aligned nanotubes via chemical vapour deposition on a flexible graphene substrate. A pressure sensor was then built with ZnO nanotubes. Due to their high aspect ratio, the device showed an outstanding sensitivity; this property in association with flexibility, made it promising for wearable applications [37].

Piezoelectric sensors generally demonstrate high sensitivity and fast response, like rapid adapting mechanoreceptors in human skin [38]. Nevertheless, these devices are unable to sense static or low frequency stimuli, because the charge collected will decay with time. Moreover, as mentioned before, piezoelectric effect provides a voltage output: hence, heavy, cumbersome and rigid batteries are not necessary for these sensors, because they are self-powered.

2.1.4 Triboelectric sensors

Triboelectric mechanism concerns mechanical energy conversion into electrical signals, as the direct piezoelectric effect. Root of the word "triboelectricity" results from the archaic Greek *tribos* which means friction between materials. Actually, this effect was known since

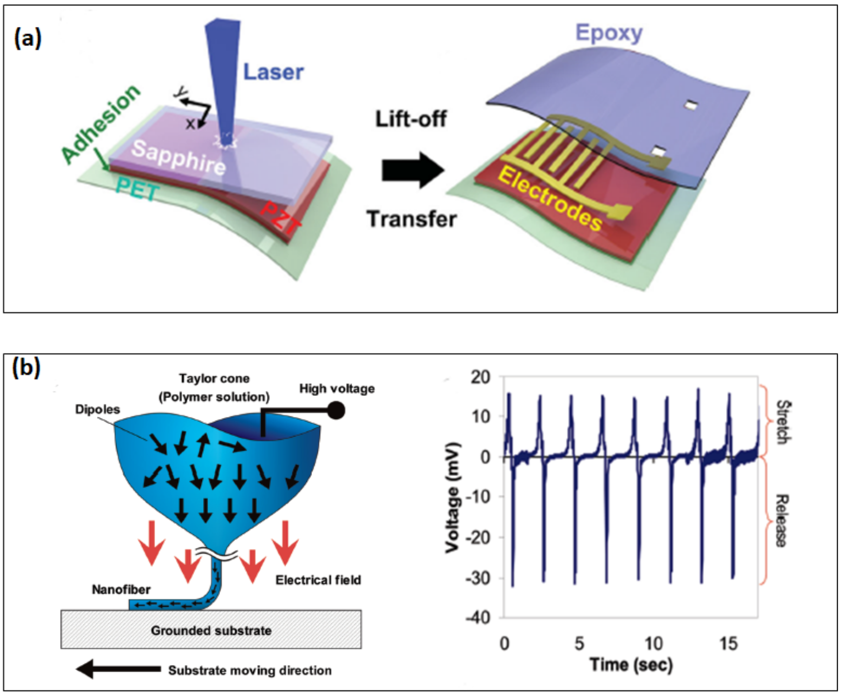

Figure 2.14: Examples of piezoelectric device: (a) On the left, LLO of a PZT thin layer on PET substrate; on the right nano-generator assembled [34] (b) On the left PVD is electrospinned; on the right, output of PVDF nano-generator under several strain cycles [36]

ancient times. Greeks discovered that amber attracted small textile pieces after being rubbed: this is due to contact electrification, namely an accumulation of charges of opposite sign on the attracted surfaces. Indeed from amber, named by Greeks *elektron*, derives the current term "electricity". This phenomenon takes place if the two materials in contact own different tendency to gain electrons. In that way "contact electrification" or "triboelectrification" happens: one object acquires electrons and its surface become negatively charged, the other loses electrons and purchases a positive charge. After release of pressure, on the back sides of the two objects, positive and negative charges respectively arise due to electrostatic induction, for maintaining electrical neutrality. Therefore a potential difference can be measured by electrodes and, if the two back sides are connected through an external circuit, a current begins to flow. When charges become balanced, electrons stop moving along the circuit and maximum potential difference is reached. Then, if the two object come closer again, difference of potential reduces until the full contact, during which becomes null, and the current flows in the opposite direction. This configuration, called "vertical contact-separation mode" [39] is shown in figure 2.15a.

Triboelectric series are a useful tool to describe electrostatic behaviour of materials, called also "tribopolarity", namely their trends to acquire or give up electrons. Materials are ordered empirically starting with those that have a greater tendency to charge positively (hence to lose electrons), and ending with those that are more inclined to gain electrons. It is necessary to choose two materials which are more distant to generate more charge

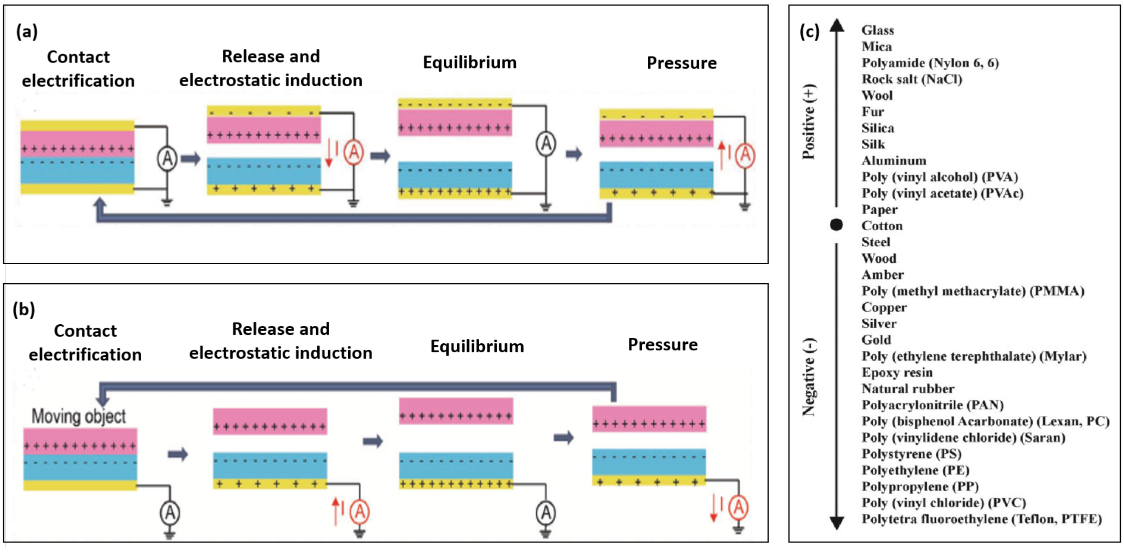

Figure 2.15: (a) Vertical contact-separation mode [39] (b) Single electrode mode [39] (c) Triboelectric series

during friction. Materials that are close to each other, have roughly the same behaviour, thus a very little charge is transferred during triboelectric effect. An example of qualitative triboelectric series is presented in figure 2.15c. Moreover, a standardized method to quantify the triboelectric charge density (TECD) was explained in the work of Zou et al.: they measured the TECD in several materials put in contact with mercury in a glove box, under controlled conditions. A liquid metal was used to provide an optimal and repeatable contact between the materials [40].

Single-electrode mode is another setup to exploit triboelectric effect (Figure 2.15b). In this case only one triboelectric materials is attached with an electrode in the back side; the electrode is then connected to ground. The other material is free. After the contact

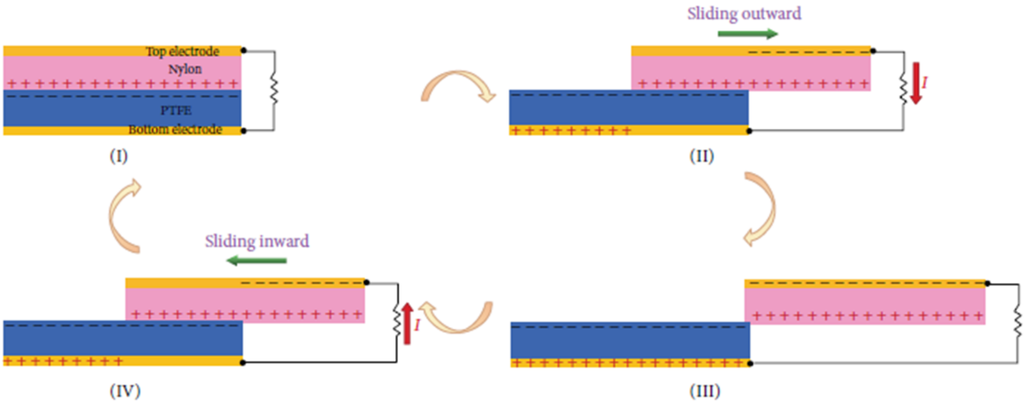

Figure 2.16: Linear sliding mode [41]

electrification, distance variation between the two materials induce charges on the electrode (electronic induction), thus an electron flow is produced in the external circuit in order to obtain an electrostatic equilibrium. This configuration is more simple and suitable for applications in which is difficult to attach an electrode, such as contact with human skin. S. Wang et co-workers proposed the "in plane sliding mode" [41] to overcome the complexity to obtain a normal movement which is necessary in vertical-contact mode. The setup is the same of before mentioned vertical-contact mode: two layers of materials which are far in the triboelectric series, like polyamide 6,6 (Nylon) and polytetrafluoroethylene (PTFE), are initially in full contact. Two electrodes are attached to them and connected with an external load. Charge at the inter-facial surfaces are generated thanks to triboelectric effect, but no potential difference is present between the electrodes because of the electrical neutrality of the overall structure. When a layer is slipped on the other, electronic induction takes place in the non-overlapping parts of the layers. Hence, electrode placed on PTFE film has an higher potential than that situated on Nylon film and thus a current flows through the external circuit. Once full miss-match between the layers is reached, difference of potential becomes maximum and equilibrium state is obtained. Finally, if the top layer is slipped inward, a negative current is produced through the external load. This steps are displayed in figure 2.16. Other different geometries can be furthermore exploited for the sliding mode and multilayer setups could be used to improve energy conversion.
Finally, the same research group [42] presented a novel triboelectric setting, called "free-standing mode" (2.17). In this case there are two fixed metal (like aluminium) layers which act as both electrodes and triboelectric layers. They are connected to each other with a electrical circuit. A free-standing layer with different tribopolarity compared with the electrodes material, such as fluorinate ethylene propylene (FEP), is initially aligned with one electrode and thus triboelectrification occurs at the inner surfaces. The FEP sheet is then moved towards the other electrode and an asymmetric charge density between the electrodes is obtained. Hence, a potential difference can be measured between the metal plates and a current flows through the external circuit until the top film overlaps the other electrode completely. Then the maximum potential is reached. If the free-standing layer slides back, electrons flows through the external load in a opposite direction. This configuration represents a versatile and adaptable solution for wearable applications.

An AC current and voltage will be generated in all four configurations, due to the periodic relative motion between the triboelectric layers. Hence, triboelectric devices are used as nano-generators (TENGs, TriboElectric NanoGenerators), namely products that harvest mechanical energy caused by subtle motions, vibrations, frictions and convert it into electrical energy. Therefore TENGs, thanks to their high efficiency, represents a sustainable and low cost way to obtain energy for powering mobile electronic devices. For example, they can be integrated into gloves, shoes or clothes to generate a small amount of power thanks to physical activities. TENGs could be also employed as flexible tactile sensors: thanks to the positive tribopolarity of human skin, different soft and biocompatible material, such as PDMS, could be used to built a triboelectric sensor, exploiting the aforementioned configurations. Self-powering is the main advantage of these devices: as for piezoelectric sensors, they can convert tiny movements into electrical signals. Han et al. created a flexible, eco-friendly and lightweight TENG to monitor physiological signals like joint motion, breathing (Figure 2.18). They exploited the friction between a film of fish gelatin, derived from fish scales, and a polydimethylsiloxane-poly(tetrafluoroethylene)

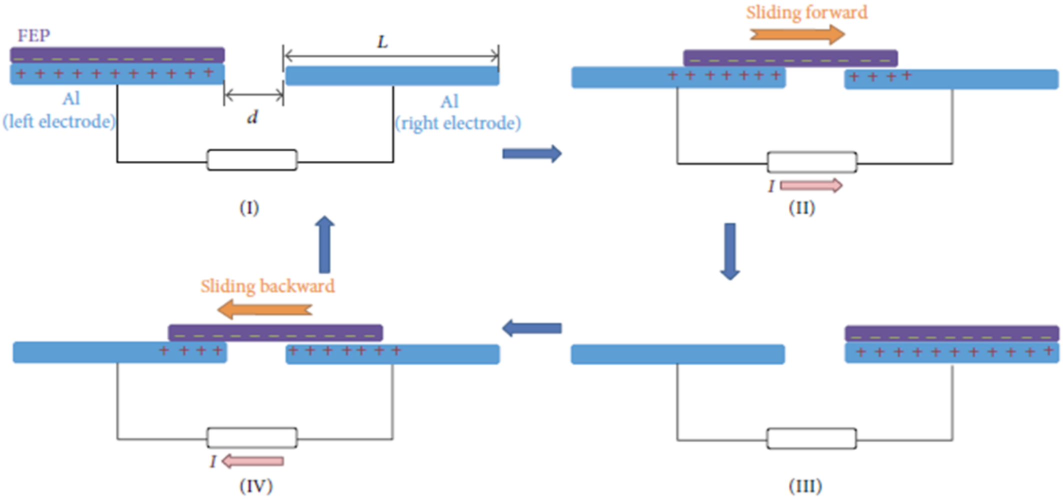

Figure 2.17: Free standing mode [42]

(PDMS-PTFE) composite layer. PTFE powder was added during PDMS curing to make its surface rough and thus for increasing contact area between the triboelectric materials and improving performances of the device. Two copper films were used as electrodes and small sponges were employed as spacers for achieving a vertical-contact mode configuration. The device was encapsulated into two sheets of printed papers, reaching an overall thickness of 6 *mm* [43].
Despite the great advantage of self-powering, triboelectric sensors are not suitable for long-lasting applications owing to wear of contact layers [5] and they cannot sense quasi-static loadings, due to the reaching of equilibrium state in all the configurations. In addition, conditioning circuits and production methods are usually more complex than those related to piezoresistive and piezocapacitive sensors.

2.2 Hydrogels

In general, hydrogels are defined as three dimensional water insoluble networks composed of hydrophilic polymers [44]. Hence, they are polymeric materials which retain at least 10% in weight (or in volume) of water thanks to the presence of hydrophilic groups such as -NH_2, -OH, -COOH, -$CONH_2$, -SO_3H [45]. Therefore their structures swell due to water uptake: this property endows hydrogels with a "soft" nature, resembling to mechanical features of living tissues. Furthermore, the excellent biocompatibility and the stimuli responsiveness (pH, temperature, chemical stimuli, light, electromagnetic fields) make them materials of choice for biomedical applications, like drug delivery [46], tissue engineering [47] and biosensors. In addition, they find also a large deployment in industrial fields as absorbers of metal ions and dyes from wastewater [48], flexible super-capacitors or batteries [49], hygienic and cosmetic products and finally water-retention agents for agricultural purposes [50].
In literature, hydrogels are categorized according to their nature and properties [45]. A

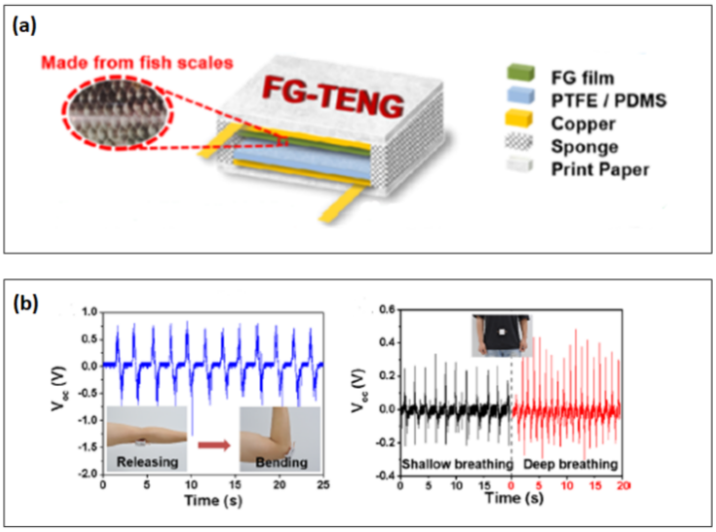

Figure 2.18: Example of triboelectric sensor: (a) Fish-gelatin TENG configuration (b) Joint motion and breathing detection [43]

summary classification is depicted in figure 2.19. A first division can be made considering the origins of polymers that constitute the hydrogel: they derive from natural sources or synthetic ones. Natural hydrogels are usually biocompatible, biodegradable, not cytotoxic and in some case they promote cells activities (bioactivity). Hence, they represents preferable materials for biomedical field. Poor mechanical properties and the possible lack of reproducibility are the main disadvantages of this class. Natural polymers basically derives from proteins and polysaccharides. Gelatin, collagen and silk fibroin are the most commonly used proteins. On the other hands, polysaccharide gels can be obtained by using

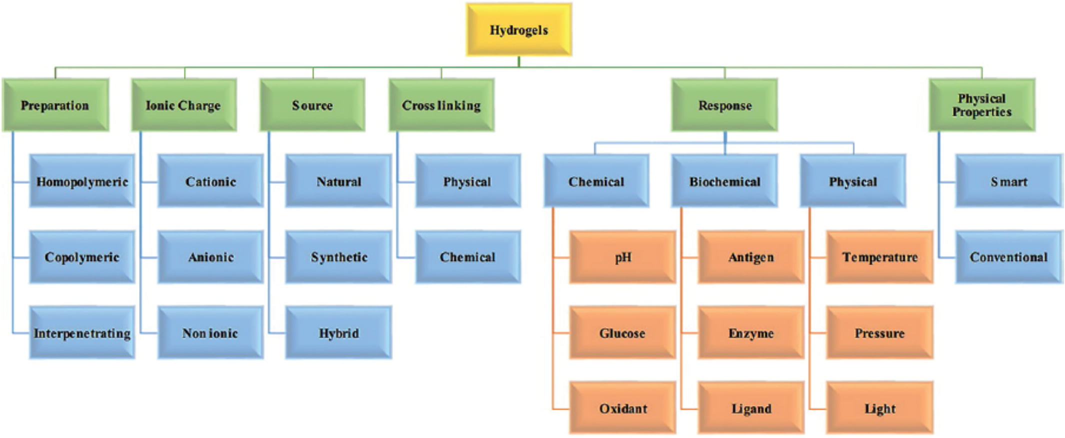

Figure 2.19: Hydrogels classification according to their nature and properties [45]

alginate, chitosan, hyaluronic acid and cellulose (it will be discussed in detail below). A list of natural polymers is presented in table 2.1 briefly.

Synthetic hydrogels generally own stronger mechanical properties and durability and thus they are usually less degradable compared to natural ones [51]. Moreover, they possess an high reproducibility and both chemical and mechanical features could be easily customized during the manufacturing processes. However, synthetic hydrogels are not always biocompatible; actually, in certain case they have a cytotoxic effect towards cells. Poly(ethylene glicol) (PEG) is an exception: it finds a wide use in biomedical applications, due to its biocompatibility, non-immunogenity, resistance to protein adsorption (no fibrotic cap is created when it come in contact with the human body tissues) and simple functionalization [52]. When poly(ethylene glicol) has an high molecular weight ($\geqslant 20000 g/mol$), it is called poly(ethylene oxide) (PEO). Others frequently used hydrogels and the chemical formula of their repeating units, are reported in figure 2.20. Usually, both natural and synthetic monomers are used together for having a trade-off between the properties of the two classes: in this case hybrid hydrogels are formed.

Table 2.1: Main natural polymers which constitute hydrogels

Hydrogel name	**Source**	**Type**
Cellulose	plants and natural fibers	polysaccharide
Chitosan	crustaceans	polysaccharide
Hyaluronic acid	animal tissues	polysaccharide
Alginate	seaweeds	polysaccharide
Silk fibroin	silkworm	proteic
Collagen	animal tissues	proteic
Gelatin	fishes and animal tissues	proteic

As regards the hydrogels preparations, a single kind or several kinds of monomer could be employed. In the first case, hydrogel is classified as "homopolymeric" while in the second case as "copolymeric". Usually copolymers are composed of at least an hydrophilic monomer. Two different polymers can also form semi-interpenetrating networks (semi-IPN) if they are crosslinked and each one does not form chemical bonds with the other. An interpenetrating network (IPN) is obtained if chemical bonds between the two networks are present and thus one polymer is synthesized in the solution where the other is already crosslinked [45]. These hydrogels are also know as "double networks hydrogels" (DN hydrogels) and will be examined later. Both semi-IPN and IPN are interesting thanks to the enhanced mechanical properties compared to single polymer hydrogels.

Furthermore, hydrogels can have a net electrical charge because of the nature of repeating unit. Hence, "anionic", "cationic", "neutral" hydrogels exist if they own a negative, positive or null whole charge respectively. Some examples are reported in the image 2.20.

crosslinking method is another way usually used to divide hydrogels. "Chemical" or "permanent" gels are those that have covalent bonds between the different polymer chains. Hence, they present an high mechanical strength and are more stable against solvent. Although, a crosslinking agent called also "crosslinker", is necessary to begin the polymerization reaction: it could be a chemical agent which acts spontaneously or is activated by radiation

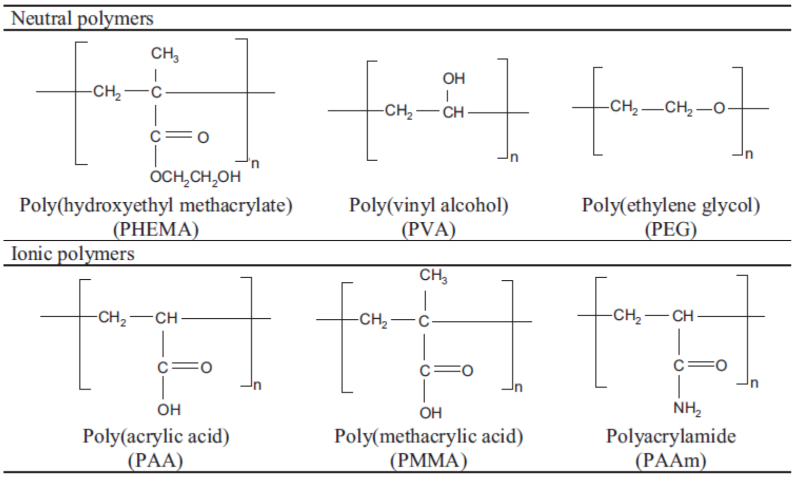

Figure 2.20: Synthetic polymers which form hydrogels and their net charge [53]

sensitive initiator or by radical one. In some cases, enzymes can also serves as crosslinkers [54]. Functional groups part of the polymer define the crosslinker to choose and the fabrication process of the hydrogel. On the other hand, in "physical" or "reversible" gels molecular entanglements and/or hydrogen, ionic, non-covalent, hydrophobic bonds constitute the connecting points between the chains. In this case crosslinking agents are not necessary and the fabrication is simpler consequently [55]. Moreover, if a polymer owing a certain net charge in the solution (polyelectrolyte) is combined with multivalent ions of the opposite sign (such as metallic ions), the latter behave as "bridges" between the polymeric chains and the so formed physical gel is also known as "ionotropic hydrogel". Actually, if ionic bonds are due to interactions among polyelectrolytes of different polarities, hydrogels are called "coacervates" or "polyelectrolytes" complexes [56]. Physical hydrogels posses lower mechanical properties than chemical ones, due to the weaker inter-chains bonds.

Finally, hydrogels which are able to respond to environmental stimuli like chemical, biochemical and physical ones (reported in 2.19) are named "smart" or "intelligent" gels. This sensitivity is due to the functional groups of the constitutive polymers. Swelling, shrinking, decrease in solubility and transformation of chemical groups of side chains are some possible hydrogels responses to external solicitations.

The performances of hydrogels are determined relying on several structural parameters. First of all, the polymer volume fraction, namely the water volume retained by the swollen hydrogel, is an important feature for characterizing the gels. Moreover, the degree of crosslinking can provide an estimation of their mechanical resistance: it is measured through the molecular weight of polymeric chains between a crosslinking point. Then correlation length has to be taken into account when diffusion of substances is relevant (like in drug delivery applications); it is a measure of the average distance between two chains. All these parameters can be measured both experimentally and theoretically [53].

Therefore hydrogels present different interesting properties and their easy customization make them suitable in a huge number of fields. Water evaporation during time is the main disadvantage. Thus hydrogel becomes dry and losses its better physical properties. Dehydration is obviously accelerated by high temperatures. Impermeable or semipermeable encapsulations are usually employed to slow down this process. That same encapsulations, if own the desired stretchability and mechanical resistance, are helpful to overcome the brittleness and low elasticity that hydrogels normally have. In literature exists other approaches that allow to solve this problem: some examples will be displayed in section 2.3. Finally, most of polymers do not show electrical properties and thus hydrogels formed by them cannot be used as flexible sensors. Making hydrogels able to conduce electricity is a crucial issue in order that they can be effectively used as "bridges" between soft human tissues and rigid traditional electronic (Figure 2.21) [57]. In the following sections several approaches for endowing hydrogels with electrical constructibility are presented.

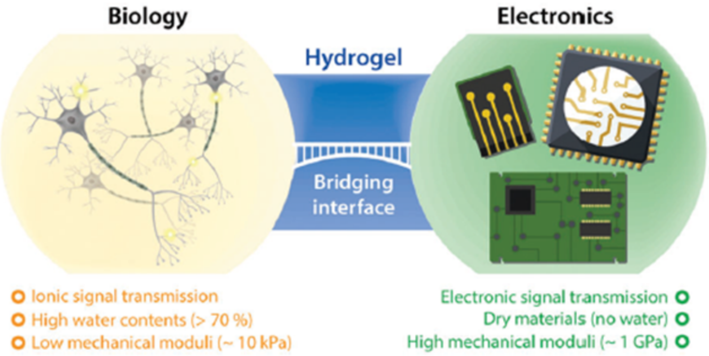

Figure 2.21: Conductive hydrogels represent a bridging interface between biological tissues and electronic devices [57]

2.2.1 Electronically conductive hydrogels

In electronically conductive hydrogels (ECHs) the current flow is due to the charges brought by mobile electrons. Some polymers, such as polypirrole (PPy), polyaniline (PANi), poly(3,4-ethylenedioxythiophene):polystyrene sulfonate (PEDOT: PSS), are intrinsically conductive. Polymerization in situ of conductive monomers is a strategy frequently used in literature for obtaining IPN gels (Figure 2.22a). A network of poly(vinil alcohol) (PVA) crosslinked through maleic acid (MA) can be soaked in a ammonium persulfate (APS) solution after drying. Then, the swollen gel is submerged in a solution of aniline hydrochloride (AnHCl) and immediately the polymerization of anyline takes place thanks to APS. In this way, Adhikari et al. obtained an interpenetrating PANI based conductive hydrogel which could be used as smart sensor [58]. Some researcher teams managed to crosslink directly conductive monomers through a specific dopant (Figure 2.22b). PANI and PPy were crosslinked thanks to phytic acid and copper phthalocyanine-3,4',4",4"'-tetrasulfonic acid tetrasodium salt (CuPcTs) respectively [60] [61]. Thereby, electric properties were not deteriorated due to a support insulating matrix, like in "in situ" polymerization techniques and optimal conductivities were achieved (7.8 S cm^{-1}).

Nevertheless, the low number of conductive polymers could limit their versatility and

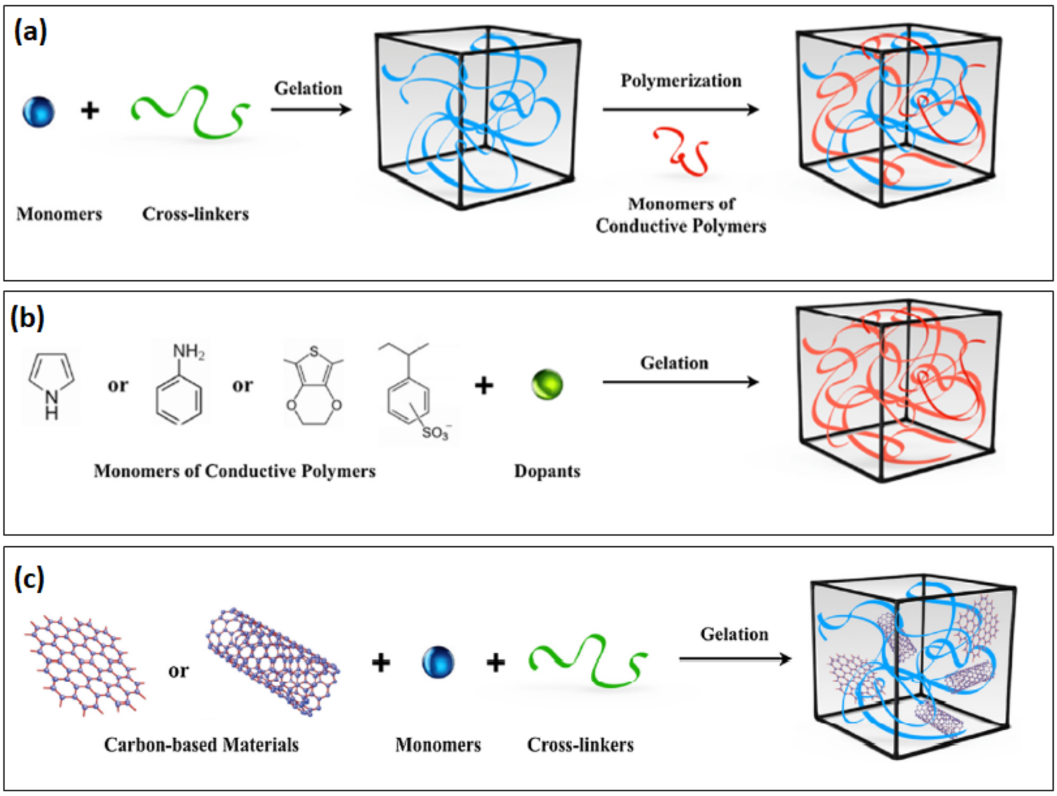

Figure 2.22: Conducting polymers based hydrogels [59]: (a) In situ polymerization (b) Conductive monomers crosslinked by dopant (c) Conductive hydrogel doped with carbon-based nanomaterials

adaptability [62]. In addition, it is frequently necessary to tailor synthesis processes because of the poor solubility of conductive polymers and additional steps are often required to remove un-reacted monomers and crosslinkers which could be cytotoxic [63].

Hence, many researchers focus on making composite hydrogels through doping strategies. Using metallic or carbon based nanomaterial as fillers is a possible approach to solve conductibility issue. These materials should have an even dispersion in the polymeric matrix to endow hydrogels with an electronically behaviour. Moreover, conductibility can be easily tailored adjusting concentrations of fillers and no extra steps for removing cytotoxic residuals are necessary. Nanomaterials are usually dispersed in the precursor solution of the hydrogel before crosslinking; then they are trapped in the polymeric network after the curing process. Carbon derived materials, such as carbon nanotubes (CNTs), graphene oxide (GO) and carbon black (CB) own outstanding electrical properties and possibility to be functionalized for promoting adhesion to the polymer. Therefore, homogeneous dispersion in the main solution is easily achieved. Xia et al. used multi-walled carbon nanotubes (MWNTCs) as both conducting materials and crosslinking agents. They functionalized MWNTCs with carboxyl groups to allow the generation of ionic bonds between chitosan chains, creating a polymeric network. Another network made of polyacrilic acid

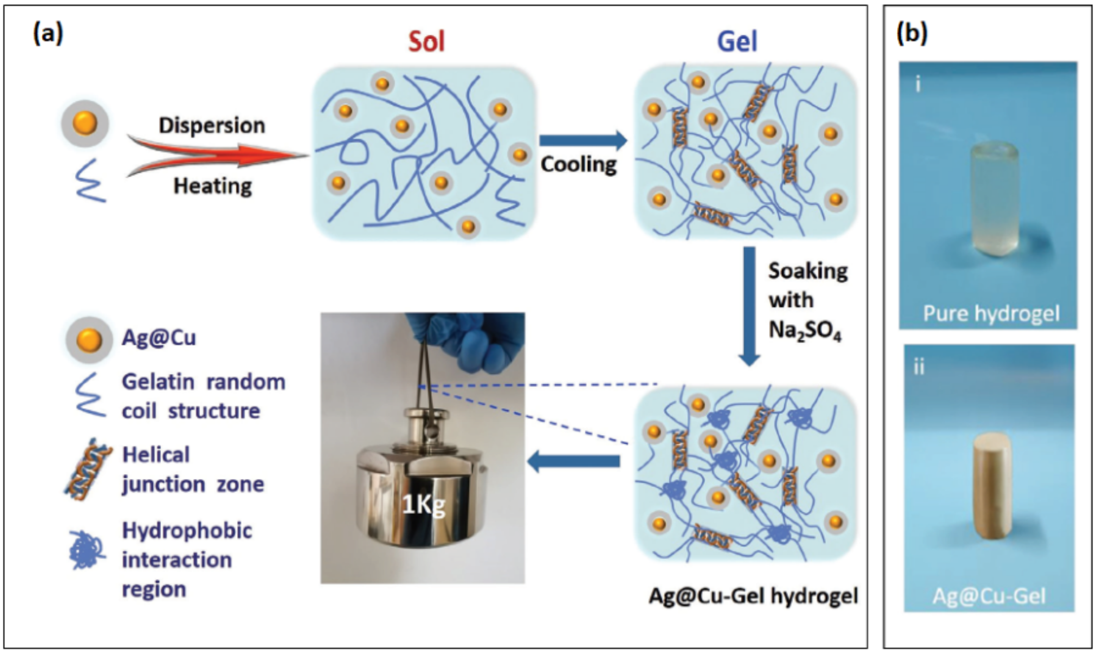

Figure 2.23: Example of ECH doped with metal nanoparticles: (a) fabrication process (b) Hydrogel without doping nanoparticles (on the top) and with Ag@Cu nanoparticles (below) [64]

(PAA) and lauryl methacrylate (LMA) copolymers crosslinked with hydrophobic bonds, was created. Chitosan and PAA-co-LMA networks were interlocked through electrostatic interactions, hydrogen bonds and physical entanglements. Gauge factor was greater for strain higher than 100% (3.2) while it was lower (1.65) for small deformations. In this way a super-stretchable, self-healing and self-adhesive sensor was produced for health monitoring purposes [6]. However, the aforementioned example and other hydrogels doped with carbon nanomaterials are often dark: the more doping agent concentration is used, the higher conductibility is achieved but the less optical transparency is obtained.
Metal-based nanomaterials are also excellent fillers thanks to their high conductibility. Nanoparticles, nanowires, nanofibers can be obtained from different metals, like gold and silver. In contrast to gels doped with carbon nanomaterials, which are no susceptible to degradation in wet environment, in this case noble metals have to be employed for avoiding corrosion [57]. Chen and co-workers used silver coated copper nanoparticles (Ag@Cu NPs) for endowing a gelatin hydrogel with high conductivity. These fillers were less expensive than pure silver nanoparticles and more resistant to corrosion compared to the copper ones. Hydrogel was immersed in a Na_2SO_4 solution, crosslinks between polymeric chains were created and thus mechanical toughness of the gel was improved. Fabrication process is briefly shown in figure 2.23. Sensors made by this ECH showed flexibility, conductibility (1.92 $S\ m^{-1}$), linearity and excellent sensitivity (GF is equal to 2.0822) [64]. Gold nanowires (AuNWs) have also attracted interest thanks to their conductibility a low toxicity. A cardiac patch made by alginate and AuNWs was employed by Dvir et al. as

scaffold for cardiac cells. In this case nanomaterials serves as electronically conductive bridges between cells to promote their growth and differentiation [65].
Nanomaterials application improves hydrogels toughness, overcoming their lack of mechanical resistance. However the fillers dispersion should be homogeneous to avoid a non-uniform conductibility and poor repeatability. Sensors based on metallic composite hydrogel normally show higher conductibility compared to carbon composite gels and an outstanding sensitivity. Here too, nanomaterials concentration should be carefully controlled to get a trade-off between conductibility and transparency of the device.

A less followed method involves the employment of liquid metals: a pattern is machined in a flexible substrate (such as hydrogels) and liquid metal is injected into it. Choi et al. used a flexible and durable interpenetrating network of agarose and poly(vynil alcohol) (PVA) to obtain layers with accurate patterns through a mold which was previously 3D-printed (Figure 2.24a). Each patterned layer was then covered with an hydrogel cap and an eutectic alloy of gallium and indium was inserted through a syringe. Viscosity of the liquid metal was increased thanks to oxidation processes; thus, metal did no get out when the device was cut. Thanks to this, self-healing, very thin and electronic conduction based sensors were made (Figure 2.24b) [66].

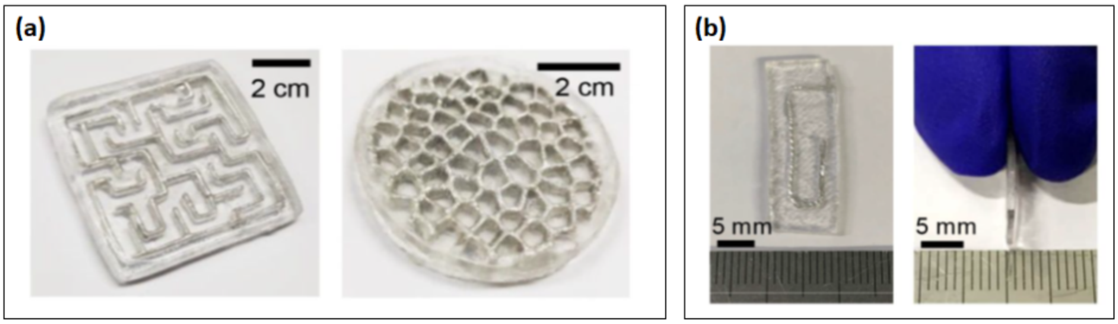

Figure 2.24: Liquid metal-hydrogel composite: (a) Patterns of various shapes (b) Thickness of the flexible electrode [66]

Despite the optimal conductibility and sensitivity given by metallic and carbon based nanomaterials, a significant issue is the possible toxicity of these fillers. Hence, careful trials about compatibility with human skin or with cells (depending on the application) must be taken into account for this kind of sensors [63].

2.2.2 Ionic conductive hydrogels

Human tissues use mobile ions to communicate to each other due to their electrolytic nature that does not allow electron flow [57]. Therefore, using ions as charge carriers is another method widely employed for obtaining conductive hydrogels which could interface with biosystems. They are usually dispersed in the precursor solution of the gel and, after gelation, they can move across its pores following the external electric field applied (Figure

2.25a). This kind of sensors are known also as ICHs (Ionic Conductive hydrogels). Ions

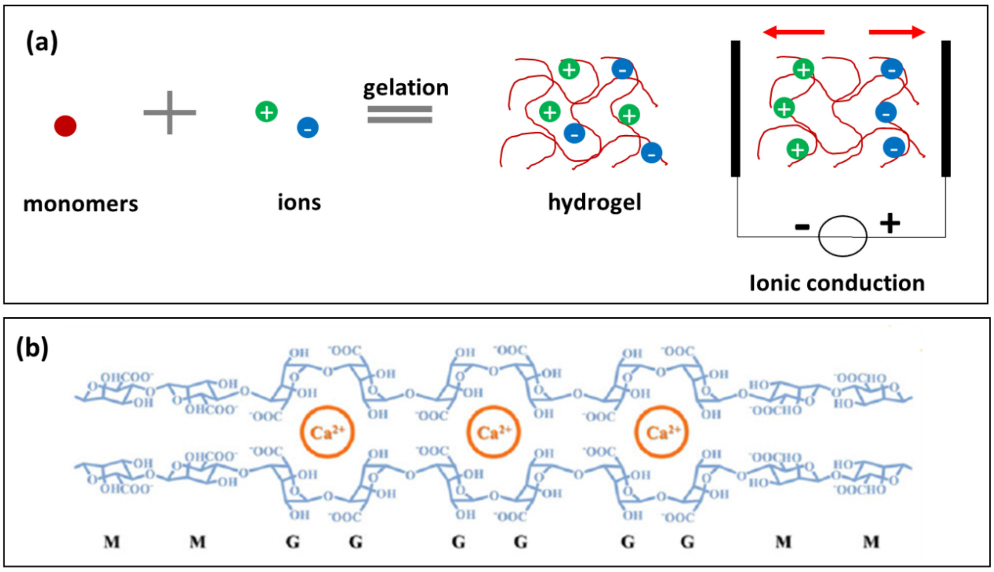

Figure 2.25: (a) Production process of a ionic conduction hydrogel (b) An example of chemical dopants: polyacrylamide chains crosslinked by bivalent calcium ions [67]

derive from water soluble salts, such as sodium or potassium or lithium chloride and others. These chemical compounds, when are immersed in a polar solvent (like water), undergo to ionic dissociation: anions and cations, that first constitute a electrically neutral salt, are separated and then surrounded by solvent molecules.

Inorganic salts are classified in physical a chemical dopants: the former do not create chemical bonds between polymeric chains and thus are free to move in the lattice, the latter act as "crosslinking centres" in the hydrogel matrix as well as conductibility agents. In this last case, multivalent ions (cations or anions) bind two or more chains of the polymer which have the opposite charge; this results in the creation of the aforementioned "crosslinking centres" which lead to a physical hydrogel, due to the ionic nature of the bonds (Figure 2.25b).

For instance, Liu et al. designed a ionic conductive sensor based on an interpenetrating network of κ-carrageenan (a polysaccharide) and polyacrilamyde (PAAm). The first polymer was physically crosslinked by potassium chloride (KCl) while N,N'-methylenebisacrylamide (MBA) was used to form the links in PAAm. Therefore, a soft κ-carrageenan network was created through ions derived from KCl salt and the AAm chains were linked via covalent bonds thanks to MBA, constituting a brittle and tough lattice. The double-network hydrogel thus created showed a great stretchability (until 1000% of strain), a good GF (the higher value was 0.68 at upper strain limit) and self healing property. Moreover this hydrogel was suitable for 3D ink-jet printing, allowing the realization of complex shapes [68]

Lithium chloride is another compound widely used as doping agent: Yang et al. prepared through a one-pot method a polyacrylamide-agar double network hydrogel in which lithium and chloride ions (Li^+ and Cl^-) acted as charge carriers. In this case, LiCl was a physical dopant because do not interact with PAAm and agarose networks. This ionic-conductive hydrogel exhibited a good sensitivity to stretching with a maximum GF of 1.8 at 1100% of strain. Moreover, it was also able to perceive temperature variations: the electrical resistance of the sensor diminished when the temperature increased, due to the higher mobility of the ions. Hence, multimodal sensing capability made it an optimal sensor for e-skin applications [69].

These examples show that ionic conductive hydrogels are generally less sensitive but own an higher stretchability compared to the nanomaterials based ones. These sensors are simpler to prepare because of the easy availability of doping salts. Others interesting features are achieved with ICHs: sensors are transparent, allowing the transmission of visual informations, and their freezing point is lowered thanks to ions, guaranteeing anti-freezing property [70]. On the other hand, higher concentrations of ions could be dangerous for cells [62] and electrochemical reactions could happen at the interfaces, as for instance between the hydrogel sensor and metallic electrodes used as connection with external devices.

2.3 Categories of hydrogel based smart sensors

ECH and ICH may represent excellent materials to produce tactile sensors based on electric transduction, since conductibility is a key features for them. Actually, hydrogels biocompatibility and softness make them ideal for this purpose. However, common homopolymeric gels are weak and have a little toughness. This lead to a poor ability to dissipate mechanical energy after external deformations and their fracture strain and stress are usually small, consequently [3]. In literature several strategies have been proposed for overcoming this issue and thus endowing hydrogels with excellent stretchability and flexibility. Nanomaterials dispersion in gels matrices is a possible solution for increase their mechanical properties, as before mentioned. Moreover, the usage of double-network hydrogels or robust encapsulations are other feasible techniques findable in literature.

The need to obtain an optimal mechanical and electrical behaviour and low-power devices is directly linked to the manufacturing procedures and the product design. Therefore hydrogel based smart sensors which exploit electric transduction may be separated into several groups. In the following sections, the main classes are examined in more detail.

2.3.1 Double-network sensors

An interesting category of smart sensor involves the double-networks hydrogels (DN HDG). Two polymeric networks which own contrary mechanical properties are intertwined through physically entanglements or chemical covalent bonds [71]. One of them is hard and brittle due to the high density of crosslinks between chains: bonds dissipate mechanical energy coming from external loadings and endow the DN hydrogel with excellent toughness. However, since crosslinks are usually chemical bonds, this first network is called "non-reversible", namely if it is broken, the whole hydrogel does not reacquire the original mechanical and electrical properties. The other network is slightly crosslinked and thus it is more flexible. Bonds between chains are reversible because are constituted by non-covalent, ionic and hydrophobic interactions, and so they reform after their rupture. For this reason, they are

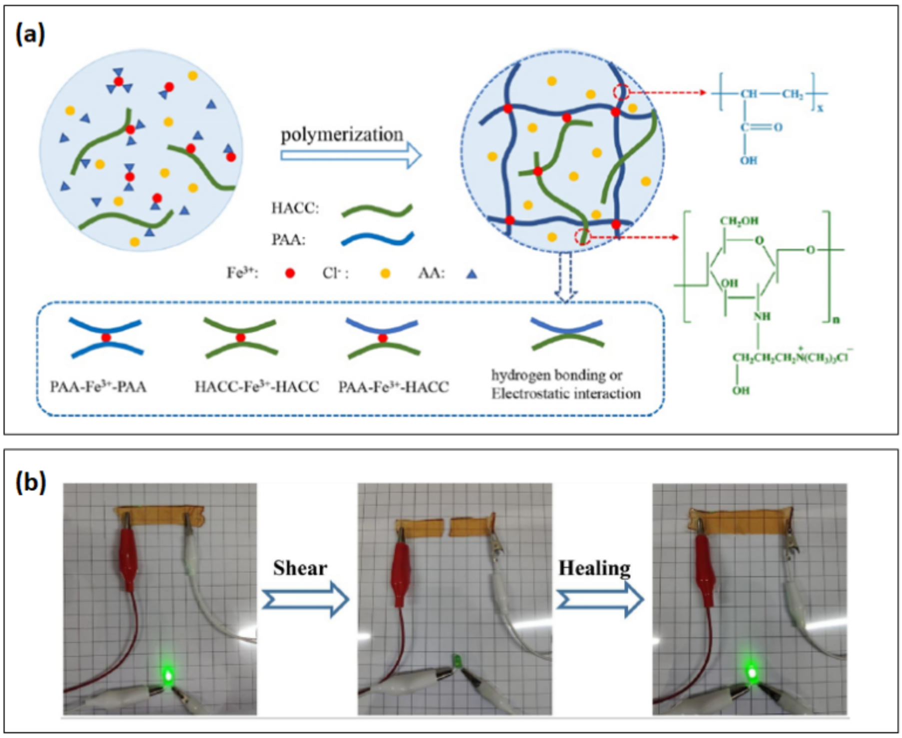

Figure 2.26: Double network hydrogel sensor: (a) One-step polymerization to obtain PAA-HACC hydrogel. At the bottom, the chemical bonds which are present in the final product (b) Demonstration of self-healing property [74]

also called "sacrificial bonds". Hence, the second network provides elasticity keeping the HDG intact during deformations and allowing the return to the initial shape. In other words, the rigid network represents the "shock absorber", while the flexible one serves as "glue" to ensure DN HDG integrity [72].
Optimization of the mechanical properties is carried out through the selection of the polymers constituting the double-network and the tailoring of their concentration: the number and the type of chemical bonds inter- and intra- networks is indeed the crucial parameter to take into account. High Young modulus (0.1-1 MPa), tensile strength (1-10 MPa), toughness (in the range of some MJm^{-3}) and great stretchability (up to 2000%) are usually achieved thanks to DN hydrogels [3] [73] . The presence of reversible bonds in the second network furthermore ensures the healing of the gels after damages. Therefore, thanks to these features, DN hydrogels represent attractive materials for building tactile sensors, despite their production methods that are often tricky and challenging.
For instance, Wang et al. designed a DN hydrogel based sensor built with a easy one-step polymerization method. Ferrum chloride ($FeCl_3$) was dissolved in distilled water in which acrylic acid monomers and HACC were previously inserted. The ionic dissociation of the salt in Fe^{3+} and Cl^- had a dual effect: Fe^{3+} created ionic bonds intra- and inter- networks and both Fe^{3+} and Cl^- gave electrical conductibility to the hydrogel. Polyacrilyc acid ionically crosslinked through ferric ions (PAA/Fe^{3+}) forms the flexible network while the

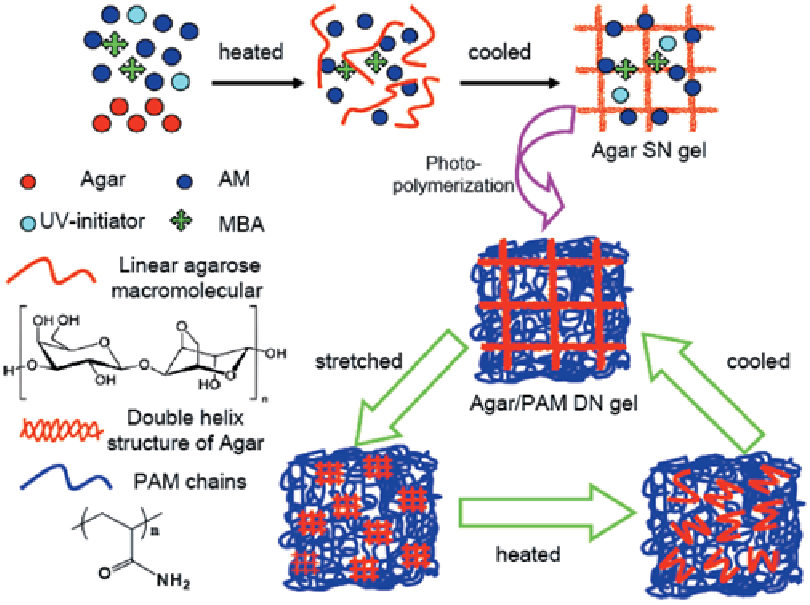

Figure 2.27: Double-network thermo-responsive hydrogel preparation

strong and brittle one was constituted by 2-hydroxy propyltrimethyl ammonium chloride chitosan (HACC) always crosslinked by Fe^{3+}. The structure and the bonds which were present in this DN hydrogel, are showed in figure 2.26a. A piezoresistance based sensor was then created through this hydrogel: it showed an excellent stretchability (1652%), toughness (5.1 MJm^{-3}) and self-healing. The latter was demonstrated connecting the sensor in series to a led and powering them. When the sensor was cut, the led was switched off. After healing the led brightness remained almost the same compared to the one before hydrogel cutting (Figure 2.26b). This sensor demonstrated adhesiveness, excellent repeatability and optimal sensitivity with higher gauge factor (11.25) corresponding to greater strains [74]. Using ionic bonds to crosslinks also the brittle network is a strategy frequently adopted for improve self-healing ability ad increase the durability of sensors against harsh conditions. The exploitation of thermo-reversible sol-gel polymers is another possibility to have mechanical and shape recovery. Chen's group successfully synthesized a DN hydrogel thanks to the thermo-responsiveness of agar. A solution (sol) with agar powder, acrylamide monomers, UV-initiator and crosslinker was heated at 90°C. In these conditions, agar formed linear chains. After cooling at room temperature, agar reorganized its structure in twisted helical bundles, forming the first network (gel), densely crosslinked. Then the photo-initiation process took place and polyacrylamide flexible network was created (Figure 2.27). This DN HDG could be stretched until 2000% of strain and returned thanks to PAM network. If it is damaged, it would restore its initial shape and features through heat treatment. In such case the first network of agar was broken dissipating energy and the second remained intact: after heating, the agar cluster formed linear chains interpenetrated to PAM network. Upon cooling at room temperature, the original gel is recovered [75]. If this hydrogel is provided with conductivity, it will represent an intriguing material

for tactile sensors due to their properties and simple production method.
In general these sensors own optimal mechanical features, notch insensitivity, resistance to knotting, twisting and damage tolerance [6] [76]. Nevertheless, the main drawback of double-network hydrogel based sensor is the water evaporation. Since the hydrogel is directly exposed to external environment, water retained by the networks will vaporize resulting in changes of stretchability and electric properties of the sensor. Therefore, this kind of sensors have often a limited working life.

2.3.2 Sandwich-like sensors

Sandwich-like sensors allow the overcoming of the problem explained before: water evaporation is slowed down or even cancelled. An encapsulation material which is impermeable or semipermeable to water vapour is used to cover the hydrogel which constitutes the sensitive part. In addition, it should own adequate mechanical properties to endow the final product with optimal stretchability and shape-recovery and to protect hydrogel from external environment. Hence, encapsulation is especially necessary for brittle and weak homopolymeric hydrogels. Elastomers like polydimethylsiloxane and commercial tapes are some example of applicable materials. They should, if possible, be transparent to provide better aesthetic results and to allow the transmission of visual informations. It is important to consider that, for wearables, semipermeable coatings should be selected for ensuring sweat permeability and to not cause inflammatory response of the skin. These sensors have a layered structure which slightly change according to the transduction method exploited. Piezoresistance sensors have a single layer of hydrogel covered by two sheets of encapsulation material (Figure 2.28a). Meanwhile, piezocapacitive ones have a dielectric flexible layer (usually made by the same material used for the encapsulation) within two layers of hydrogel; the whole structure is then protected by covering sheets (Figure 2.28b). Electrodes, required for sensing the electrical parameter variations, are inserted during the device assembly and are trapped between the encapsulation and hydrogel layers.

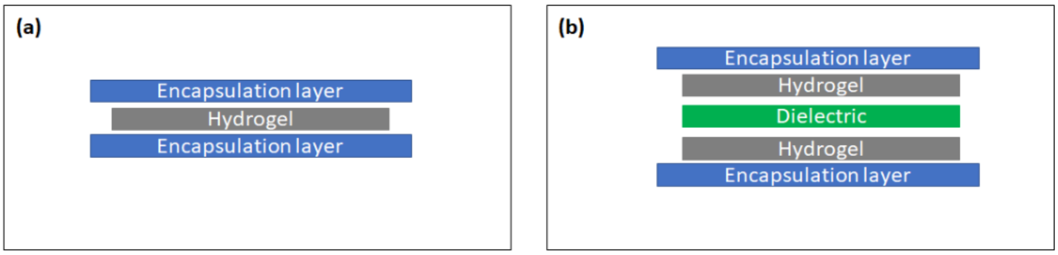

Figure 2.28: Configurations of sandwich-like sensors: (a) piezoresistance device structure (b) Piezocapacitive device structure

Sun et al. presented a sensor, inspired by the human skin, made by a weak homopolymeric hydrogel (polyacrylammide) doped with ions derived from sodium chloride dissolution, encapsulated by an acrylic commercial tape (VHB, 3M). Therefore, a capacitive sensor was created with a layered structure (Figure 2.29a). It was modelled with the electric equivalent showed in figure 2.29b: the overall capacitance was given by the series of the dielectric

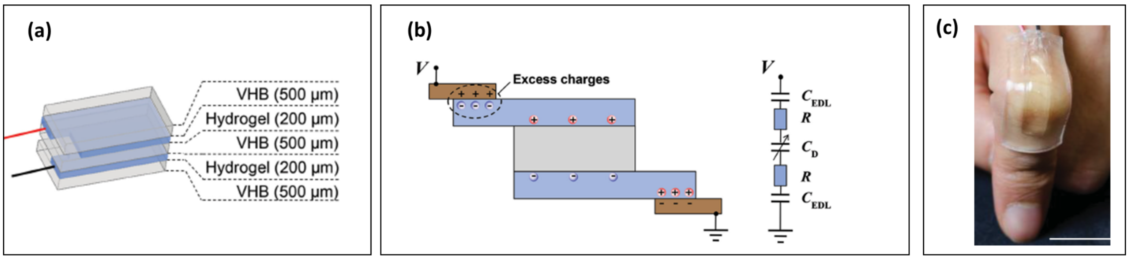

Figure 2.29: Ionic skin [28]: (a) Structure of ionic skin (b) Electrical equivalent (c) The final product

capacitance (C_D) and the capacitances of the electrical double layers (C_{EDL}). These last ones were referred to the interface between the metallic electrodes and the ionically conductive hydrogel and were caused by the double layer of ions (of opposite sign) which accumulated near each charged electrode [77]. Therefore the overall capacitance can be computed as $1/C = 2/C_{EDL} + 1/C_D$. Since the charges of the double layers are separated of nanometers and capacitance is computed according to equation 2.9, C_D is the dominant parameter. In this way transparent piezocapacitive device (Figure 2.29c) which was able to sense both stretching and pressure with optimal repeatability, was obtained [28].

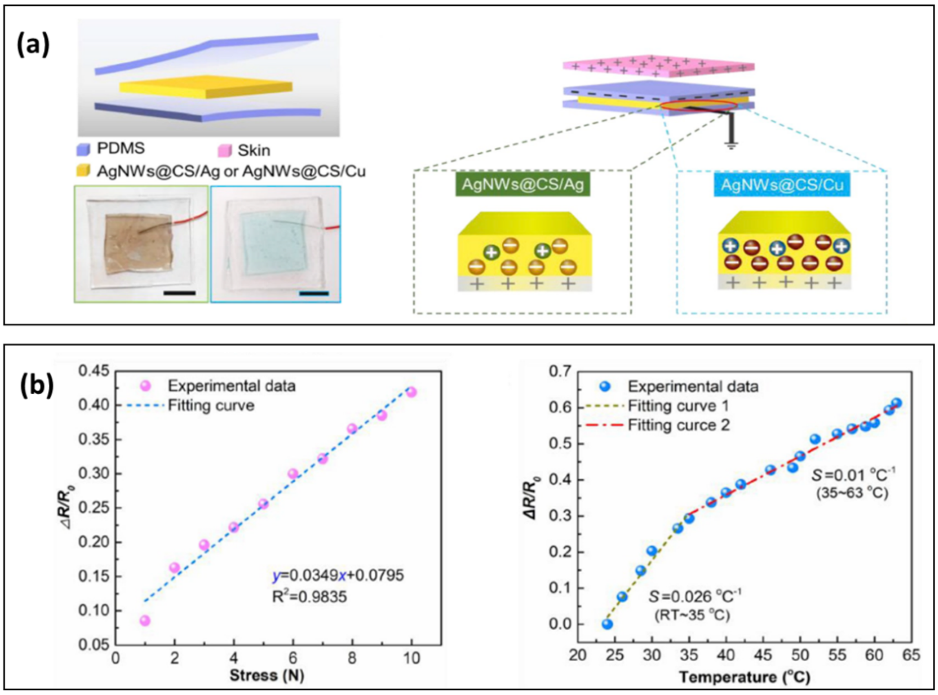

Figure 2.30: Hybrid conduction sandwich-like sensor [78]: (a) On the right, structure of the sensor. On the left, single-contact mode working principle and EDL in the two configurations (b) Transfer curves of different sensing modes

Sandwich-like structures are also adopted to encapsulate nanocomposite or double-network hydrogel. Wang's group realized a motion-energy harvester (MEH) which was furthermore employed as stress and temperature sensor. They exploited the hybrid (both ionic and electronic) conduction of a nanocomposite hydrogel; chitosan with silver nanowires (Ag-NWs) dispersed in the solution, was actually crosslinked by metallic ions (Ag^+ or Cu^{2+}). The network so obtained, was encapsulated between two sheets of transparent VHB tape. The configuration and the two types of hydrogel, one crosslinked with Ag^+ and the other with Cu^{2+}, are showed in figure 2.30a. MEHs were realized through triboelectric single-electrode mode explained earlier in section 2.1.4. In addition, using two electrodes, it was possible to adopt the same structure for creating a multi-modal piezoresistance sensor. In fact, in figure 2.30b the transfer curves for stress and temperature stimuli are showed . As concerns the stress, a linear relationship between input and output was found, meanwhile it was possible to divide the temperature curve into two linear region with different sensitivity. An interesting feature was the washability": the hydrogel, after complete dehydration, was subjected to water for trying to restore the initial performances. It was found that after 30 minutes, the electrical output of the MEH was comparable to the original one [78]. As can be seen from these examples, production processes of sandwich-like sensors are generally simpler compared to those of the other classes. The main problem is the absence of self-healable ability because encapsulations employed do not own this property. Moreover, other interesting features, such as self-powering, transparency and adhesiveness may be achieved in easier way.

2.3.3 Self-powered sensors

Another issue which has not been dealt with so far is the power supply of the sensors. They need a continuos and stable power for performing an un-interrupted sensing and to transfer data. Thus, power sources must be reliable, durable and appropriate as regards the supplied tensions. Batteries are the most common type of power supply units since they have been studied for a long time. Their working principle consists in the conversion of chemical energy, derived from redox reactions, into electrical energy. Although the large scale production of batteries makes them the preferred power sources for wearable applications, the considerable weight and encumbrance of batteries often limit their usage in this fields. Another problem is the self-discharging of batteries: their output voltage is not constant over the time. Today, thanks to the continuos development, several interesting

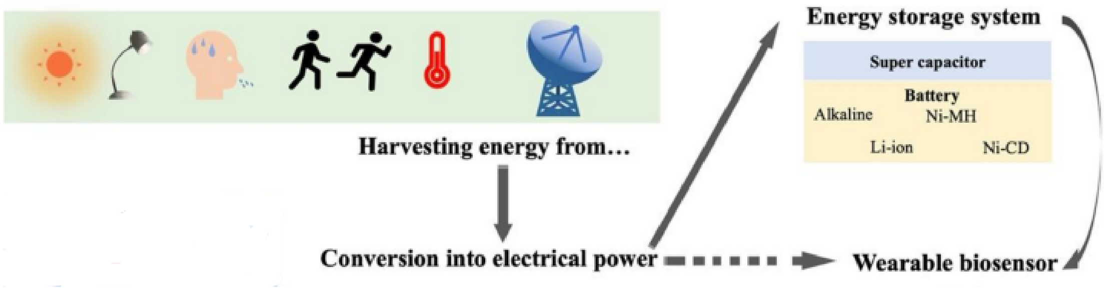

Figure 2.31: Harvesting energy from environmental sources

solutions have been found. For instance lithium-ion batteries own an high working voltage, great specific power and outstanding lasting. However, in some cases miniaturizing batteries is not possible because of the high power density required by sensors. In addition, the possible leakages of toxic electrolytes used in batteries, may cause adverse reactions on the human skin [79].

Therefore, alternative energy sources were widely investigated in literature: studies are actually focused on harvesting energy from external environment. Heat, light, friction, radio-waves, chemical reactions may be exploited to obtain electrical power which can be stored in batteries or supercapacitors with the problem related to toxicity explained before, or can be applied directly to wearable devices 2.31. Piezoelectric and triboelectric effects, examined in detail in sections 2.1.3 and 2.1.4, are possible ways to overcome the issue of the power supply. Piezoelectrical or triboelectrical sensors manage to convert mechanical stimuli to a voltage or current output in a direct manner, resulting in self-powered devices. This feature, combined with the normally easy production processes, low cost materials and versatility, makes them very intriguing for wearable applications [81].

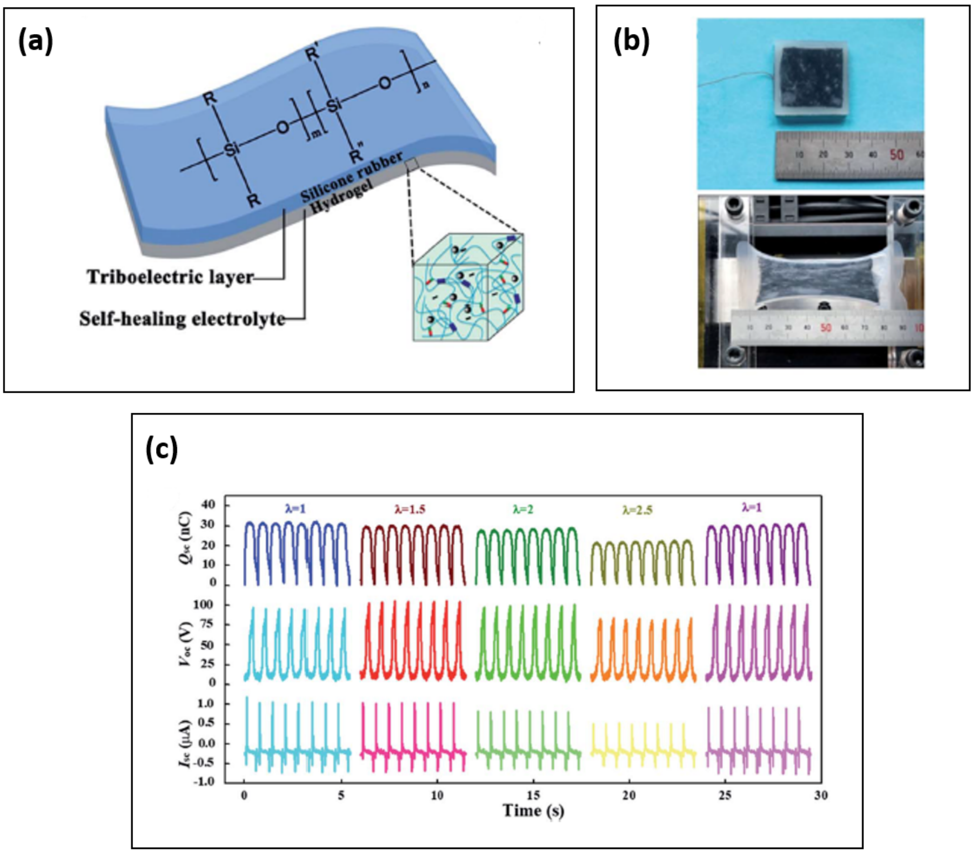

Figure 2.32: Example of triboelectric nano-generator and sensor [80]: (a) TENG configurations (b) Images of TENG relaxed and stretched (c) Output performances (transferred charge, open circuit voltage and short circuit current) of the TENG at different strains

For instance Guan et al. created a self-healing triboelectric nano-generator (SH-TENG) which could be also employed, hypothetically, as smart sensor. A co-polymeric hydrogel of poly(vynil alcohol) and agarose (PVA/agarose) was synthesized through freezing/thawing process; multi-walled carbon nanotubes (MWNTCs) were inserted in the precursor solution to provide electronic conductibility. Moreover, particles of photo-termally active polydopamine (PDAPs) were added to improve mechanical properties (they were linked to PVA microcrystallites) and to allow the self-healing ability through near-infrared light exposition. In this hydrogel, borate bonds were present, thanks to the existence of borate ions: these covalent, dynamic and reversible crosslinking could be reformed through water exposition. Therefore a double-mediated self-healing hydrogel was obtained. A silicon rubber layer (which is far from human skin in the triboelectric series) was then casted onto hydrogel layer and the single-electrode configuration was exploited (section 2.1.4). Experimental tests were performed at different strains with a nylon film which was repetitively accosted to the sensor: when the device was stretched, its resistance increase and thus voltage output diminish. An optimal repeatability of voltage output and stretchability (400%) were reached (Figure 2.32) and thus it could be employed as smart sensor.

Not only piezoelectric and triboelectric effects can be harnessed for building self-powered sensors: Wang's group proposed a strain sensor based on galvanic cell configuration, actually. An hydrogel composed of gelatin and tannic acid (TA) doped with silver nanowires (AgNWs) was used as electrolyte. An electrode of air and a layer of zinc respectively acted as cathode and anode, like in common batteries. In this case, the chemical energy produced by the redox reactions showed in figure 2.33b was converted into electrical energy, resulting in a open circuit voltage of 1.5 V. The sensor was constructed connecting the fixed resistor R_f (Figure 2.33a); when it was deformed, the hydrogel resistance (R) varied and the voltage measured on the fixed resistor chaged. If sensor was pressed and so its resistance diminished, voltage output increased, consequently (Figure 2.33c). In addition, the device showed a good repeatability after being subjected to different pressure cycles. This sensor also demonstrated an excellent stretchability (1600%) and self healing thanks to the reversible crosslinks, formed by TA, between gelatin chains. The benefit of using a galvanic cell configuration is the possibility to sense constant loadings which cannot be measured by piezoelectric and triboelectric sensors.

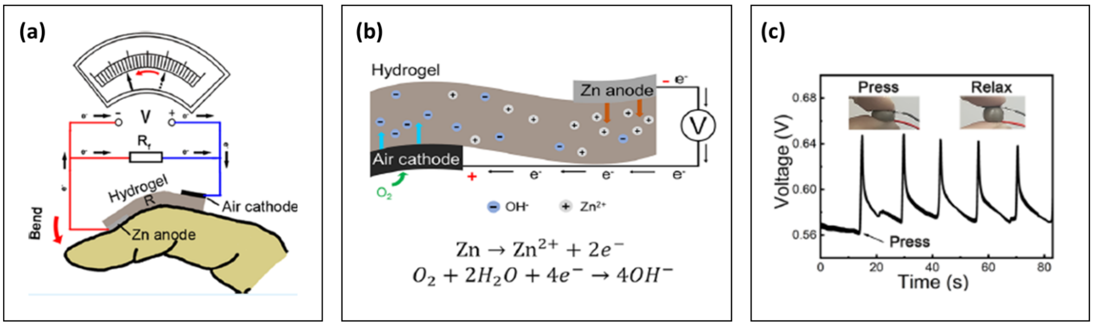

Figure 2.33: Example of self powered sensor based on galvanic cell [82]: (a) Configuration of galvanic cell sensor applied on a finger bended (b) Redox reactions that take place inside the galvanic cell (c) Voltage output resulting from several pressure cycles

Besides the advantages given by the absence of external batteries, self-powered sensors may be encapsulated through elastomeric materials for reducing hydrogel water evaporation. Moreover, signals conditioning electronic is usually more elaborate than that used in other sensors. Almost all these device can be used in a dual way, as sensors and as nano-generators for harvesting mechanical energy developed by the human body, finally.

2.4 Applications of tactile sensors

Number of smart sensor applications is unimaginable. They find use in a wide variety of fields, such as biomedical one, industry, domotics, military field, entertainment (gaming) and safety. In a world in which connectivity, digitalization and big data are becoming increasingly important, smart sensors play a major role: they enable the acquisition of raw data and signals that may be converted in meaningful informations. The advantages are multiple: for instance in medical field, remote sensing of vital parameters of a patient could avoid the need for physician's visits, and hence healthcare costs diminish. For a video game player, the use of tactile sensors in a gesture-based interface could make the game more immersive and realistic [83]. As another example, systems for identifying fatigue are common accessories for ensuring safety in vehicles: they could be also based on wearable sensors. These examples show how, in the new millennium, smart sensors surround us both in every day life and in specific applications and their market is consequently in continuous ferment. Biomedical sector is one of the field which has benefited most from the evolution of tactile sensors. The recent progress on robotics and artificial intelligence actually requires soft devices so that humans can interface safely and friendly with machines [84]. Some

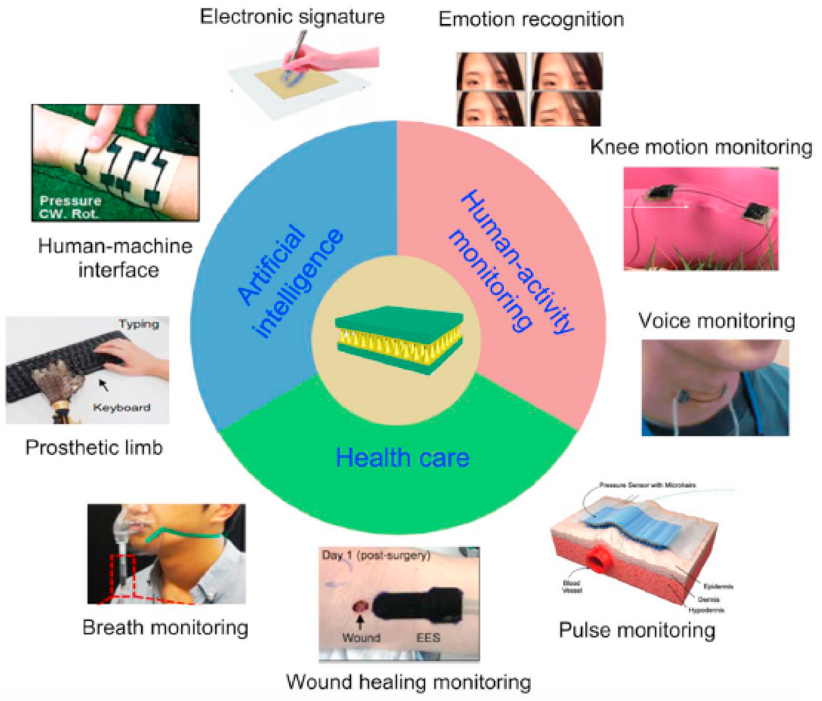

Figure 2.34: Examples of smart sensor applications [84]

possible applications in biomedical field shown in figure 2.34, include health-monitoring, sof-robotics and prosthetics. In the following sections some of them are analysed in more detail.

2.4.1 E-skin and soft robotics

The human skin is the biggest sensory unit of our body which allow us to interface with the external world through a very complex system of different sensors. In recent year, numerous efforts to mimic its outstanding features have been made, leading to the birth of the term "electronic-skin" (e-skin). The idea is to succeed in collecting data from outside, which can be elaborated through artificial intelligence methods in order to provide feedback informations, like the mechanoreceptors-brain system does (Figure 2.35) [22]. Flexibility, stimuli responsiveness, multi-sensing ability, self-healing are some of the properties that an artificial skin should have for getting closer to the organic one. Therefore, smart sensors based on hydrogels could represent an optimal solution for this purpose. Moreover adhesiveness could be an important attribute for attacking the e-skin to prosthesis and robots. Transparency is also necessary for having a finest aesthetic result and so a better social acceptance. Although the first goal is mimicking only human skin features, e-skin could be endowed with additional sensing capacities, such as gas recognition, chemical and biological sensors [85]. Electronic-skin represents the optimal tool for human-machine interfaces (HMI), due to its connectivity and its mechanical compliance with soft tissues. As example, a prosthesis endows the amputee, which wears it, functionality, but it is unable to replace haptic sensation, because the afferent neural pathway is interrupted. Therefore, it is difficult to understand the forces applied to the objects handled [86]. Hence, e-skin could provide the amputee with informations about contact pressure, allowing him to distinguish object textures and materials. Kim's group designed a multifunctional artificial skin able to sense pressure, strain and temperature stimuli. Stretchable and flexible polydimethylsiloxane was employed as substrate for building a layered structure in which each sheet

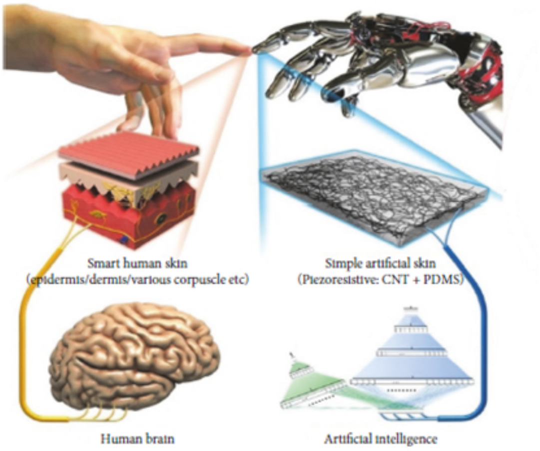

Figure 2.35: Electronic and organic skin by comparison [22]

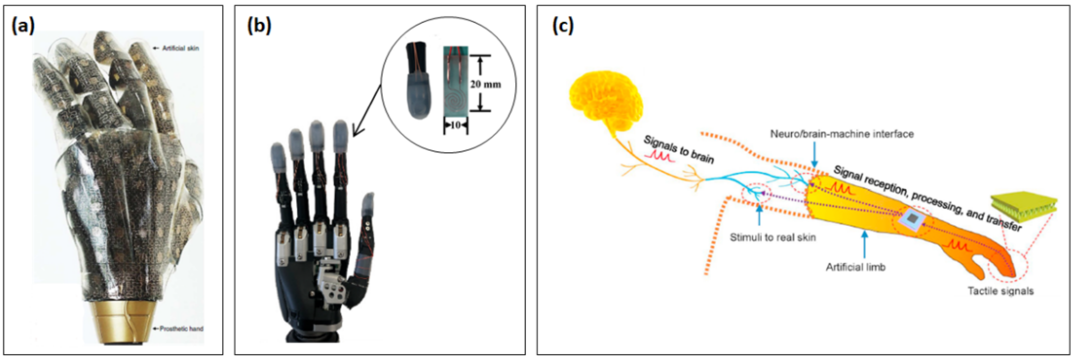

Figure 2.36: E-skin applied on prosthesis: (a) Multifunctional PDMS based e-skin applied on a prosthetic hand [87] (b) Liquid metal based tactile sensors applied on the i-limb prosthesis [88] (c) Ideal feedback loop for a prosthetic hand [84]

corresponded to a specific sensor (Figure 2.36a). In addition, integration of humidity sensors, electrodes and heaters was possible for ensuring multi-sensing and actuation abilities [87]. Instead Abd et al. created a liquid metal sensor applicable on the fingers of the prosthetic hand i-Limb (Figure 2.36b). The substrate with hollow canals of different geometries was realized with the elastomer Dragon-skin 30; then liquid metal was inserted through syringe and the sensor was applied on the distal phalanges of the prosthesis. This device was able to recognize different speed of sliding and various textures thanks to a neural network classification algorithm [88]. Therefore, tactile sensors are essential for endowing prosthesis with sensitive ability and thus allowing more subtle and precise movements. In future, haptic informations should be ideally transferred to the brain via brain-machine interface in order to have a feedback loop (Figure 2.36c).

Today, also robotics is going towards mimicking living organisms: flexible robots have gaining more importance due to their improved ability to adapt to the surrounding working environment and thanks to the better safety which they have when are in contact with humans. This field, called "soft-robotics" involves collaborative robots, surgical assistance robots and exoskeleton for patients rehabilitations. In these cases, the need to use flexible and stretchable materials leads to the applications of soft sensors. A soft robot enables lower inertia and few kinematics limitations and thus is an optimal solutions for both rehabilitation and assistance of those patients that underwent to strokes, neurological disorders and musculoskeletal injuries. Traditional rigid exoskeletons actually do not align their centres of rotation with that of the human joints because of the difficulty of their detection without in-vivo imaging techniques [89]. This results in improved loads on the limbs and joints. Using completely soft exoskeleton, called exosuits, is a possible solution: hence, smart flexible sensors are necessary for tracking the forces and displacements applied for driving actuators placed in these devices.

2.4.2 Health monitoring and human motion detection

As early as the first spatial trips, the need to monitor health of the crew in a remote manner arose: electrocardiogram, heartbeat, body temperature and quality of expired air were already measured through wearable sensors during the NASA missions in the '60. These sensors had to continuously monitor the health conditions of the astronauts, providing informations in quasi real-time to the medical staff. In addition, they had to be comfortable enough for being worn throughout the entire duration of the trip, without limiting movements [90]. Today, with the advent of telemedicine, smart wearable sensors have became very widespread. The possibility to continuously and remotely monitor health is essential for critically ill patients and, in any case, allows the reduction of waiting times of medical visits and hospitalization costs. The four human main vital signs are body temperature, heart rate, blood pressure and breath rate. In addition, oxygen saturation in blood could be also interesting. If they are monitored and data are sended to the physician, it is possible to detect pathologic conditions or to check the efficiency of a rehabilitation treatment and eventually modify it (Figure 2.37) [5]. Therefore, non-invasive sensors with an appropriate sensitivity, durability and compliance with human skin must be employed for having quality data. Comfort and aesthetic aspect are others two features to take into account, because these sensors have to be worn for long periods.

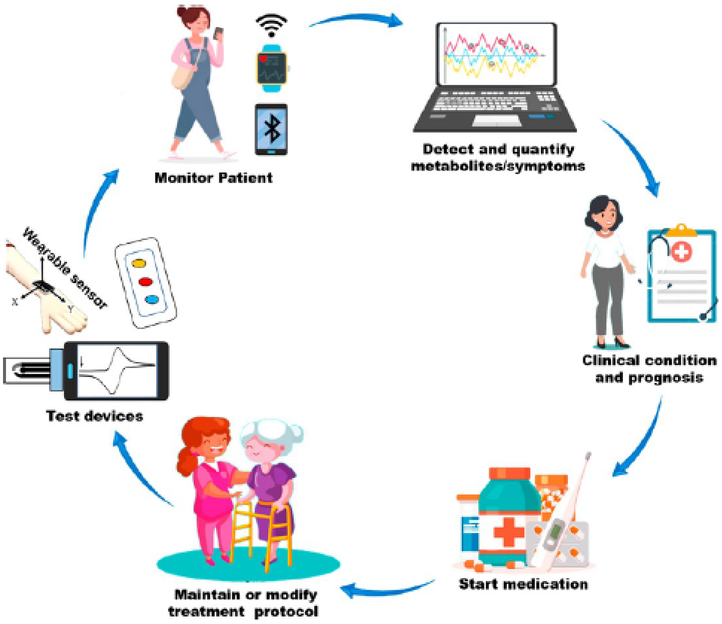

Figure 2.37: Wearable sensors workflow for health monitoring [91]

Liu et al. proposed a piezoresistance strain/pressure sensor based on a double-network hydrogel. The soft network was made of poly(vynil alcohol) (PVA) and poly(vynil pyrrolidone) (PVP), while the hard one was constituted by cellulose nanocrystal (CNCs) crosslinked by ferric ion (Fe^{3+}). The so called "F-hydrogel" was then encapsulated through transparent VHB tape and conductive wires were added. The sensor showed high stretchability (0-200%), high gauge factor (0.478) and low hysteresis. It could be used for subtle deformations: breath rate was detected attaching the sensor to the lower rib cage allowing the distinction among rapid or regular breathing or breath holding. In addition, the sensor was

attached to the wrist and pulse rate was measured before and after a running of sixty second; the heart beats augmented after the exercise and thus electrical resistance increased due to the greater deformation (Figure 2.38a). It was possible to find the number of beats per minute, counting the peaks of relative resitance signal in sixty second.
The electronic conductive hydrogel composed of polyacrylamide/chitosan hybrid network doped with multi-wall carbon nanotubes (PAAm/CS-c-MWCNTs) prepared by Xia et al. demonstrated a good sensitivity, especially for small deformation (GF of 1.65), fast response and excellent reproducibility. It was able even to sense vocal cords vibrations: actually the sensor was applied on the throat of a subject which was speaking different words. The figure 2.38b shows how the piezoresistance based sensor output was repeatable when the subject laughed or said the word "telephone", demonstrating its applicability for voice monitoring.

The two examples above reported sensors able to sense both small strain and large deformations. This also enables the human motion detection, which is an important attribute in different fields of biomedicine. In sports medicine, for instance, monitoring of athletes performances during training is crucial for planning specific exercises to boost their abilities and understand their physical condition . In addition, wearables sensors could inform the coach whether an exercise is done well or not, avoiding injuries to the players [93]. Biomechanical analysis are usually performed by expensive and complex optical tracking methods. As a cheaper alternative, electro-goniometer or inertial sensors could be used. However, they often limit the movements due to their encumbrance and weight. Hence, low-invasive and lightweight wearable sensors represent an optimal solution to monitor joint motion during physical activities.

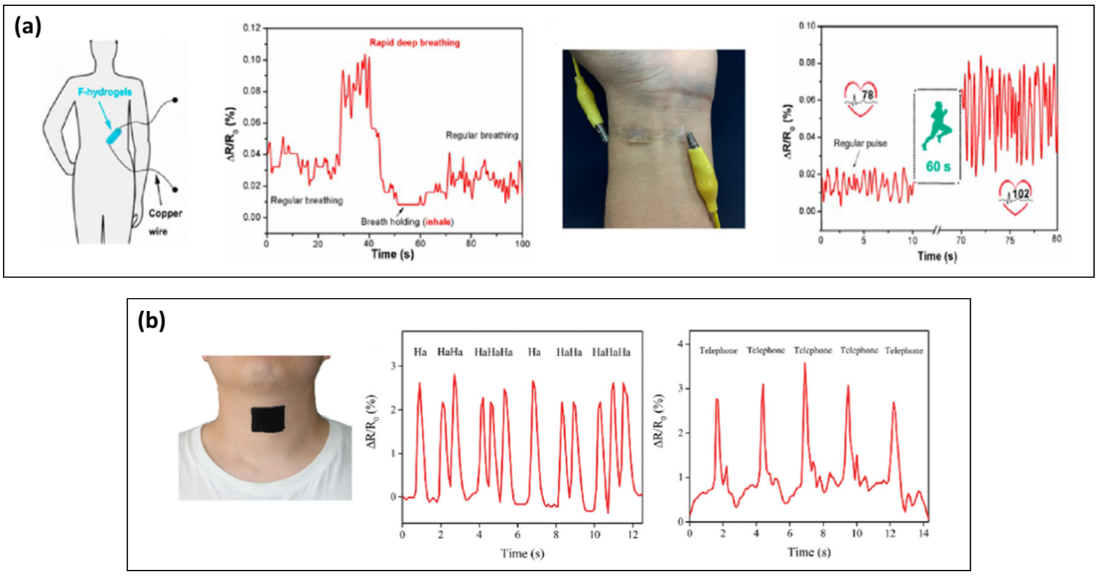

Figure 2.38: Smart sensors applications in health monitoring: (a) F-hydrogel smart sensor applied in breath rate monitoring (on the left) and heart rate detection before and after a running (on the right) [92] (c) PAAm/CS-c-MWCNTs hybrid hydrogel sensor applied for voice monitoring [6]

Similarly, human motion monitoring is fundamental in rehabilitation. Neuromuscular and cardiac diseases, like spinal cord or peripheral nerves injuries, cerebro-vascular accidents, multiple sclerosis and strokes, imply a partial or total paralysis of certain areas of the human body, due to the damage of the nervous efferent and afferent systems or to the lack of oxygen supply. Assessing the severity of the pathology and evaluating its exacerbation or remission are fundamental to actively follow the patients, especially those affected by progressive diseases. In this way the treatment could be personalized for each subject, improving their quality of life. Therefore, a continuous and minimally invasive monitoring is necessary for evaluating the range of motions of joints. Gait analysis, which involves ankle, knee and pelvis joints study, and upper limbs motion evaluations (concerning elbow, wrist and phalanges) are the most common test performed.
The same PAAm/CS-c-MWCNTs hydrogel sensor presented before, was applied to detect the bending of a finger, showing an higher electrical resistance when the angle of bending increased. Moreover, the output was repeatable for an angle of 90° as is shown in the inset in figure 2.39b. Knee, elbow and wrist bending and release were also measured, obtaining excellent results (Figure 2.39a and 2.39b). Therefore, sensors that own a large working range, with a good sensitivity, robustness, lightweight, durability and low invasiveness are suitable for wearables. For a large scale production, low cost materials usage and simple construction methods are also desirable. Moreover, an efficient signal elaboration stage,

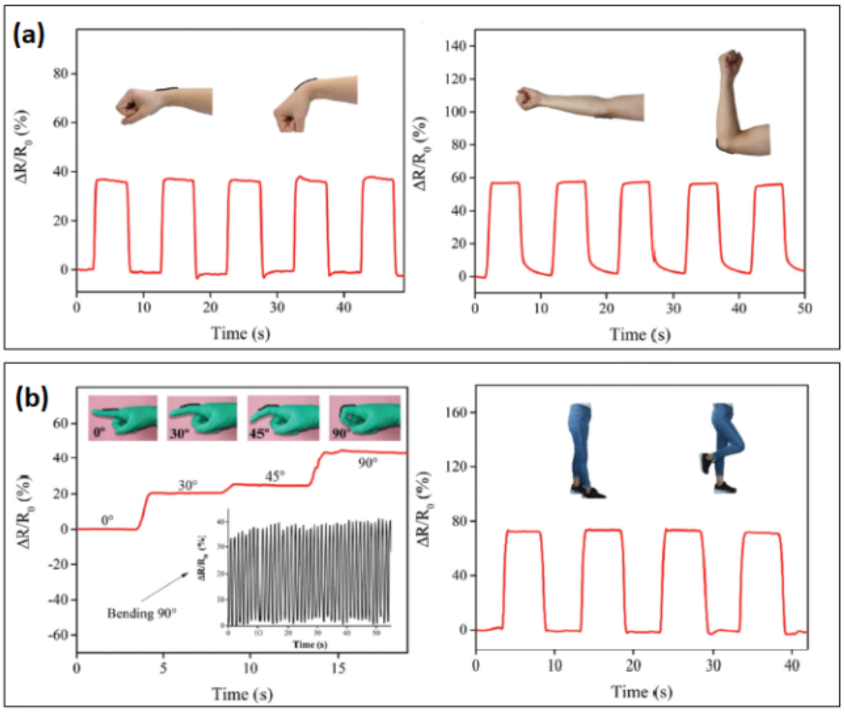

Figure 2.39: Smart sensor applications in human motion detection [6]: (a) Wrist bending (on the left) and elbow bending (on the right) (b) Finger bending (on the left) and knee bending (on the right)

which is little prone to motion artefact and electrical noise, is necessary for obtaining high quality data, which could be more easily analysed by physicians.

2.4.3 Robotic minimally invasive surgery

Robots are becoming interesting tools in surgery. They may assist surgeons providing informations about the patient in real-time through 3D rendering and ensuring a better precision. Physiological tremors of the surgeons hands are actually avoided. A less invasiveness is achieved, resulting in little blood loss and thus a better final aesthetic result, shorter recovery period and lower risk of post-operative infections [4]. Traditional robot assistance systems, like da Vinci one (Intuitive Surgical, US), are controlled directly by the surgeons, in a master-slave mode: the operator utilizes manipulators and pedals placed in the console and the system reproduce its movements through robotic arms. Each arm is endowed with surgical instruments, and one of them keeps a camera which provide a 3D view of the operating area in the monitor module. The console, robotic arms and vision cart of da Vinci robot are shown in figure 2.40. These robots are mainly employed in minimally invasive surgery (MIS), such as prostatectomy, thoracic and abdominal surgeries. The disadvantages include the cost of the robots, the long lasting surgeons training and the lack of haptic perception. The latter aspect could represent an important challenge to overcome: the touch together with the view are the two principal senses applied for handling objects [95]. Without a tactile feedback, surgeons are not able to understand the force applied to the tissues by the end-effector of the surgical robot, leading to errors and safety problems. Therefore, smart sensors could constitute a way to solve this issue. Tactile informations could be presented to the surgeons through visual or auditory devices or tactile displays based on pneumatic, shape-memory alloy or piezoelectric systems. The latter are more intuitive obviously.

Figure 2.40: Da Vinci surgical system [94] : on the right the four robotic arms module; in the middle the console cart; on the right the vision cart

King's group presented the first tactile feedback system applied on da Vinci robot. It consisted in a piezoresistive sensor mounted on the end-effector robotic arms (Figure 2.41a); informations were transferred to a control system which elaborated them and drove a pneumatic tactile display. This latter system was made of several polydimethylsiloxane balloons in which compressed air was inflated: they were placed on the fingers of the user, through a velcro strap (Figure 2.41b). Hence, the pressure stimulus applied to the user finger through the balloons was related to the force sensed by the sensor mounted onto the robotic arm [96]. In literature several others works that deal with tactile sensors applied on robotic minimally invasive surgery (RMIS) can be found. Besides the traditional piezoresistive or piezocapacitive sensors, other transduction mechanisms could be exploited, such as Hall effect [97]. However, the ultimate goal is the same: reproducing the tactile sensation in robots in order to improve surgeons' performance and thus the results of surgical interventions.

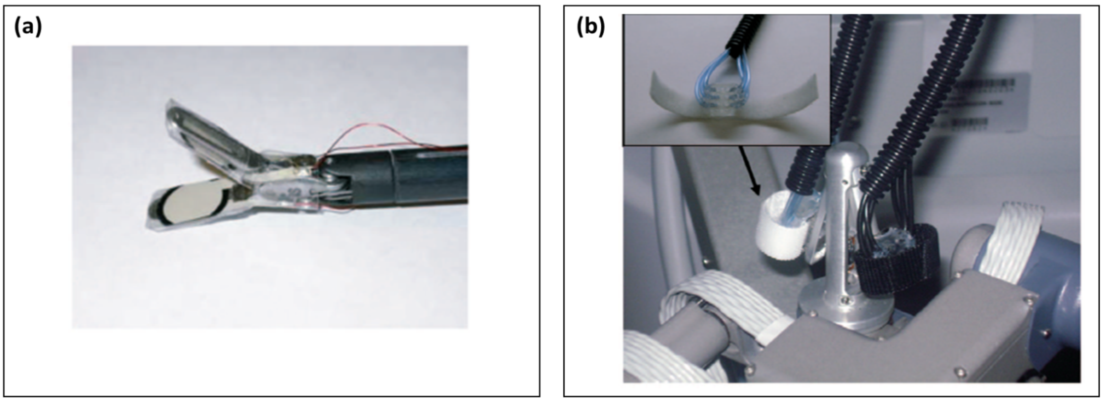

Figure 2.41: Tactile feedback system applied on da Vinci robot [96]: (a) Flexible pressure sensor mounted on Cadiere graspers (b) Pneumatic display applied to the console (in the inset, the ballon tactile display with velcro strap)

Chapter 3

Materials and methods

3.1 Device manufacturing

In this work the production and the characterization of a sandwich-like sensor based on hydrogels, which exploits ionic conduction, are investigated. The structure is presented in figure 3.1. The hydrogel constitutes the inner layer of the sandwich and carries out the role of sensitive part thanks to ions present in the precursor solution. Therefore, the hydrogel is also called "ionogel". Herein, a carboxymethylcellulose water solution with sodium chloride (NaCl) was used to prepare the ionogel. Since hydrogel network is brittle and weak, the encapsulation layers shall ensure flexibility, protection from external stress and prevention of water evaporation. In addition, transparency and adhesiveness are useful properties for biomedical applications: the former could make the sensors more aesthetic for daily usages, the latter allows a better integration with the human body as was previously explained. In literature, several materials have been examinated, but there is no work that deals with the influence of different encapsulations on sensor production and performances. Hence, the shells of a flexible sensor with the same sandwich configuration and the same sensitive inner layer, were prepared through the following materials:

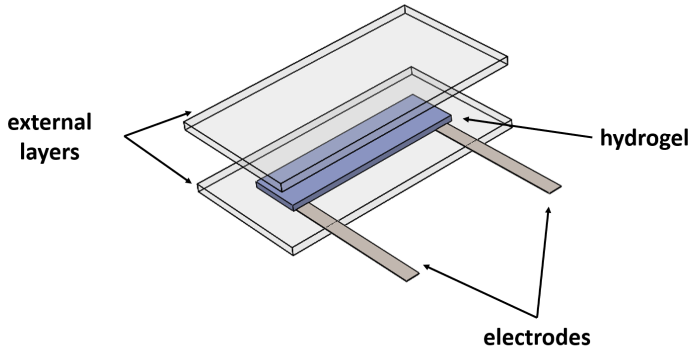

Figure 3.1: Sandwich-like sensor structure

- polydimethylsiloxane (PDMS), a transparent and biocompatible elastomer;
- TEGO®rad 2800, a 3D printable silicone;
- VHB tape, a bi-adhesive, transparent tape;

Each of them presents some advantages and disadvantages which will be discussed later. A pair of flat electrodes were added during the sandwich assembly, for sensing the variation of electrical properties. And, even in this case, different materials (stainless steel, titanium, copper-Kapton. copper-Kapton-copper) were investigated to find the most sensitive setup.

3.1.1 Carboxymethylcellulose ionogel preparation

Cellulose is one of the most available organic polymer. It is a polysaccharide composed by several hundreds of cellobiose units (figure 3.2). Cellobiose derives from the condensation of two molecules of D-glucose: a chemical bond between the carbon atoms located in position 1 and 4 in the glucose molecules is formed through the bridging oxygen atom. Hence, this linkage is called β-1-4-O-glycosidic bond. Cellulose structure is composed of crystalline domains, in which hydroxyl groups of glucose form hydrogen bonds among them, and amorphous regions (figure 3.2). The higher the percentage of crystalline areas respect of the whole polymer, the greater are mechanical resistance and hydrophobicity. The interest in cellulose is high thanks to its biocompatibility, availability, low cost, biodegradability and renewability [98]. Cellulose mainly derives from plants, by which cellulose nanofibers (CNF) are obtained through different mechanical and chemical processes. Cellulose with high purity and cristallinity can be also produced by bacteria. Nevertheless, this bottom-up approach is still difficultly applicable on large scale, due to the high cost of materials

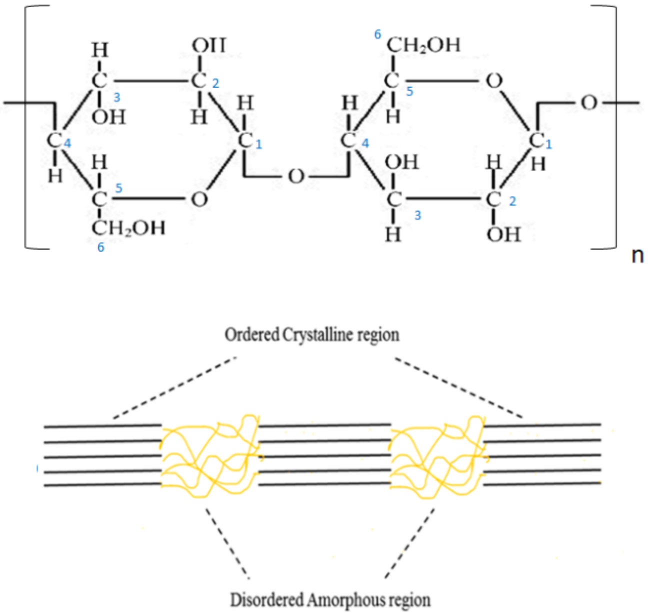

Figure 3.2: Upward the chemical formula of cellobiose; downward the structure of cellulose

[100].
Cellulose mechanical and chemical properties can be easily tuned through the modification of the hydroxyl groups present on its carbon backbone. Esterification and etherification are two common processes for obtaining cellulose derivates with different features. Water solubility is crucial to produce an hydrogel: hence, carboxymethyl cellulose (CMC) represent an optimal candidate for this purpose. In CMC most of hydroxyl groups are substituted by polar carboxymethyl groups (-CH_2-COOH), which make it water soluble (figure 3.3a). The degree of substitution determines its properties. Pure CMC can give physically crosslinked hydrogels in the presence of coordinating ions or at low pH. As an alternative, aiming to obtain a more stable chemically crosslinked hydrogels, CMC can be further modified trough a methacrylation process [101]. The synthesis of methacrylated CMC (M-CMC, figure 3.3b) open the possibility to chemically crosslink the CMC chains exploiting the photopolymerization reaction.

Photopolymerization is a common and environmentally friendly process used for curing liquid monomers thanks to light of various wavelength. A photocurable solution need monomers and a photoinitiator (PI) that, upon irradiation, generates the reactive species that starts the polymerization. Photopolymerization processes are usually separated into radical and ionic ones: in the former the reactants are radicals, in the latter they are anions or cations. The compounds which contain acrylic/vinyl group are the most used for radical photopolymerization: in fact, the double bond undergoes to rupture, when it is attached by another radical, allowing the generation of macro-radicals. M-CMC can then be crosslinked exploiting a radical reaction; bismesitoylphosphinic acid (BAPO-OH) can be used as a water soluble photoinitiator. It derives from phenylbis(2,4,6-trimethylbenzoyl)phosphine

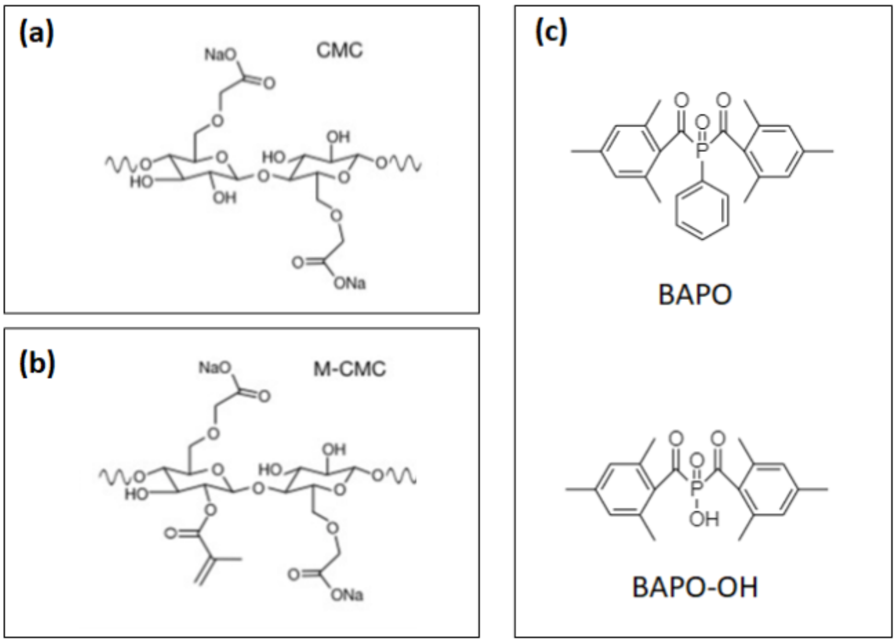

Figure 3.3: (a) CMC (b) M-CMC (c) BAPO and BAPO-OH

oxide (BAPO), a common photoinitiator reactive to UV/visible light. BAPO was functionalized with an hydroxyl group to make it more soluble in water solutions and thus BAPO-OH was synthesized [102]. The differences between BAPO and BAPO-OH are shown in figure 3.3c. The photoinitiator, when is exposed to the UV light, forms the initial radicals. They react with a M-CMC monomer. Then the reaction continues with the involvement of others monomers: this is the phase called "propagation". Finally, the polymerization ends when two macro-radicals join together or for disproportion and consequently radicals inactivation. Therefore, photopolymerization allows fast reactions that take place at room temperature, with a reducing of costs due to the non-use of heat and the less time spent. It is a versatile procedure that could be applied to various materials, if the correct photoinitiator is chosen.

In this research, the common sodium chloride (NaCl) was embedded into the M-CMC hydrogel for endowing it with ionic conductivity. First of all, NaCl was dissolved in distilled water, which was used as solvent. Then, M-CMC was added to the solution and it was magnetically stirred at a temperature of 40°C until an homogeneous blend was obtained. BAPO-OH was finally inserted at a concentration of 2wt% with respect to M-CMC and the solution was left to mix for few more minutes at room temperature. Different salt concentrations and cellulose molarities were investigated. The table 3.1 summarizes the compositions of hydrogels used in subsequent steps. Each solution thus obtained was sonicated for 10 minutes to remove bubbles deriving from stirring. At last, each precursor blend was exposed to UV light (HAMAMATSU, LC8 UV lamp) for 5 minutes at 20 mW/cm^2 for photopolymerization. In this way M-CMC hydrogels, called "ionogels" due to the ionic conductivity given by NaCl, were achieved. Moreover, an additional solution with 4 wt% of carboxymethylcellulose (CMC) with respect to distilled water and 1 mol/L of salt was prepared and it was not exposed to UV light since it do not manage to react due to the absence of methacrylic groups. In the following steps, this last one solution is named "4% not cured" (4%_NC).

Name	**M-CMC [wt%]***	**NaCl [mol/L]**
2%_05	2	0.5
2%	2	1
2%_15	2	1.5
3%	3	1
4%	4	1

Table 3.1: Compositions of hydrogels prepared (* wt% with respect to distilled water)

3.1.2 Polydimethylsiloxane sensors

Polydimethylsiloxane (PDMS) is a material widely used in the field of sensors, due to its mechanical properties and its dielectric nature. It can act as both encapsulation and triboelectric layer [78], indeed. The PDMS (its chemical formula showed in figure 3.4a) is a transparent, biocompatible, heat resistant and hydrophobic silicon elastomer. These properties make it suitable for applications in various fields, like in biomedicine, cosmetic, micro-electronic and industry. Different shapes could be easily obtained through moulding: it is actually able to conform to nanometric details. In this research the thermopolymerizable polydimethylsiloxane Sylgard@184 (Dow Corning Corporation) was employed. It is supplied as a two-parts component kit (3.4b), the viscous precursor and the liquid curing agent, which need to be blended at a mass ratio of 10:1. Its curing process is controlled varying the temperature. For creating the encapsulations, the solution of precursor and curing agent was poured in a rectangular plastic mold, once the air bubbles, incorporated during mixing, were removed through the immersion in a ultrasonicator bath (Sonorex Digiplus, Bandelin) for 10 minutes. crosslinking of PDMS took about 24 hours at room temperature: in this case the mold with the solution was inserted into the oven (Memmert) at 80°C, to accelerate the curing process. After one hour, the PDMS became solid with a rubber-like appearance; it was easily removed from the mold and then cut into desired shapes. In this manner two rectangular layers about 0.5 mm thick are obtained. Following this, electrodes were placed on the PDMS sheet and 125 mg of cellulose solution was poured above them (on a rectangular place of 2.5x1 cm^2). Then it was photo-polymerized as explained before in section 3.1.1. The sandwich is closed with another sheet of PDMS, using always PDMS not cured as "glue". The PDMS was left curing at room temperature for 24 hours. It was not put into the oven because the high temperature would have enhanced hydrogel water evaporation. The entire production process is shown in figure 3.5. The final product was a stretchable and transparent sensor. Moreover PDMS proved to be slightly adhesive to the skin in its early applications; however, after some time, it was not sticky any more, due to the dust collected on its surface. The main drawback of this production method was the presence of bubbles inside the sandwich. During the closing of the sensor with the other PDMS shell, air in fact remained entrapped between the cellulose hydrogel and the PDMS encapsulations. This could result in unstable electrical properties.

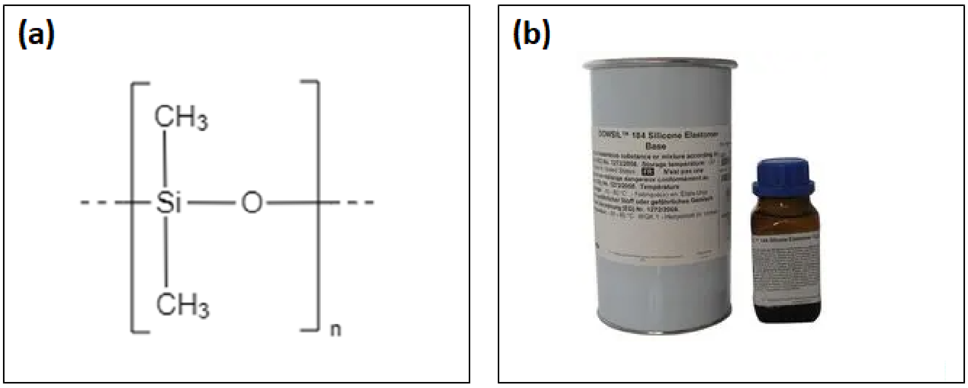

Figure 3.4: (a) PDMS repetitive unit formula (b) Two component kit of monomer and curing agent (Sylgard@184)

3.1.3 TEGO®rad sensors

The main problem of the previous encapsulation was the time that PDMS employs to cure: since the PDMS used as "glue" to close the sandwich became totally cured in 24 hours at

room temperature, the hydrogel water evaporated during this time. Hence, durability of sensors was dramatically reduced. Moreover the difficulty of sandwich closure due to the incorporation of air bubbles, resulted in electrical properties un-stable at static conditions. Therefore, reproducibility of sensors was not achieved.
TEGORAD 2800 (TRAD), an silicon-acrylate oligomer provided by Evonik Industries AG (Essen, Germany), was employed in order to overcome the previous issues. It is a PDMS-like elastomer photopolymerizable, through a radical reaction, thanks to the acrylate groups. Also in this case, BAPO (described in section 3.1.1) was exploited as photoinitiator for the formation of the first reactive species under the exposition to UV light. Nevertheless it is not soluble in TRAD. Hence, it was easily dissolved in Darokour, a liquid UV photoinitiator, under magnetic stirring. The weight ratio between BAPO and Darokour was set equal to 1:4 to obtain an homogeneous blend of photoinitiators. Then, three different solution of TRAD were prepared varying the concentration of the PI solution in order to investigate how mechanical properties, reactivity to UV light and external appearance changed. As regards the exterior aspect, it was possible to see that transparency diminished when an higher concentration of PI blend was used (figure 3.6a).Therefore, for the following steps, the TRAD solution with 0.8wt% of blend of photoinitiators was used. The BAPO and Darokour blend was added to TRAD and the mixture was magnetically stirred; the container was covered with a aluminum foil to avoid the ingress of light which could initiate the photopolymerization. Thus, a yellowish solution was obtained. As a first approach, it was poured into a rectangular plastic mold; after that the solution was covered by a thin glass to avoid radical scavenging due to the direct air oxygen contact (figure 3.6b), and was exposed to the UV light (25 mW/cm^2 for 10 minutes). Oxygen inhibition is, in fact, a problem when photopolymerization takes place in air: oxygen quenches photoinitiators or it bonds with radical on the surfaces, forming non reactive peroxides (radical scavenging) [104]. This effects lead to incomplete photopolymerization and thus

Name	**blend of PI [wt%]***
TEGO08	0.8
TEGO15	1.5
TEGO2	2

Table 3.2: Compositions of TRAD solution investigated (* wt% with respect to TRAD)

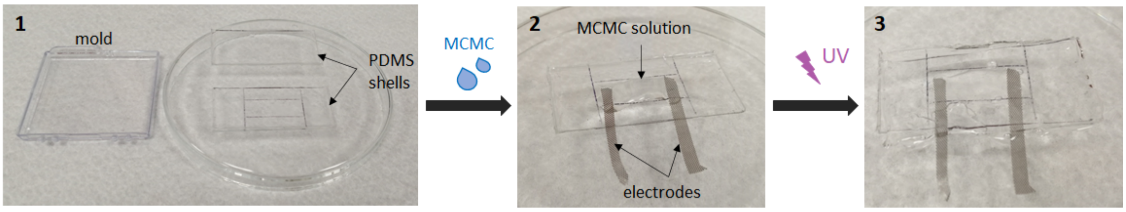

Figure 3.5: PDMS sensors production: (1) The mold in which PDMS precursor is poured and the two shells of cured PDMS (2) Electrodes positioning and M-CMC solution pouring (3) Sandwich closure after photo-polymerization of M-CMC solution

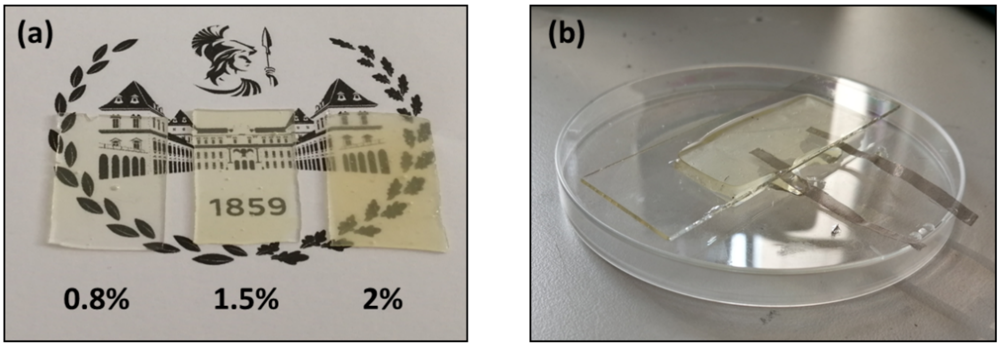

Figure 3.6: TRAD solutions: (a) Transparency of TRAD samples with different concentration of PI blend (b) Positioning of thin laboratory glass for avoiding contact with atmospheric oxygen

the sample surfaces remain sticky with possible toxic monomers not reacted.
After the curing, rectangular TRAD shells (0.5 mm thick) were realized through a cutter. Then, electrodes were placed on them and 125 mg of M-CMC solution was poured on a 2.5x1 cm^2 place and it was cured for 5 minutes at 20 mW/cm^2. The procedure is the same of PDMS sensor building (section 3.1.2). As the last step, a thin layer of TRAD solution was poured on the M-CMC hydrogel and, after covering the sensor with glass to prevent radical scavenging, it was cured under UV light for 5 minutes at 25 mW/cm^2. This method ensures an optimal enclosure of the cellulose because the viscous TRAD solution spreads on the sandwich sensor without the entrapment of air bubbles; moreover, the faster production time guarantees a minor hydrogel water evaporation.

In recent years, 3D printing is gaining more interest due to its attractive features, such as low material waste, high precision, repeatability and reduction of production costs. Among the 3D-printing technologies, Digital Light Processing (DLP) is one of the most employed

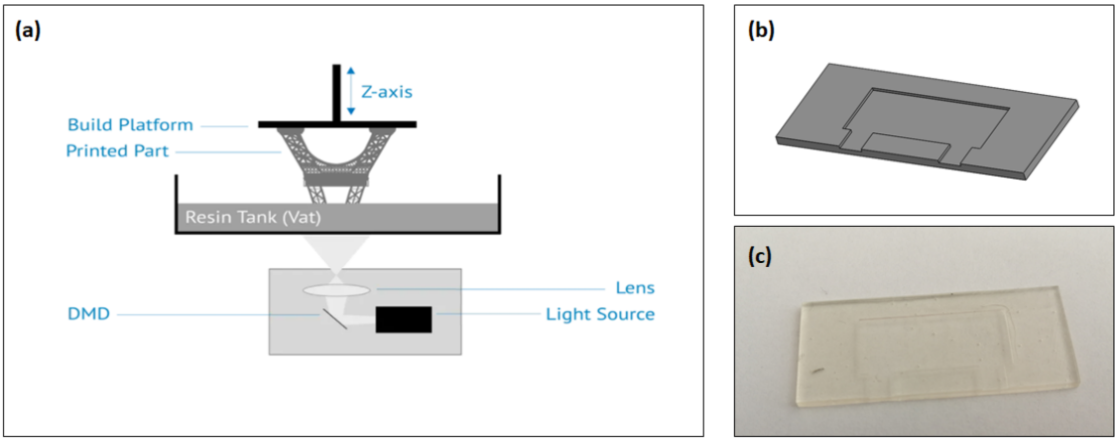

Figure 3.7: Digital light processing printer: (a) Working scheme (b) CAD model of shell (c) Printed TRAD encapsulation

due to its precision and versatility. This technique is applicable when it is necessary to use photopolymerizable resins. DLP consists in a transparent vat, in which the liquid resin is inserted, and a build platform connected to a stepper motor, which moves vertically. The light source which performs the photopolymerization is placed under the vat; the light is properly deflected by a matrix of digital micro-mirrors devices (DMDs), the orientation of which is numerically controlled. DLP works layer by layer: after the irradiation of a certain layer, the stepper motor moves up and the following layer is hit by the light. Hence, the object is built from bottom [105]. The 3D model of the product is created through common Computer-Aided-Design (CAD) software; then it is sliced for obtaining 2D layers with software provided by the printer's manufacturer or by third party. For each step, DMDs are oriented for creating the mask corresponding to the slice considered, and light source is activated [106].
Printability of silicones acrylates has been received interest and was already analysed because of polydimethylsiloxanes application in electronic and microfluidic devices, in which an high precision is required [107] [108]. Therefore, DLP printing is suitable also for sensors encapsulations made of TRAD. This alternative approach was consequently exploited. The DLP printer UV Max (Asiga, Australia) was employed because it operated with a UV light source. Before the insertion in the printer vat, the TRAD and PI solution was heated through the hotplate at 50 °C, for reducing its viscosity and thus facilitating its printing. As concerns the printer parameters, the burn-in layers, namely the initial ones, varied from 0 to 0.250 mm and were exposed for 4.5 s to a UV-light intensity of 49.53 mW/cm^2. The other layers were subjected to the same light intensity for 2.5 s. The separation velocity between two consequent layers was set to 1 mm/s. The heater temperature of the printer

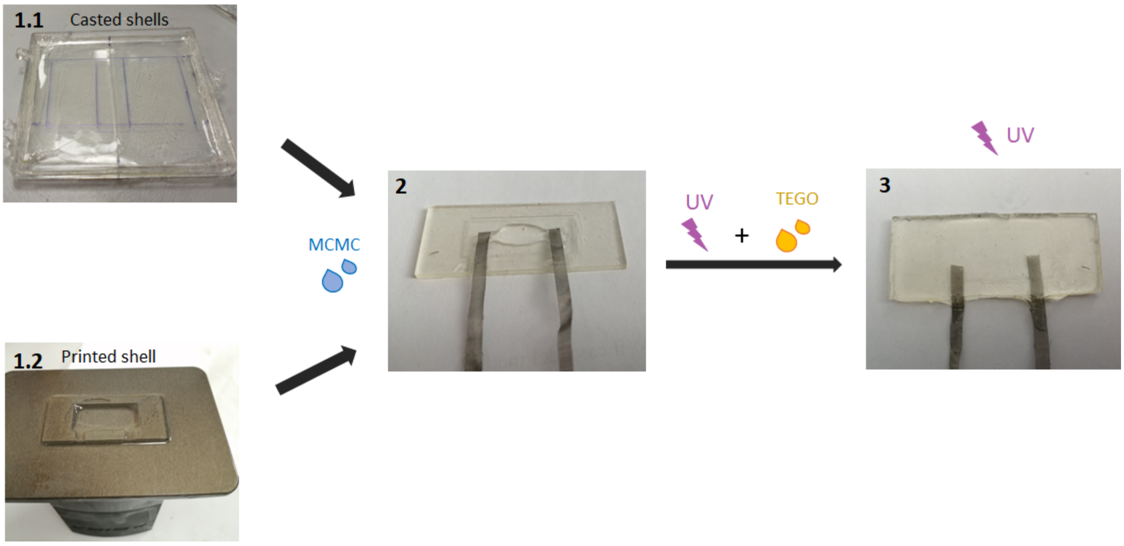

Figure 3.8: TRAD sensor production: (1.1) Shell obtained from casting of TRAD solution into mold (1.2) Shell printed with UV Max DLP printer (2) Electrodes positioning and M-CMC solution pouring (3) TRAD solution pouring and photopolymerizing to close the sandwich, after M-CMC curing

was set to 50 °C for the entire process and slice thickness was 0.050 mm. After the printing, the build platform was removed and the encapsulation was cleaned with ethanol to remove non-reacted monomers. TRAD encapsulation is shown in figure 3.7c: the model, created on Solidworks (Dassault Systemes), consisted in a rectangular shell 1.5 mm thick, with a cavity of dimensions 2.5x1x0.05 cm^3 in which the M-CMC was poured. Two tiny corridors were also generated for placing the electrodes (figure 3.7b). The following steps are the same presented in the first approach. Both the procedures and the final products are outlined in figure 3.8.

TRAD encapsulations overcome the issues concerning the production time and air bubbles of the PDMS shells and, especially for printed shells, allows an higher repeatability in the manufacturing of sensors. However, TRAD owns lower mechanical properties compared to PDMS: sensors thus built result little stretchable. Hence, they could be more suitable for sensing of bending and pressure stimuli. Moreover, investigations about skin compatibility need to be made.

3.1.4 VHB tape sensors

Several studies in literature use commercial tapes instead of PDMS to encapsulate hydrogels, for preventing water evaporation and to endow them with optimal mechanical properties. Transparent and durable materials are preferable for the reasons mentioned earlier. Very High Bond (VHB) tapes of the 3M company are a series of high-performance bi-adhesive products which are widely used as flexible dielectrics and/or substrates in soft-electronics and wearable application [28] [78]. In this work the model 4905 is employed, due to its transparency and its thickness of 0.5 mm. It is an acrylic tape with a pronounced non linear viscoelastic behaviour and a very high stretchability. Its properties are highly dependent on temperature: when it increases, VHB polymer becomes more soft, diminishing its hysteresis and its residual strain in stretching tests [109]. Therefore the tape, actually, reacquires its original dimensions not instantly after deformation.

Sandwich-like sensors could be easily prepared overlapping three rectangular layers of VHB tape. In the intermediate sheet a rectangular hole of 2.5x1 cm^2 was cut through the cutter. Then the backside protection film was removed and the intermediate layer was stuck on the outer layer and was pressed for ensuring an optimal adhesion. The M-CMC solution (125 mg) was poured in the hole of the intermediate layer and electrodes were placed so that they were in contact with the conductive solution. The M-CMC was cured through UV light as before explained. Finally, the other external shell was used to close the sensor taking care to remove air bubbles through pressure. A protective film was left in a side of the sensor and the other side was covered with silicon oil to make it not adhesive. These expedients made the sensors simpler to handle for the next analyses. The manufacturing process is shown in figure 3.9.

These kind of sensors are the easiest and the fastest to built because there is no waiting time for PDMS or TRAD curing. Moreover, if the closure has been made carefully, air bubbles are avoided resulting in more repeatable sensors with stable electrical properties. For these reason, sandwich-like sensors made with VHB tape were employed to make the further electrical and electrochemical characterizations.

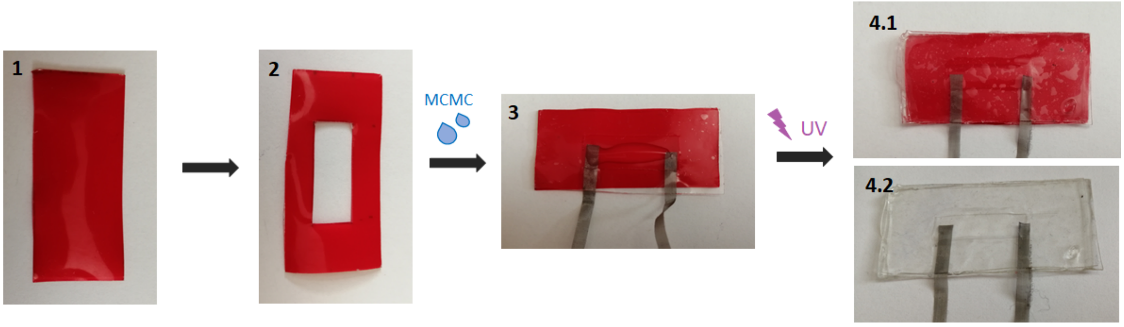

Figure 3.9: VHB sensor production: (1) Inferior shell (2) Intermediate layer (3) Electrodes positioning and M-CMC solution pouring (4.1) VHB superior layer positioning, after M-CMC curing; the sensor is with its protective film (4.1) The transparent VHB sensor without protective film

3.2 Sensor characterization

Sensors characterization is separated into M-CMC hydrogels and encapsulation analysis, electrochemical tests and electrical evaluations. M-CMC solution was thoroughly studied to demonstrate its reactivity while varying salt molarity and for investigating how the mechanical properties changed with increasing cellulose concentration. VHB, TRAD and PDMS have been compared with respect to mechanical properties and permeability to water vapour, to choose the best configuration for further applications. Moreover, the optimal solution of TRAD was chosen through the investigation of different concentration of photoinitiators blend (BAPO and Darokour). The electrodes material, that guarantees the best performances, was selected through electrochemical analyses. Finally, the whole sensor based on VHB tape, was analysed both in piezocapacitive and piezoresistive mode under stretching and bending stimuli. Finally, sensors were tried in some wearable applications after the best setup was found.

3.2.1 FTIR spectroscopy

Fourier transform infrared (FTIR) spectroscopy is a technique widely used for finding out the chemical composition of a certain mixture. It is based on the concept of interaction between energy delivered by IR radiation and chemical bonds. For any electromagnetic radiation its wavelength is inversely proportional to its frequency according to the following formula:

$$f = \frac{c}{\lambda} \tag{3.1}$$

where f is the frequency (Hz), c is the light speed in the vacuum ($c = 299792458\ m/s$) and λ is the wavelength, usually measured in cm. Radiation energy is directly proportional to its frequency through the Planck constant ($h = 6{,}2607015 \times 10^{-34}\ J \cdot s$):

$$E = \frac{hc}{\lambda} = hf \tag{3.2}$$

In literature, wave number is frequently used in the place of wavelength: it is the reciprocal of the wavelength and indicates the number of oscillation of the wave in the unit of length.

Its unit of measurement is m^{-1} or cm^{-1}.

The infrared (IR) radiation is comprised between the visible light and the microwaves; its bandwidth roughly includes the wavelengths between 750 nm and 1 mm. IR are partially adsorbed by molecules which, as a consequence, change the vibrational state of their chemical bonds. Therefore, each functional group interact with a certain frequency of IR radiation, absorbing its energy. Moreover, the whole molecule shows a precise "fingerprint" that depends on the combinations among vibrational states of all the chemical bonds that constitute it.

In the FTIR spectrophotometer, a IR beam originated by the light source, passes through an interferometer. Therefore, an interferogram, in which intensity of light is plotted in the time domain, is produced: it contains the informations about all the frequencies of the radiation emitted from the IR source. In this manner, it is avoided the emission of beams for each single frequency. The beam exiting from the interferometer is sent towards the sample. A detector measures the intensity of radiation after the passing through the sample, creating another interferogram and converts it into an electrical signals which can be elaborated. The Fourier transform of the two interferograms is then computed to pass from the time domain to the frequency one. Thereby the intensity of light can be plotted versus each frequency of the IR range. The spectrum of the sample is thus obtained: on the x-axis the wave number is usually reported instead of the frequency, meanwhile on the y-axis there are absorbance (A) or transmittance (T). Both properties, expressed also as a percentage, are computed by comparing the light intensity before and after the sample crossing. If the transmittance is equal to 1, the sample has not absorbed radiation and thus absorbance is null. On the contrary, if the transmittance is zero, the sample has an absorbance which is infinite since the sample has absorbed all the radiation. Therefore transmittance and absorbance are linked through the following equation:

$$T = \log_{10} \frac{1}{A} \tag{3.3}$$

The spectrum obtained is compared to those find in literature or in web databases: like that it is possible to find the correspondences between the peaks of transmittance or absorbance, located at certain frequencies, and the functional groups. Hence, the composition of the sample is determined.

There are two main techniques to perform the FTIR spectroscopy: the transmission method and the attenuated total reflection (ATR) one. In the former, the IR beam passes through the sample before being collected by the detector. Therefore, the samples must be properly prepared: their thickness must not be too high and, often, they have to be reduced as pellet, film or mull [110]. Instead, in the ATR method, the sample, which can be both liquid and solid, is placed on a material with greater refractive index (the ATR crystal): the IR beam enters this material with an angle higher than its critic angle (θ_c) and thus the total internal reflection takes place (figure 3.10a). The total internal reflection happens when there is no refracted beam and an evanescent wave, which is absorbed by the sample, arises at the interface between the two media [111]. The intensity of light measured by the detector is compared to that of the incoming light and absorbance or transmittance are derived. The schematic of the sample placed on the high refractive ATR crystal in a ATR system is shown in figure 3.10b. Only the surface of the sample (between 0.5 and 2 μm of thickness) is analysed through this method.

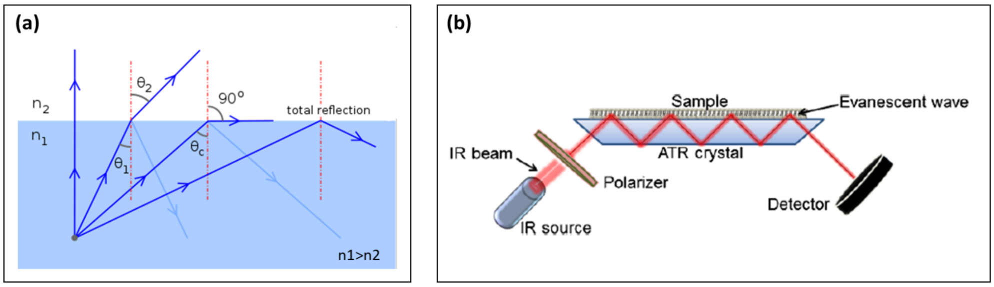

Figure 3.10: FTIR-ATR working principle: (a) The internal total reflection phenomenon in two generic media with refractive index n1 and n2 (b) representation of a FTIR-ATR system [111]

In this work, a Nicolet iS50 (Thermo Fisher Scientific) FTIR spectrometer, equipped with the ATR module, was employed for analysing the TRAD solutions with different concentration of photoinitiators blend before and after exposure to UV light. This study was necessary to asses the reactivity of the three samples, underlining eventual differences among them. Each non-cured solution was placed on a silicon sample holder (which constitute the ATR crystal) through a film applicator bar of 500 μm of thickness. The ATR crystal was placed into the spectrometer and a background spectrum was first collected: this acquisition is always necessary to remove the contributes of the environment and the sample holder in the following spectra. Then, for each sample, 32 spectra were collected and averaged with a wave number range between 400 and 4000 cm^{-1}. Samples were then cured through exposition to UV lamp (Dymax) for 5 min in nitrogen atmosphere for avoiding radical scavenging caused by oxygen. Finally, the spectra of the cured samples were collected through the same procedure described earlier. All the data were elaborated through the software Omnic (Thermo Fisher Scientific).
When the solution is exposed to UV light, acrylates double bonds of the TRAD undergo to homolytic rupture allowing the propagation of the photopolymerization reaction. Therefore, comparing the spectrum of non-cured sample with that of the cured one, the lowering of the peak placed approximately at 1190 cm^{-1}, corresponding to carbon-carbon double bond typical of acrylates compounds, was assessed.

3.2.2 Photoreology

Rheology tests are used for analyzing the mechanical response of a certain material to external shear stress. The deformation and the viscosity of the sample are related to the intensity of the applied stress, the application speed and its duration to understand its viscoelastic behaviour. Therefore rheology is mainly applied to liquid or semi-solid materials like polymers. Viscoelasticity is a property which is assigned to those materials which are not completely elastic and not even completely viscous. A purely elastic solid behaves according to the Hooke law ($\sigma = E\epsilon$). Hence its deformation depends only by the stress applied and it is immediate. Instead, a viscous liquid follows the Newton law $\tau = \eta\dot{\gamma}$: the shear stress τ (Pa) linearly depends on the shear rate $\dot{\gamma}$ (s^{-1}), namely the velocity of the deformation perpendicular to the direction of the stress. The constant of proportionality is represented by the viscosity η, measured in $Pa \cdot s$; it only depends on temperature. The viscoelastic behaviour is a combination of the elastic characteristics typical of solids and viscous properties of fluids. Polymers, soft tissue, wood an metal at high temperatures show this effect [112]. It is common to separate the linear viscoelastic region from the non-linear one. The former consists in a range of small deformation in which the viscoelasticity can be described by an ordinary differential equation. In this case the elastic and the viscous components can be considered independent and the total response of the material is obtained overlapping their effects. Instead, for large deformation, the system change its properties during the solicitation and thus it is described by non linear differential equations.

Dynamic modulus and the phase shift between stress and strain are normally used for describing viscoelastic materials. They are obtained applying through the rheometer a sinusoidal shear stress ($\tau(t) = \tau_0 sin(\omega t)$) and measuring the response in deformation of the sample. It will be always a sinusoid, $\gamma(t) = \gamma_0 sin(\omega t - \delta)$, delayed of the factor δ with respect to the input. If stress and deformation are in phase (δ=0), the material is purely elastic. If the deformation is 90° out of phase with respect to the input solicitation, the sample is totally viscous. Therefore a viscoelastic object owns a δ comprised between 0° and 90°. From the ratio between $\tau(t)$ and $\gamma(t)$ it is possible to obtain the dynamic modulus G which is a complex number divisible in:

$$G = G' + iG'' = \frac{\tau_0}{\gamma_0} cos\delta + i \cdot \frac{\tau_0}{\gamma_0} sin\delta \tag{3.4}$$

where $G' = \frac{\tau_0}{\gamma_0} cos\delta$ is the storage shear modulus (a measure of energy stored and recovered per each cycle) and $G'' = \frac{\sigma_0}{\tau_0} sin\delta$ is the loss modulus (a measure of the energy dissipated by the internal frictions). From the mechanical point of view, G' represents a measure of the stiffness of the sample [112]. The ratio between the latter and the former ($tan(\delta) = G''/G'$) is also called "loss factor". The greater the loss factor, the more viscous is the sample. On the contrary, when the $tan(\delta)$ is close to zero, the material can be considered elastic. Rheometer could be equipped with an UV lamp for analysing the kinetic of photo-polymerization: photo-reactivity is studied checking the variation of mechanical properties (G', G") under UV light exposition.

In this work, rheometer was first used to assess the possible effect of salt molarity in M-CMC solution curing. Then, the different mechanical properties of hydrogels obtained varying M-CMC concentration are studied through the same method. Test were performed through an Anton Paar rheometer (Physica MCR 302) in parallel-plate mode (upper plate diameter of 25 mm), equipped with UV lamp (Hamamatsu LC8). The intensity of light was set at 20 $mWcm^{-2}$ and all the trials were performed at constant temperature (25°C). A bottom quartz plate, on which samples were placed, was employed. First of all, amplitude sweep test were done for finding the linear viscoelastic range (LVR): the frequency of oscillations was kept constant at 1 Hz and both G' and G" were measured varying the strain amplitude from 0.01% to 1000%. The two moduli approximately are stable in the LVR; for higher strains they decay as a results of variation of the samples structure. Thereby it was possible to choose an appropriate deformation amplitude (1%) in the LVR to be applied in the further test.

Then time sweep test were carried out to examine how long the curing process took for the M-CMC solution with different salt molarities. These trials were executed at a fixed frequency (1 Hz) and at a constant strain comprised in the LVR (1 %), measuring changes in time of the dynamic modulus of samples. After a time of 60 s, the UV lamp was switched on and curing process began. When the solution is not cured, the viscous modulus G” is greater than G”. If the photo-polymerization starts, the elastic modulus G’ begin to rise until it exceeds G” and reaches a plateau. This proves the hydrogel formation. The transition point between the viscous solution and the hydrogel is when G’ is equal to G”: it is named "gel point". The time in which the gel point is reached represents an optimal parameter to asses the photoreactivity of the solutions.

3.2.3 Tensile test

Tensile test were performed to evaluate the mechanical properties of the three materials used as encapsulation. Rectangular specimens of PDMS and TRAD were obtained through casting and curing processes, as was explained before in sensor manufacturing (section 3.1). VHB tape was simply cropped in a rectangular shape thanks to a cutter. An Instron tensile machine with a load cell of 10 kN was used for these test. Samples edges were grasped on two knurled clamps. Trials settings and data storing were carried out through BlueHill software. Tensile speed was set at 5 mm/min for PDMS and TRAD samples. Instead, VHB specimens were stretched at 25 mm/min due to their higher stretching performances. For each kind of material, four specimens were tested until rupture.
One of the two clamps of the machine is fixed. The other is moveable: it is carried up by a linear motor and in doing so the sample is stretched. The load cell mounted on the moving clamp measure the force applied. The corresponding stress value (σ) is derived from the formula $\sigma = F/A$ where F is the force measured and A is the cross sectional area of the sample, set manually through the software. At the same time strain is measured knowing the position of the linear motor. Before the test start, zero position is set and sample length is configured; then the software computes the strain (ϵ) using the formula $\epsilon = (l - l_0)/l_0$, where l is the current length of the sample, determined by the position of the motor, and l_0 is the length of the sample at rest.
Stress-strain curves were thus plotted and mechanical parameters were derived. The slope of the straight line in the initial linear part of the graph represented the Young modulus or elastic modulus. Toughness, namely the energy absorbed by the sample before rupture, was computed as the area under the $\sigma - \epsilon$ curve. Fracture elongation and tension were the values of strain and stress at the sample breaking point. Average values and standard deviations of these parameters were then computed: they described the mechanical behavior of the three materials, allowing the selection of the best solution for the different applications.

3.2.4 Electrochemical analysis

Electrochemical analyses were necessary for both understand the electrical behaviour of the sensors and to choose the best material for the electrodes. Electrochemical impedance spectroscopy (EIS) was the tool used to achieve these purposes. EIS, performed through a potentiostat, is a method to study the complex impedance of system in which ionic conduction is prevalent [113]. It consists in the application of an AC voltage at a certain frequency ($V(t) = V_0 e^{i\omega t}$) and the measuring of the resulting AC current $I(t) = I_0 e^{i\omega t - \theta}$, in which θ represents the phase shift. A DC constant voltage is usually superimposed to the AC input. The amplitude (V_0) of the input should be enough small in such way that the system can be approximated as pseudo-linear [114]. Then, the complex impedance is computed through the Ohm's law:

$$Z = \frac{V(t)}{I(t)} = \frac{V_0}{I_0} e^{i\theta} = Z_{Re} + i \cdot Z_{Im} \tag{3.5}$$

This process is repeated for a certain range of frequencies; in fact, it is normally named frequency response analysis (FRA). Modulus, phase, real and imaginary part can be derived for each frequency, thanks to the complex numbers algebra. Results are usually presented through the Nyquist plot in which the real part of impedance (Z_{Re}) is on the x-axis and the imaginary part (Z_{Im}) on the y-axis. In this type of graph the frequency is not shown. Therefore a system that is fashioned through a simple resistor has an horizontal line on the Nyquist plot, due to the presence of only the real part of impedance. On the contrary, if the model is a capacitance and so the impedance is purely imaginary, a vertical line occurs on the Nyquist plot. In addition, a parallel between a capacitance and a resistance gives a semicircle. Bode plots is another way to show the data: they show the modulus of the impedance ($|Z| = \sqrt{Z_{Re}^2 + Z_{Im}^2}$) or the phase ($\theta = \arctan(\frac{Z_{Im}}{Z_{Re}})$) with respect to $\log f$.

After data being acquired from potentiostat, an electrical model of the system is suggested thanks to the observation of the impedance trends in the before mentioned plot. In addition to the common ideal electrical components (resistance, capacitance and inductance), several other elements exists to take into account the non ideality of the samples [114]. In this work the constant phase element (CPE) was employed. It is a generalization of the capacitance and its contribution in impedance is the following:

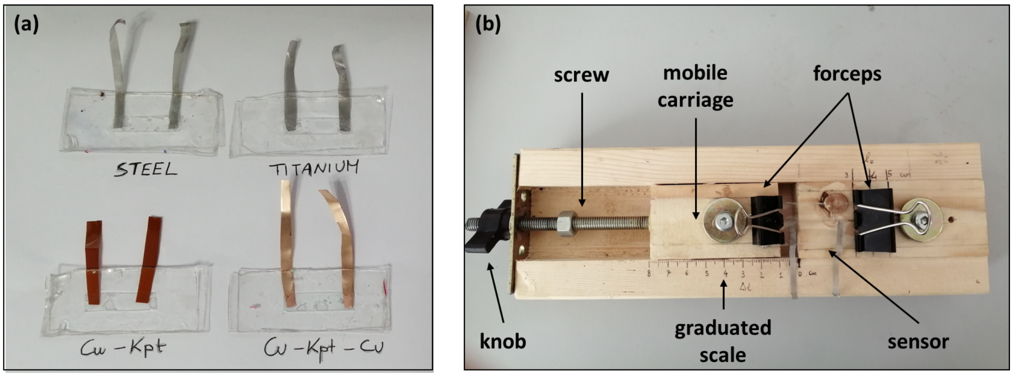

Figure 3.11: Materials of electrodes and stretching instrument: (a) VHB sensors with electrodes of different materials (b) stretching home-made machine and its parts

$$Z = \frac{1}{Q(j\omega)^{\beta}} \tag{3.6}$$

In this equation, Q represents the CPE prefactor and β is the CPE index which varies between 0 and 1. The more it is close to 1, the more the system is similar to an ideal capacitor. On the other hands, if it is closer to 0, the sample behaves like an ideal resistor.

Therefore, it is necessary to choose the best combination (series and/or parallels) of electrical elements to fit, through appropriate algorithms, the experimental raw data. There are several software proper to do this process. Then, the values of parameters of the chosen electrical model can be extracted from the fitted data. Hence, the samples subjected to different external static stimuli can be examinated through EIS and thus the electrical parameters variations can be checked.

In this manner it was possible to find the material for electrodes which ensures the highest sensitivity to external deformations and to study the behaviour of sensors at various frequencies. Four different materials were taken into account for electrodes: titanium (Ti), steel (St), copper-Kapton (Cu-kpt) and copper-Kapton-copper (Cu-kpt-Cu). The first two were organized in knitted foils. The others were sandwich-like sheets: a Kapton foil overlapped to a copper one in the Cu-kpt arrangement, and a Kapton intermediate layer between two copper layers in Cu-kpt-Cu foils. These sheets were cropped with a cutter in a rectangular shape for obtaining the electrodes. Hydrogel with the M-CMC concentration of 2wt% with respect to water and a salt molarity of 1 M, was used to build the sensors used in these test. Hence, for each kind of electrodes three sensors based on VHB tape, were produced following the process explained in section 3.1.4. A FRA, with range of frequencies between 0.01 Hz and 100 kHz was made for each sensor at rest and when it was subjected to strains of 20%, 40% and 60%. A DC voltage of 0.5 V and an amplitude of AC voltage of 20 mV were set and for each decade were acquired 10 points. EIS analyses were performed through the Multi Autolab/M101 (MetroOhm) potentiostat in a 2-electrodes configuration controlled by the software Nova. Deformations were applied to the sensors through the home-made tensile machine shown in figure 3.11b. Sensor edges were clamped between two forceps; one of them was mounted on a carriage which was put in motion through a screw properly tightened thanks to a knob. A scale indicated the stroke of the carriage and thus, knowing the initial length of the sample, it was possible to derive the strains applied.

For data fitting, the free software EIS spectrum analyser was employed [115]. Raw data in the Nyquist plot owned a shape referable to two semicircles for all the types of sensors. Moreover, the graphs did not begin at the origin of the axes. Hence, the model shown in figure 3.12a was chosen as a representation of samples. The series resistance R1 indicates

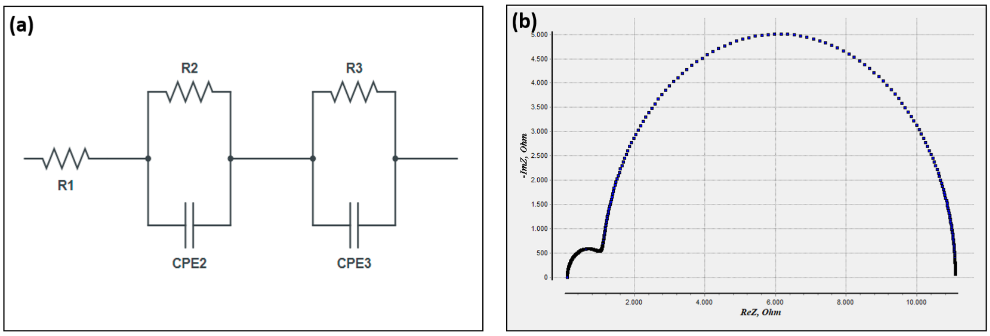

Figure 3.12: Sensor electrical model: (a) elements of the model (b) simulated response of the model when ideal capacitors are used instead of CPEs

the electrolyte resistance and describes the offset with respect to the origin in the Nyquist plot. The first parallel between a CPE2 and R2 represents the contact resistance and the interface between electrodes and electrolyte; it acts at higher frequencies and is depicted by a small semicircle. Finally the second parallel (CPE3-R3) constitutes the contributes at lower frequency due primarily to the ionic diffusion in the electrolyte and is represented by a bigger semicircle in the Nyquist plot. CPEs were used instead of capacitance because of the non ideality of the system deductible from the fact that semicircles were flattened in raw data. In the Bode plot the parallels between R and C corresponds to two separated peaks of the phase, associated with the time constants ($\tau = R_p C_p$) of model. The ideal Nyquist plot of this system is reported in figure 3.12b: in this case impedance value were simulated using CPEs with β factor equal to 1. Values of parameters (R1, CPE2, R2, CPE3, R3) were extracted by the same software. Capacitance value (C2,C3) corresponding to the CPE2 and CPE3 were derived from the formula [114]:

$$C = Q^{\frac{1}{\beta}} R^{\frac{1}{\beta}-1} \tag{3.7}$$

in which R is the parallel resistance to the CPE described by the parameters Q and β.
After values of electrical elements were obtained for all the sensors subjected to the strains previously mentioned, the relative variation of resistance ($(R - R_0)/R_0$) and capacitance ($(C - C_0)/C_0$) were computed for each sample and then were plotted. These graphs assisted the electrodes material choice.
In addition EIS analyses, with the same procedure described above, were applied to choose the best electrical excitation frequency and to confirm data obtained from the electrical characterization. In this case, strains of 10%, 20%, 30%, 40%, 50% were taken into account.

3.2.5 Electrical characterization

An LCR meter (BK Precision 894) was employed for studying the variation of electrical properties under external deformation. Parameter settings and data collection were performed through LabView (National Instruments). The whole test bench is shown in figure 3.13b. A parallel between a resistor and a capacitor (Rp and Cp, shown in figure 3.13b) was used as model of impedance. Stimulation frequencies of both 20 Hz and 1000 Hz were applied and the signal voltage amplitude was set at 0.5 V. Electrical characterization was useful to determine the concentration of M-CMC which ensured the best sensitivity to external strain and to understand which of the parameters (Rp or Cp) and at what frequency (20Hz or 1000Hz) it was better to work. As regards the hydrogel solutions, the molarity of NaCl was kept constant since the ionic contribution is dominant at lower frequencies and it is more useful a sensor with higher electrical excitation frequencies. Instead, M-CMC concentration was varied due to its pronounced effects on both mechanical behaviour and electrical properties recoverability of sensor. Hence, solutions with 2%, 3%, 4% M-CMC photo-polymerized and the solution with 4% M-CMC not cured (4%NC) were taken into account. For each M-CMC ionogel, three VHB sensors were built with the electrodes chosen through EIS analyses.
Each sensor underwent to static measurements at rest and under two kind of deformations: stretching and bending. Stretching stimuli were performed through the same instrument described in section 3.2.4. Strains from 10% to 50% with step of 10% were employed. Bending stimuli were applied through the handmade machine shown in figure 3.14b. The

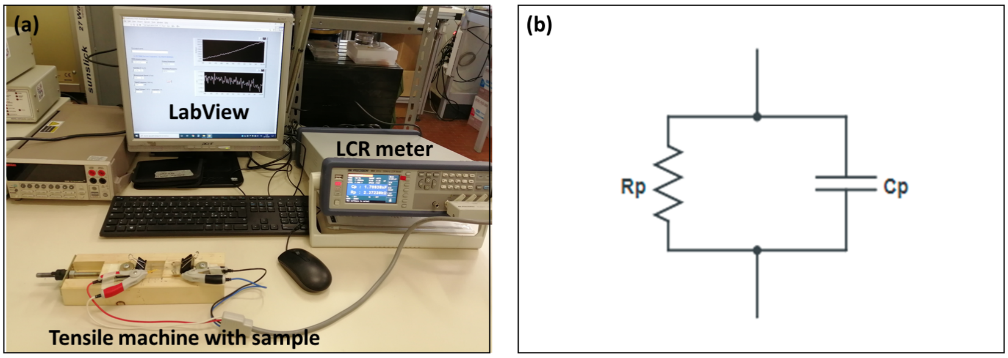

Figure 3.13: LCR meter: (a) LCR meter test bench (b) model of impedance measured

sensor was first closed in the middle between two rubber strips in order that electrodes were left exposed (figure 3.14a). Thus, it was simple to connect the LCR meter probes to the electrodes. This sensor holder was then placed perpendicularly to the basement of

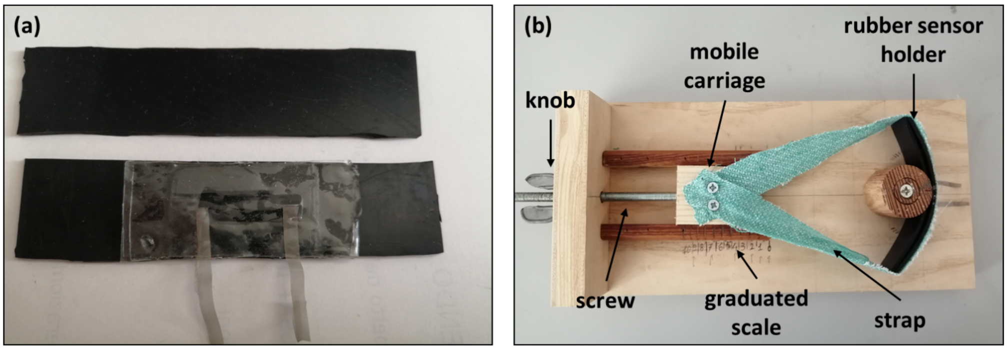

Figure 3.14: Bending home-made instrument: (a) sample holder made of rubber (b) bending machine and its parts

the bending instrument, near a fixed cylindrical pillar, and it was held in position though a textile strap. The strap was fixed on a carriage which could move linearly thanks to the tightening of a screw. When the carriage was moved, the strap lengthened and it consequently bent the sample holder. It is important that the rubber holder was placed centrally in relation to the supporting pillar in order to reproduce a symmetric arc when it was bent. In this way it was possible to make repeatable the bending test. Like in stretching test, five different curvature radii were chosen to be analysed: 15 cm, 9 cm, 5 cm, 3 cm and 2,5 cm.
An acquisition of 1 minute was performed through the LCR meter for each step of the two test. Then the means and the standard deviations of Rp and Cp value were computed and relative resistance or capacitance changes were plotted against to the deformation steps (both for stretching and bending test). For each M-CMC concentration were tested three samples in order to make a relevant statistical analysis: hence, the averaged transfer curves

were thus obtained. After the samples loadings, data were also acquired during the unloading phase in order that to evaluate the hysteresis and to verify the possible recovery of initial properties. This trial was repeated also after samples were stored one month at 25°C, to evaluate the possible changes due to the water evaporation.
After the selection of concentration of M-CMC, of electrical frequency and of parameter to be analysed, sensors were stretched until rupture through the tensile machine (Instron, tensile speed of 10 mm/min), while they were monitored through LCR meter, for obtaining the complete transfer curves of sensors. Moreover, cyclic acquisitions (20 cycles at 50% of strain) were also carried out to evaluate the repeatability of measures.
The dependency of the electrical parameters with respect to the temperature was further evaluated. The sensor was put in a oven (Memmert) while Rp and Cp were measured through the LCR meter. Temperature was varied from room temperature (25°C) to 60°C with 5°C of step and static acquisitions of 1 minutes were done for each temperature step. An electric excitation frequency of 1000 Hz was used for all the trials. Three samples were analyzed in this manner, to have statistical more robust results. After these characterizations, sensors were applied to the body to monitor joint motions, muscular activities, heart rate and voice.

Chapter 4

Results

4.1 Ionogel characterization

First of all, photorheologies were carried out to characterize the reactivity and the mechanical properties of the cellulose ionogel. The linear viscoelastic range, in which the moduli (G’, G”) are stable, was found performing amplitude sweep test on non-cured solutions with 2wt% of M-CMC with respect to water and different salt molarities (0.5 M, 1 M, 1.5 M). In that way it was possible to choose the value of strain to apply in the following time sweep test in order that it was comprised in the LVR. A deformation amplitude of 1% is a reasonable value as it is shown in figure 4.1a. Then, time sweep test, with the chosen strain amplitude, and 1 Hz of oscillations frequency, were performed. After 60 sec from the start of the trial the UV lamp (20 mWcm^{-2}) was switched on and the solutions began to crosslink. In figure 4.1a are reported the moduli of the 2%_05, 2%, 2%_15 solutions (table 3.1). The gel point, namely the time in which the storage modulus overcome the loss one, indicating the gel formation, is approximately the same for the three samples. Therefore, the concentration of salt does not influence the reaction speed of the ionogel.

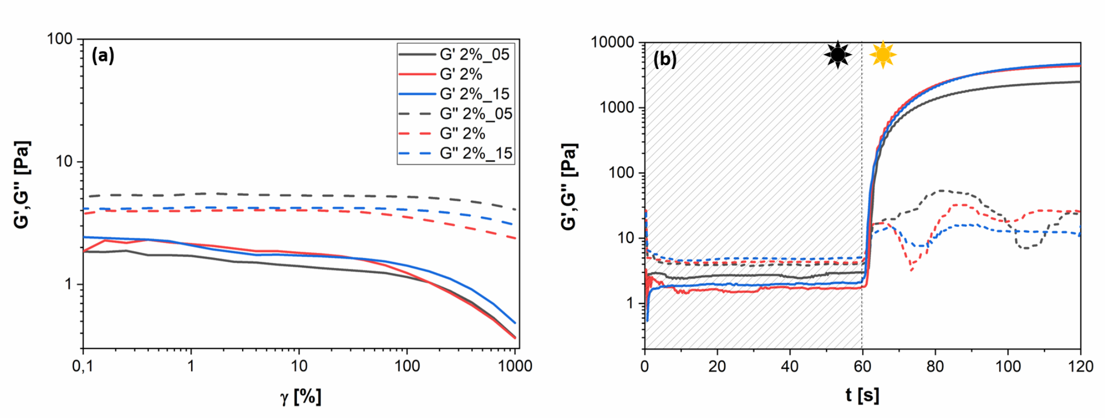

Figure 4.1: (a) Amplitude sweep test of ionogel solutions (b) Time sweep test of the same solutions: in the dashed area the UV lamp was switched off

Moreover, the similarity among the storage moduli after complete gelation suggests that the salt does not affect the stiffness of the hydrogels.

The reactivity is not even influenced by the M-CMC concentration: in figure 4.2a, where time sweep test are shown, the gelation point does not vary for the three UV curable solutions. Subsequently the crosslinked hydrogels with various M-CMC concentration (2%, 3%, 4%) and the hydrogel with CMC not crosslinked (4%_NR) were subjected to amplitude sweep test to find out their mechanical behavior (figure 4.2). The 2% and 3% M-CMC hydrogels shows a similar G' and thus comparable stiffness. Instead the 4% ionogel is stiffer than the others, due to the higher amount of M-CMC chains and thus the greater number of crosslinks among them. This results also in a increased brittleness. On the other hand, the 4%_NC hydrogel is similar to a viscous colloid solution and, consequently, its storage modulus and stiffness are lower than those of the other samples. Moreover, the LVR is broader, indicating that the mechanical properties of this sample are stable for an greater range of deformations.

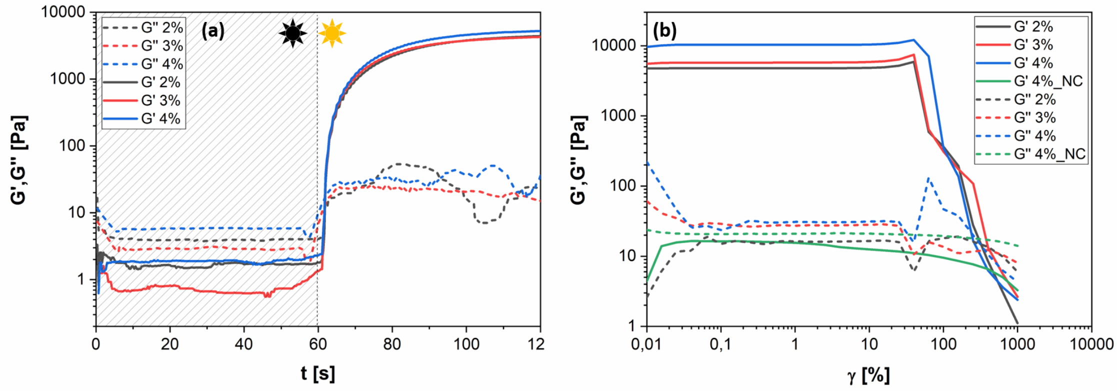

Figure 4.2: (a) Time sweep test of curable hydrogels (b) Amplitude test sweep of hydrogels with different M-CMC content

4.2 Encapsulation characterization

Since TRAD is a material poorly investigated in literature, at first, the influence of the photoinitiators blend concentration was analysed. Hence, reactivity of solutions TRAD08, TRAD15, TRAD20 (table 3.2) was compared through the FTIR-ATR method. First FTIR spectra of the solutions not crosslinked were acquired. As can be seen in figure 4.3a, spectra of the three specimens are almost identical. After TRAD solutions irradiation for 5 min, FTIR-ATR analyses were performed again. In all three samples the peak of the spectrum placed at 1190 cm^{-1}, which corresponds to the double carbon bond typical of acrylates, flattens. Moreover, in figure 4.3b it is clear that the area under the peak which represents the acrylates conversion, is almost the same for the samples, indicating a good reactivity of all the three formulations. This also confirms the possibility to print 3D shapes through the DLP method.

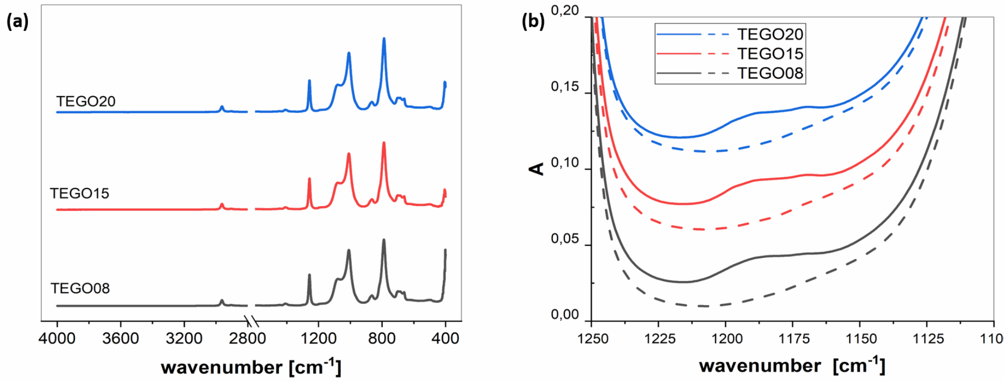

Figure 4.3: FTIR-ATR test: (a) spectra of the three solutions prior irradiation (b) lowering of the peak related to the double carbon bonds conversion; the dashed lines indicate the irradiated samples

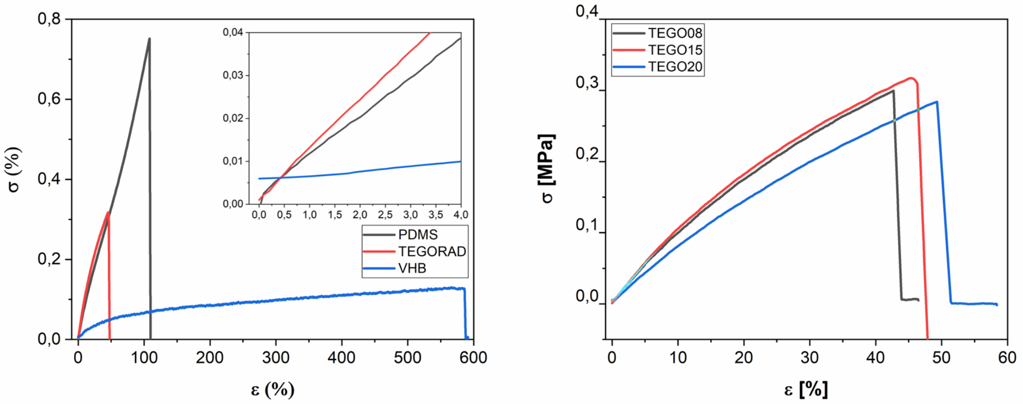

Figure 4.4: Examples of tensile curves: (a) PDMS, TEGO15, VHB samples. In the inset, the magnification of the elastic region (b) different TRAD formulations

Then, tensile test were carried out for evaluating the mechanical properties of the three solutions of TRAD, PDMS and VHB tape. For each kind of material, four rectangular specimen were prepared. The specimens were stretched until rupture. However, all VHB tape samples have slipped from the clamps due to the exceptionally high deformation reached. Therefore, tension and strain at breaking point have been computed at the slipping point for VHB specimens. Examples of single samples curves are reported in figure 4.4. From a quick look it is already clear that the VHB tape owns the highest stretchability, while TRAD sample is the less extendable. PDMS holds intermediate properties. In the inset in figure 4.4 a magnification of the curves is shown: in this linear elastic region, the Young modulus was computed as the slope of the curve. In figure 4.4b TRAD samples with different concentration of photoinitiators blend are compared, showing that there are

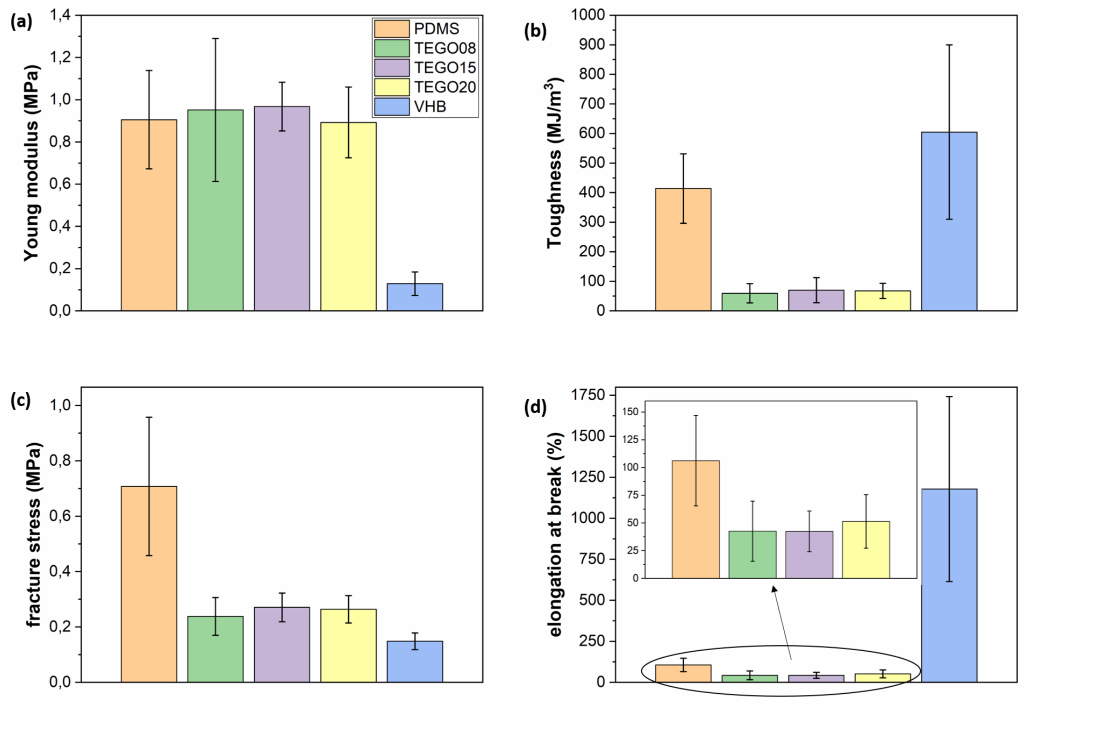

Figure 4.5: Mechanical parameters statistic: Young modulus (a), toughness (b), ultimate tensile strength (c) and elongation at break (c). In the inset the magnification of the PDMS and TRAD elongation at break

no relevant differences among them. This is also proved by the achieved properties of the samples (figure 4.5). The main mechanical features, such as the previous mentioned Young modulus, the toughness, the elongation at break and the ultimate tensile strength (UTS), were extracted from the $\epsilon - \sigma$ graphs. Even though PDMS and TRAD holds similar stiffness (represented by the Young modulus), the latter is more brittle: its toughness, namely the area under the $\epsilon - \sigma$ curve, and elongation at break are much lower. Therefore, TRAD based sensors are not applicable where large strain are required. The UTS means the maximum stress that the sample manage to bear before rupture: the PDMS shows the higher UTS, although VHB tape data shall not be considered since VHB samples have not undergone to breaking. This is the reason why the error bars are greater for VHB ultimate strain and toughness. Nevertheless, the average elongation at break of VHB is much higher than that of the other materials (about 1200%): hence, its superior stretchability, compared to PDMS and TRAD, makes it the ideal candidate for building strain sensors. VHB holds also a low Young modulus and thus it is softer than the others specimen, suggesting that it is more compliant to the irregular surfaces of soft tissues and robotics. However, the return to the initial shape after large deformations is slow owing to the viscoelastic properties of the VHB tape.
Moreover, the transparency of the sensors made with the three different encapsulation is

compared in figure 4.6. It is clear that the TRAD sample, although the solution with the lowest concentration of photoinitiators blend was employed, is the less transparent, due to its slightly opaque yellowish color. This results in a less aesthetic result if the sensor is applied on the skin surface. Rather, both PDMS and VHB samples are perfectly transparent. However, in the central area of the PDMS sensor there are several bubbles resulting from the non perfect closure. In addition, some whitish residuals are present in the same area: they consist of the salt (NaCl) precipitated due to the water evaporation during the waiting of PDMS curing. Therefore, VHB tape is the best solution as regard the external aspect of sensor.

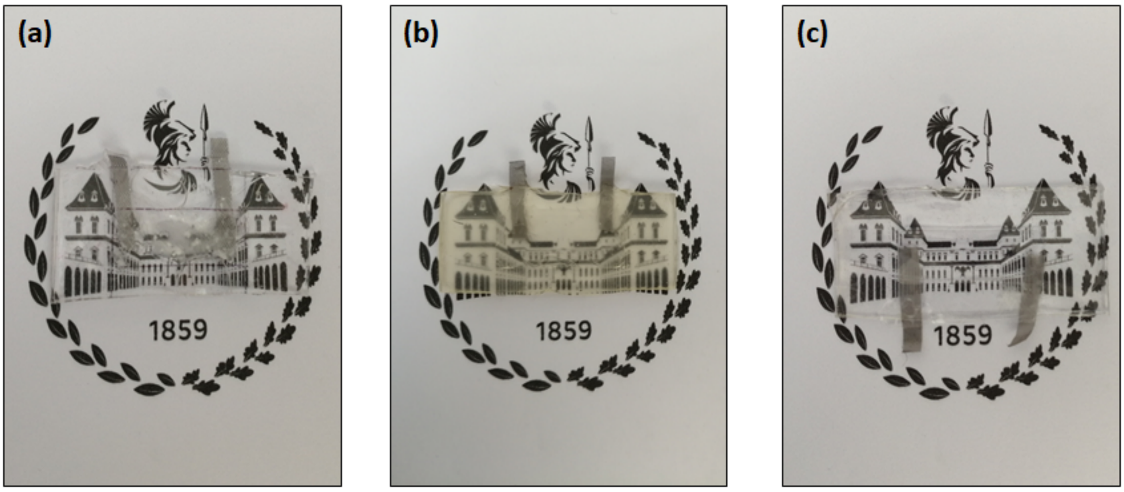

Figure 4.6: Transparency of sensor with shells of different materials in comparison: PDMS (a), TRAD 2800 with 0.8% of PI blend (b), VHB tape (c) sensors

4.3 Electrodes and electrical excitation frequency choices

Electrochemical impedance spectroscopy analyses were performed on the sensors with 2% M-CMC hydrogel and different electrodes. FRA method was applied to acquire data of samples at rest and subjected to 20%, 40%, 60% of strain. The electrical model presented in section 3.2.4 was used for fitting the raw data through the software EIS spectrum analyzer. Figures 4.7, 4.8, 4.9 and 4.10 show Bode and Nyquist plot of both the raw data and the fitted curves. Observing especially the devices with Cu-Kpt and Cu-Kpt-Cu electrodes (figures 4.7 and 4.8), the presence of two semicircles in the Nyquist plot is quite clear; therefore the system was modeled by two parallels between resistor and capacitor. CPEs were then chosen instead of capacitors because the semicircles are slightly flatten, indicating a non-ideal system. From the graphs it is also noticeable the offset with respect to the origin along the x-axis: it was modeled through a series resistance. A similar behavior was found also for sensors with steel and titanium electrodes. Although it is more difficult to associate the ideal Nyquist graph 3.12b in section 3.2.4 to the plots presented in figures 4.9 and 4.10, the same model fitted well also data of these specimens. For all the kind of

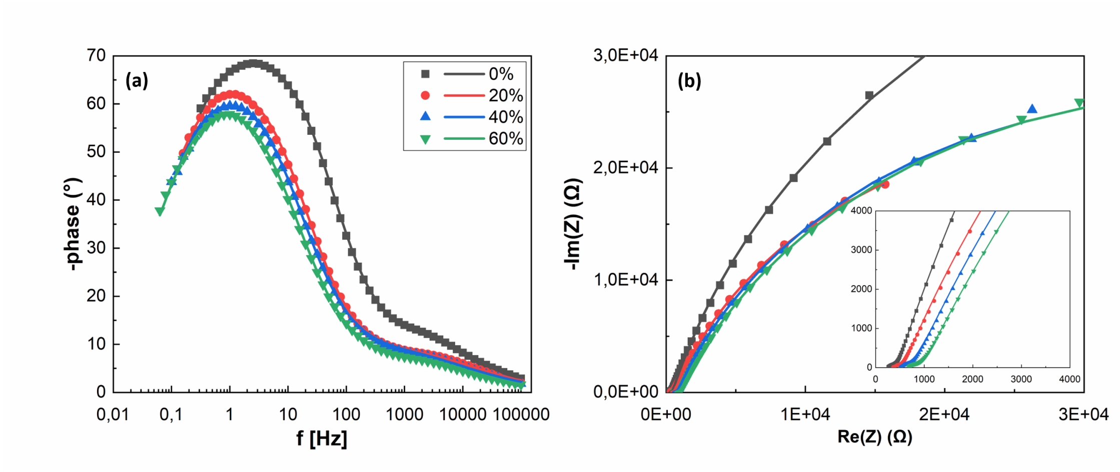

Figure 4.7: Bode (a) and Nyquist (b) plot of sensors with Cu-Kpt electrodes at rest and under strains (20%, 30%, 40%). In the inset, the magnification of the Nyquist plot. The points represent the raw data; the solid lines constitute the fitting curves

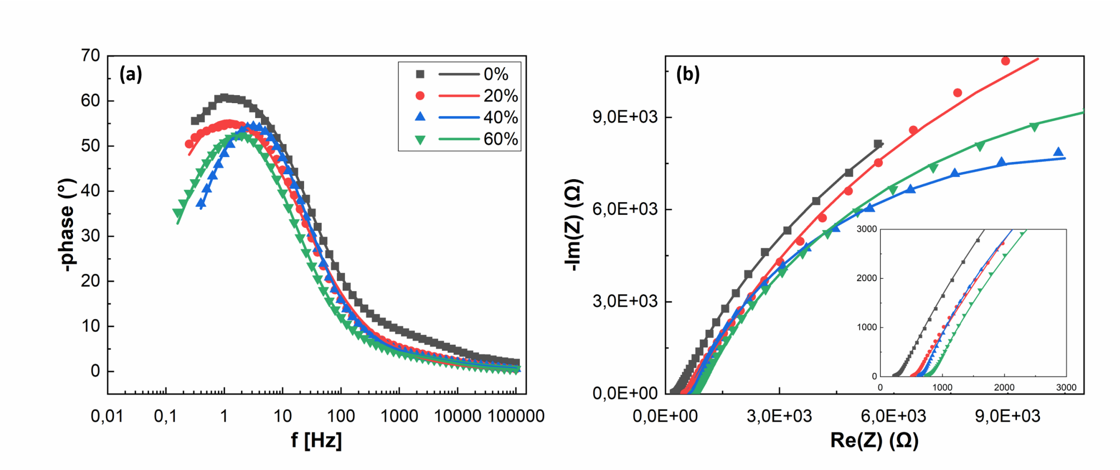

Figure 4.8: Bode (a) and Nyquist (b) plot of sensors with Cu-Kpt-Cu electrodes at rest and under strains (20%, 30%, 40%). In the inset, the magnification of the Nyquist plot. The points represent the raw data; the solid lines constitute the fitting curves

sensors the impedance data substantially changed when they were subjected to external strains: this is evident from both Bode and Nyquist plots. In the former a shift of the phase peaks is present. This corresponds to a lowering of the semicircles and an increasing of series resistance noticeable in the enlargements of the Nyquist plots.

Electrical parameters (R1, R2, CPE2, R3, CPE3) were extracted from the fitted data and C2 and C3 were derived thanks to the equation 3.6. Since three samples for each kind of electrode were tested at different strains, it was possible to analyze statistically

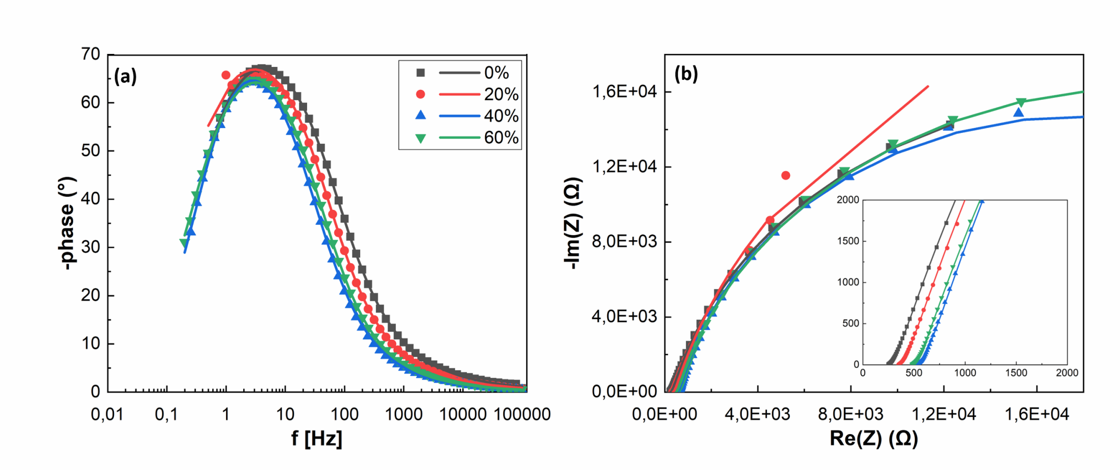

Figure 4.9: Bode (a) and Nyquist (b) plot of sensors with stainless steel electrodes at rest and under strains (20%, 30%, 40%). In the inset, the magnification of the Nyquist plot. The points represent the raw data; the solid lines constitute the fitting curves

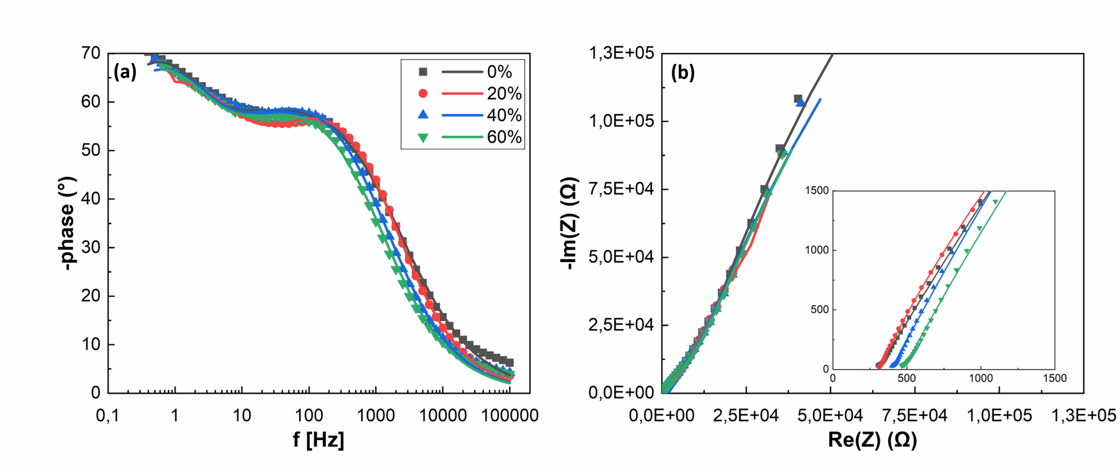

Figure 4.10: Bode (a) and Nyquist (b) plot of sensors with titanium electrodes at rest and under strains (20%, 30%, 40%). In the inset, the magnification of the Nyquist plot. The points represent the raw data; the solid lines constitute the fitting curves

the parameters variation of the model. In figure 4.11 the relative variations of single parameters, with respect to their values at rest, versus the strain applied for the four types of electrodes considered, are reported. In general, the series resistance (R1), namely the resistance of the electrolyte, tends to increase when the strain becomes greater for all the sensors, as seen before. In fact, the polymeric network, if sensor is stretched, shrinks and the ions dissolved in water cross it more difficultly. The parallel constituted by R3 and C3 which represents the diffusion contribute at low frequencies, shows the highest variation for sensors with titanium electrodes. On the other hand, regarding the part that involves the contact resistance and the interface electrodes-electrolyte, represented by the parallel R2-C2 at high frequencies, the steel electrodes seem to be the best choice to ensure the greatest sensitivity.

After this initial analysis, the devices with copper based electrodes (Cu-Kpt and Cu-Kpt-Cu) have been discarded due to the corrosion which took place at the interface between copper and hydrogel and thus the consequently instability of the electrical properties. The figure 4.12 shows four samples with different electrodes just produced and after being tested and stored for three weeks. Since the electrolyte was rich of salts and different working voltages have been applied for the test, the copper was subjected to a very corrosive environment and released corrosion products of a bluish-green color in the solution. It is interesting to note that the bluish color is more pronounced in the sensor with Cu-Kpt-Cu electrodes due to the double layer of copper exposed to the solution (figure 4.12b). Titanium is protected from corrosion by its passivation oxide. In the same way, the stainless steel is protected by an oxide patina formed by the chrome contents in the alloy. In fact, no noticeable differences can be observed in the samples with titanium and steel electrodes before and after the storing period. Therefore, since the contribute given by the type of electrode mainly regards the parallel at higher electrical frequencies (R2,C2) and diffusion is a phenomenon characterized by greater time constant and thus of little interest, stainless steel was preferred as material of electrodes for the following analyses.

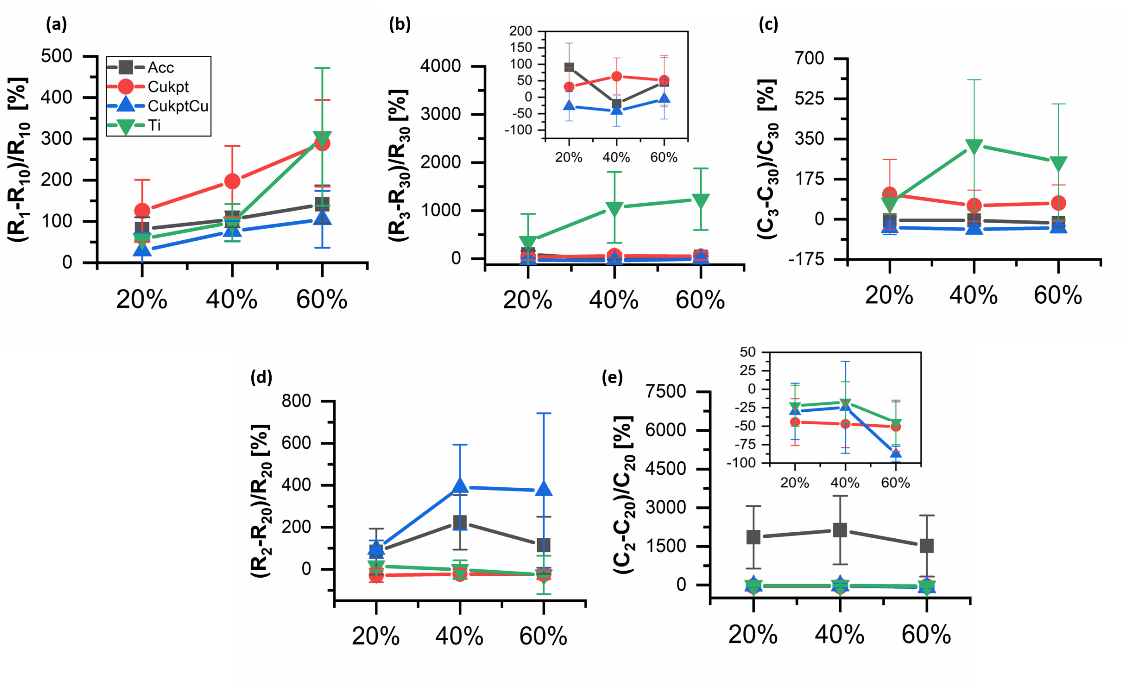

Figure 4.11: Electrical parameters statistics: (a) series resistance (b) parallel resistance at low frequencies (in the inset an enlarged area is shown) (c) parallel capacitance at low frequencies (d) parallel resistance at high frequencies (e) parallel capacitance at high frequencies (in the inset an enlarged area is shown)

Then, others EIS trials were carried out on the sensors with steel electrodes to find out the

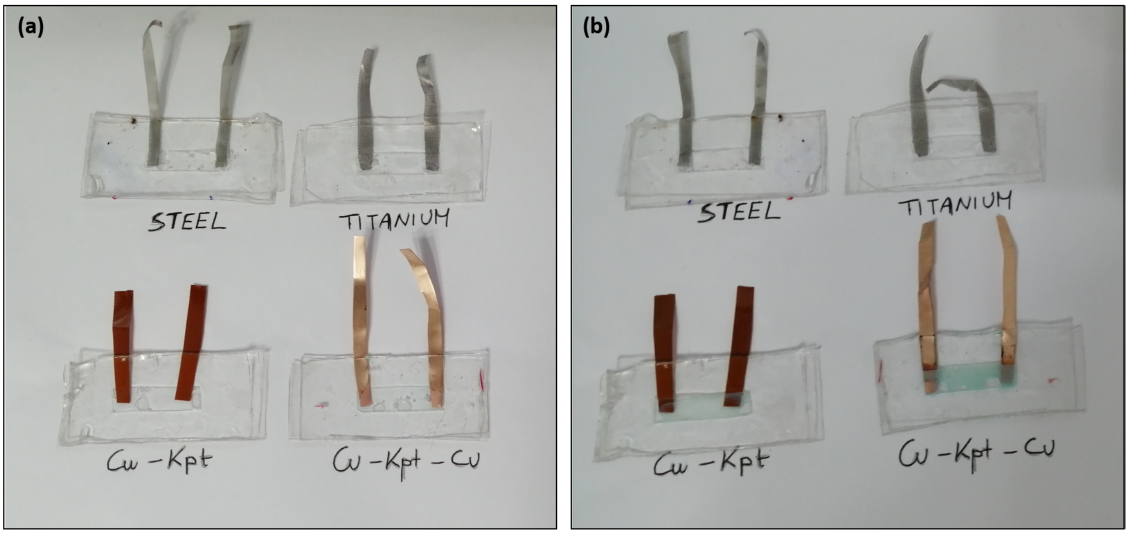

Figure 4.12: Corrosion of different kind of electrodes: (a) samples just produced (b) the same samples after being tested and after being left for 3 weeks in the fridge

best electrical frequency and what concentration of M-CMC ensured the highest sensitivity. Since the impedance is a complex number and its real part represents the resistance of the system and, on the contrary, its imaginary part constitutes the reactance (thus involves both capacitors and inductors), several information about the working mode were additionally found out. Hence, FRA method was applied for sensors at rest and subjected to 10%, 20%, 30%, 40%, 50% of strain. For each M-CMC concentration (2%, 3%, 4%, 4%_NC) one sample was tested. Data fitting and parameters extraction were performed through the same software employed before. In this case, plotting the real and the imaginary part of impedance versus frequency was more convenient to assess the behavior of each kind of sensor. Enlargements in the range between 10 Hz and 2000 Hz are reported because in the electrical test through the impedance meter were chosen both a low electrical frequency (20 Hz, the lower limit of the instrument) and an high one (1000 Hz), to study the devices behavior. From figures 4.13 and 4.14 it is clear that all the sensors work better if the real part of impedance is took into account. In fact, the variation among the curves in the stretched states and the one at rest is more pronounced in the real part than in the imaginary one. Therefore, since the real part shows the dissipative behavior typical of resistance of the system, piezoresistance mode seems to be preferable. Nevertheless, it depends on the electrical model of impedance chosen for the time measurement: hence, a more detailed analyses on the working mode is carried out further in sections 4.4.1 and 4.4.3. In addition, higher frequencies are preferable because the differences between the curves are slightly bigger than those at lower frequencies in the real part plots. Moreover, the hydrogel seems to be more sensitive as M-CMC concentration grows. However the hydrogel with CMC not crosslinked (4%_NC) does not follow this trend: it is more similar to the 2% hydrogel owing to its structure not crosslinked which makes it more soft. The variation between subsequent strains is not constant especially for 3% and 4% samples. In fact, 3% and 4% hydrogels are more stiff and brittle than the others: this means that,

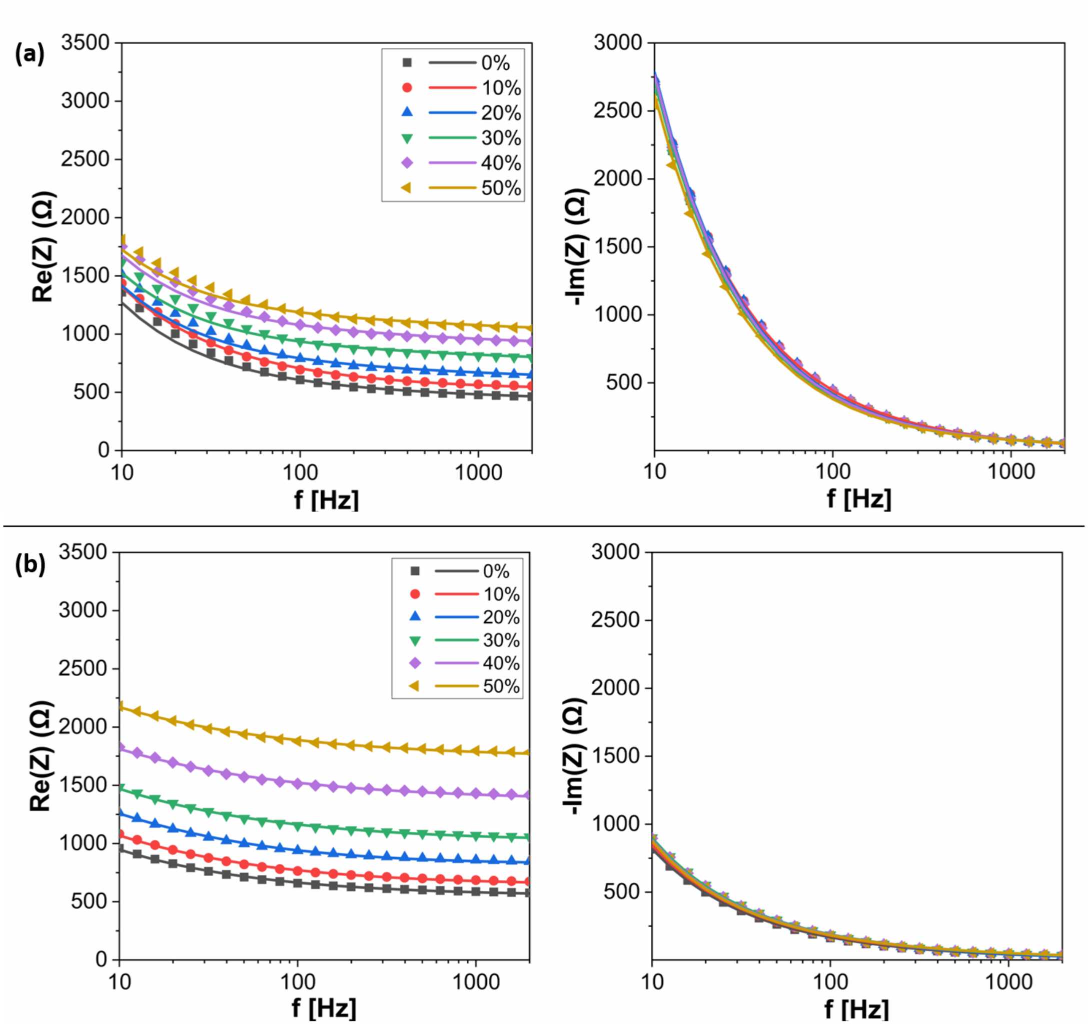

Figure 4.13: Impedance real and imaginary part variation under strains of one sensor for 2% (a) and 3% (b) M-CMC concentrations. The points represent the raw data; the solid lines constitute the fitting curves

when they are stretched, their networks get broken and can not reform itself resulting in formation of poorly conductive regions due to the air entrapped. For these reasons these hydrogels do not hold stable electrical parameters in their life cycle. Despite the achievement of these interesting results visually, a deeper statistical analysis regarding the working characteristics of sensors was subsequently performed through the impedance meter.

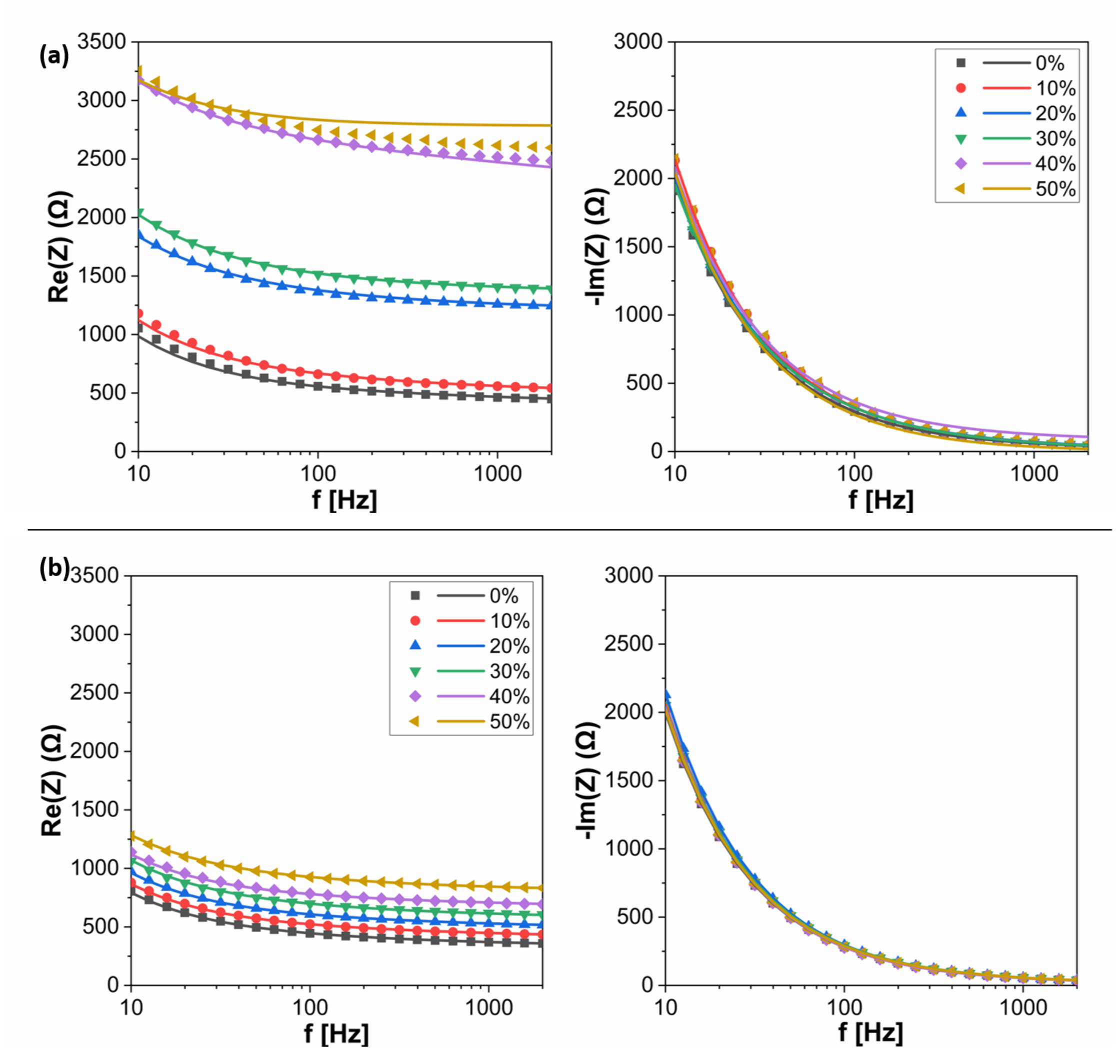

Figure 4.14: Impedance real and imaginary part variation under strains of one sensor for 4% (a) and 4%_NC (b) M-CMC concentrations. The points represent the raw data; the solid lines constitute the fitting curves

4.4 Device performances

After the selection of the electrodes material, LCR meter was employed to confirm in a statistical way the data obtained through the EIS analyses:

- the best excitation frequency to use;
- transduction mode exploitable to achieve the best performances;

- concentration of M-CMC which ensures the best trade-off between sensitivity and repeatability of measures;

Three VHB sensors with steel electrodes were prepared for each concentration of cellulose (2%, 3%, 4%, 4%_NC). They were subjected to external deformations of strain and bending during the acquisition of electrical parameters (Rp, Cp) by the impedance meter. The tensile and bending home made instruments and the Instron tensile test machine were used for these analyses.

4.4.1 Tensile test

First of all, static acquisition of 1 minute were performed for each step of the tensile home-made machine (0%, 10%, 20%, 30%, 40%, 50%). Then average values on acquisition time of Rp and Cp were derived. Since these values were rather stable for each acquisition, the standard deviations were neglected. This procedure was repeated for each sensor and thus the transfer curves were obtained. The variations of the electrical parameters (Rp and Cp) with respect to their initial values (Rp_0 and Cp_0) were plotted versus the strain applied. Trials with excitation frequencies of both 20 Hz and 1000 Hz were carried out: for each one, a new set of samples was prepared. Transfer curves of each kind of sensor were then averaged and plotted (figures 4.15 and 4.16). Firs of all, it is clear that, in piezoresistance mode, each type of sensors is more sensible to external deformations if an higher electrical frequency is applied (4.15a). On the other hand, if the capacitance is exploited, the differences between the acquisition at 20 Hz and those at 1000 Hz are significantly reduced (4.16a and b). Both in piezoresistance and piezocapacitive mode sensors hold a non-linear characteristic for this range of strain.

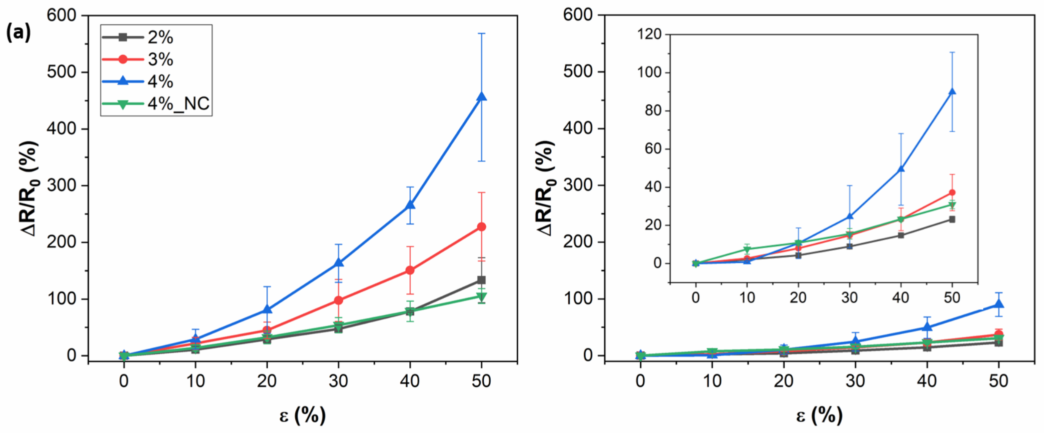

Figure 4.15: Average transfer curves of sensors used in piezoresistance mode tested at 1000 Hz (a) and 20 Hz (b). In the inset, an enlargement of the figure (b) is reported

Comparing the variations in capacitance and in resistance for each kind of device, it is evident that the latter are greater in absolute value. This fact suggest that it is better to exploit the piezoresistance transduction method for these sensors.

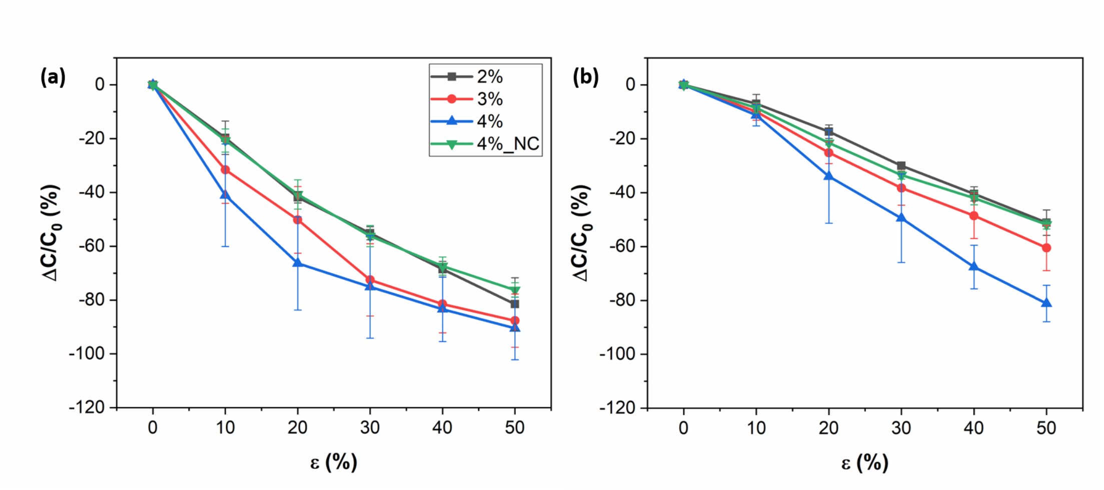

Figure 4.16: Average transfer curves of sensors used in piezocapacitive mode tested at 1000 Hz (a) and 20 Hz (b). In the inset, an enlargement of the figure (b) is reported

Observing the samples as M-CMC concentration changes, the 4% one shows the best performances: actually, the higher is the M-CMC concentration, the bigger are the variations of the electrical parameters (both Rp and Cp) for each strain step. The one exception is represented by the sensor with the hydrogel not cured (4%_NC): it holds performances similar to that with 2% hydrogel. On the other hand, the problem is that more rigid

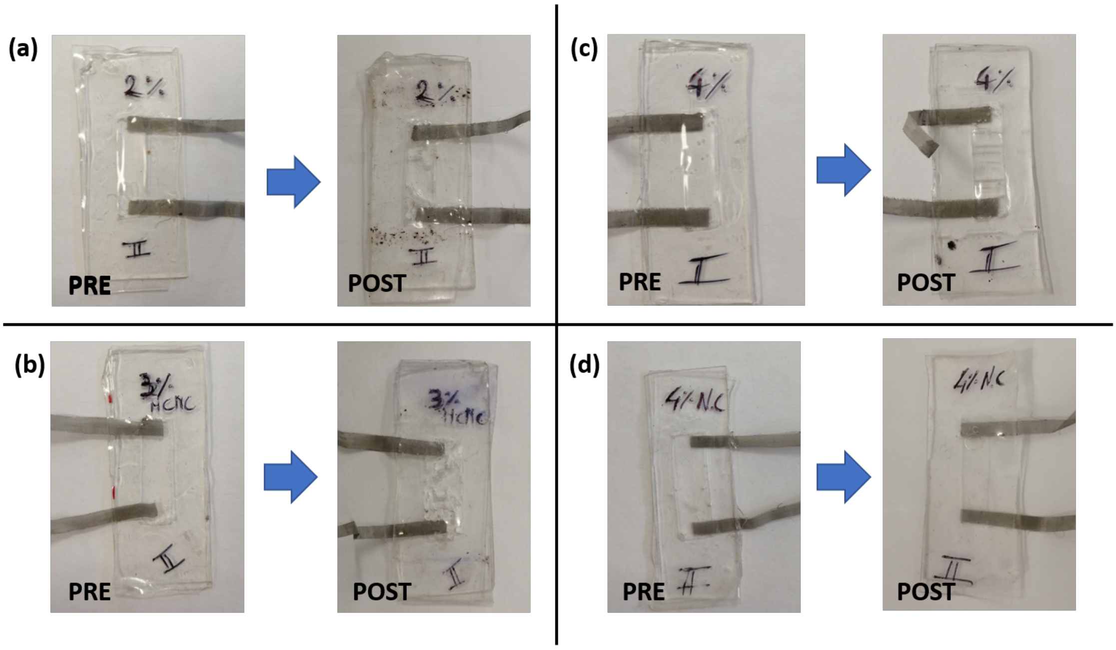

Figure 4.17: Sensors prior and after a cycle of deformation; 2% (a), 3% (b), 4% (c), 4%_NC (d) samples;

hydrogels, when are stretched, get irreversibly broken because they are brittle. Hence regions with low conductivity arise and this results in an higher variation of the electrical resistance and capacitance. Since these regions where the polymeric network undergo to rupture are not the same for all the sensors of a certain type, the error bars of the stiffer hydrogels are broader. It is possible to note visually this effect comparing the sensors prior and post a deformation cycle (figure 4.17): while the 4%_NC hydrogel does not show consistent variations, the others, after the strains, result damaged. The 4% hydrogel, the more rigid, even exhibits fractures perpendicular to the strain direction. To demonstrate this phenomenon, sensors were subjected to increasing strains, like before, and then the deformation was gradually diminished, following the same steps of the ascent. In this case, only the 1000 Hz electrical frequency was employed. Only one sensor per type was checked. Moreover, the same sensors, after the trials, were stored at room temperature for one month and then the same analyses were performed again. This last test it is useful to understand how the electrical properties could change over time. Looking the up-down

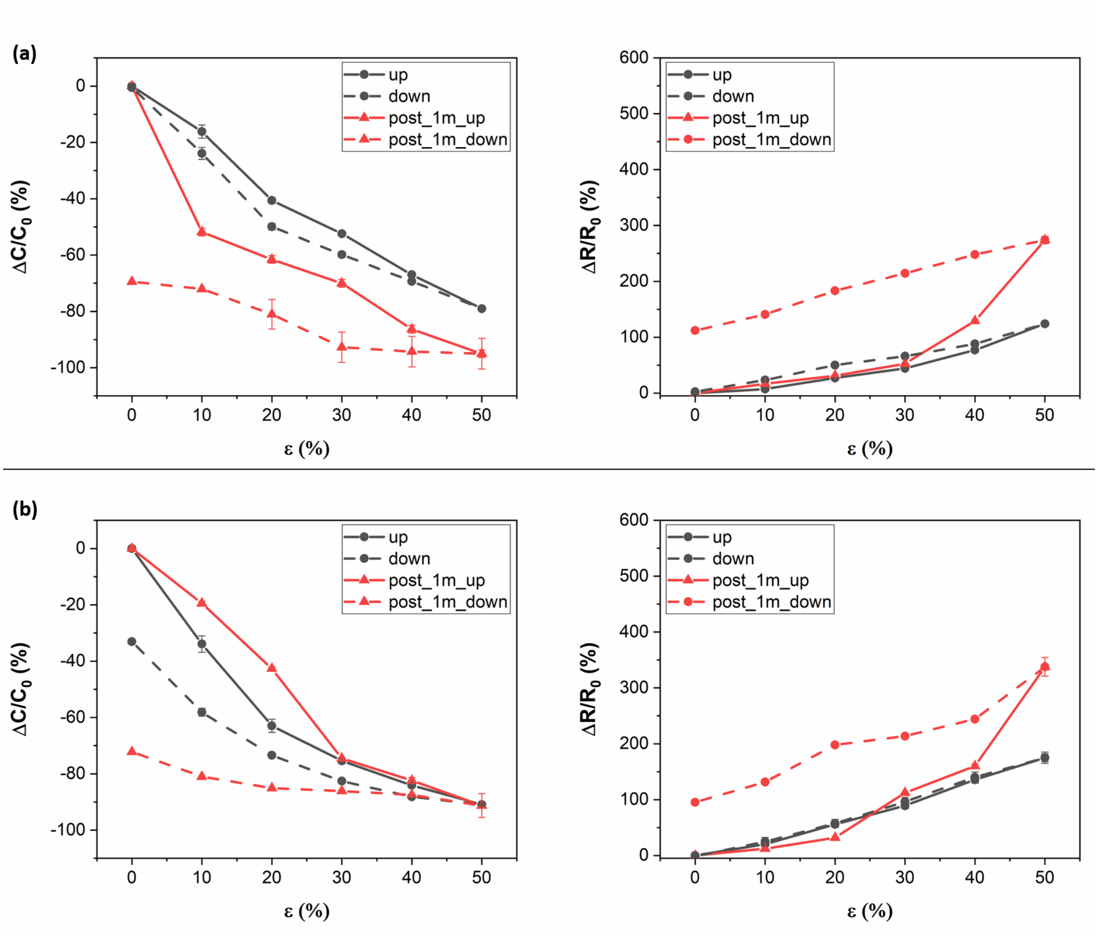

Figure 4.18: Relative variations of resistance and capacitance during loading and unloading cycle, prior and after a month of storing at 25°C, of sensors with 2% (a) and 3% (b) hydrogels

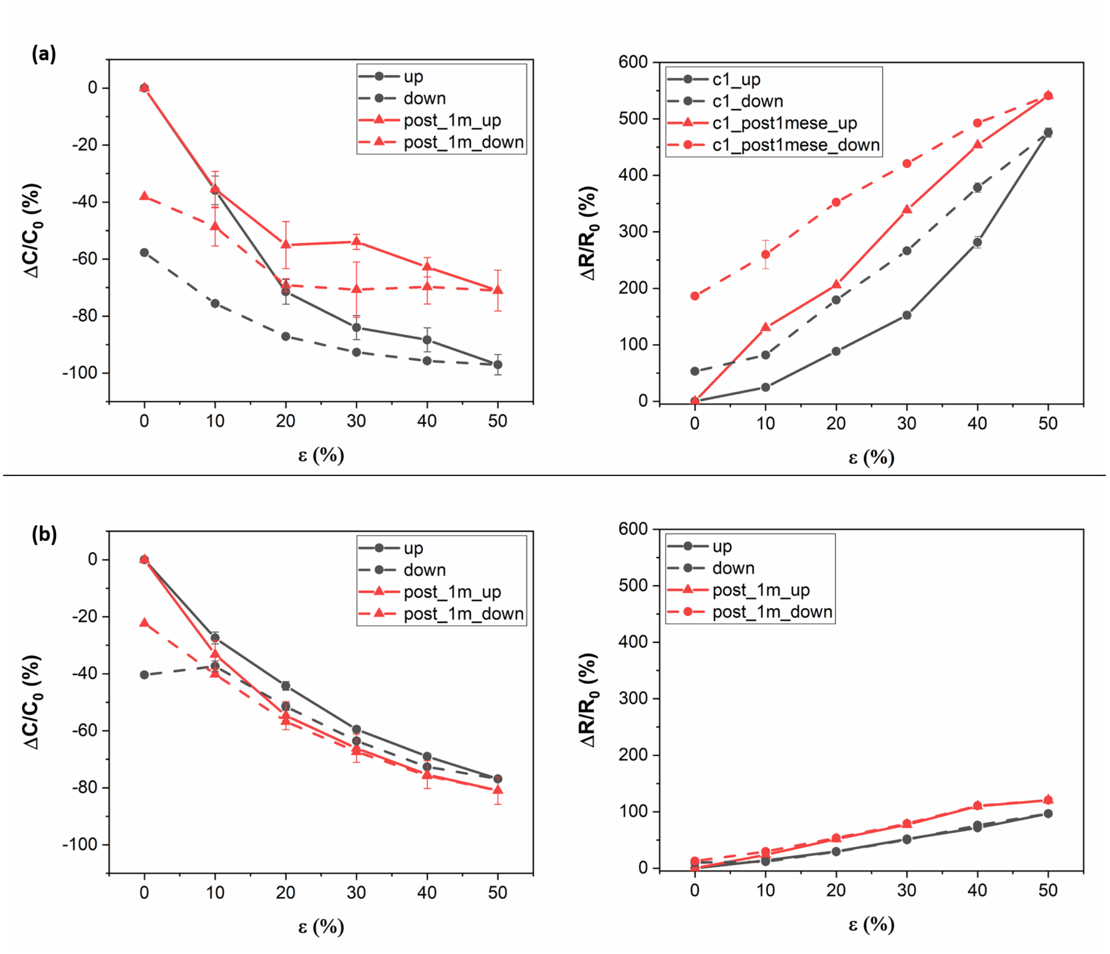

Figure 4.19: Relative variations of resistance and capacitance during loading and unloading cycle, prior and after a month of storing at 25°C, of sensors with 4% (a) and 4%_NC (b) hydrogels

cycles of the sensors prior the storage period (black lines) in figures 4.18 and 4.19, it is evident that devices with 3% and 4% of M-CMC holds electrical properties (Rp and Cp) not reversible after the deformations. This is caused by the phenomenon described earlier. In fact, the variations of resistance and capacitance of the softer hydrogels (2% and 4%_NC) return back almost at their initial values. After one month, in which water retained by the network is partially evaporated, the difference between loading and unloading curves drastically grows: the hydrogel become more dry, areas with low conductivity increase and thus the parameters variations are greater and less predictable. However, the sensor with 4%_NC shows optimal recovery of the resistance and the capacitance: this is mainly due to the absence of irreversible crosslinks among the polymeric chains and thus to the non-rupture of the hydrogel. Moreover, the electrical behavior almost does not change over the time because, even if the water evaporates, the hydrogel remains homogeneous. Therefore, according to the strain analyses, the hydrogel with 4% of CMC with respect of water is the solution that ensures the best balance between sensitivity, recovery and stability over the time.

Since the transfer curves were obtained through static measurements point by point, it

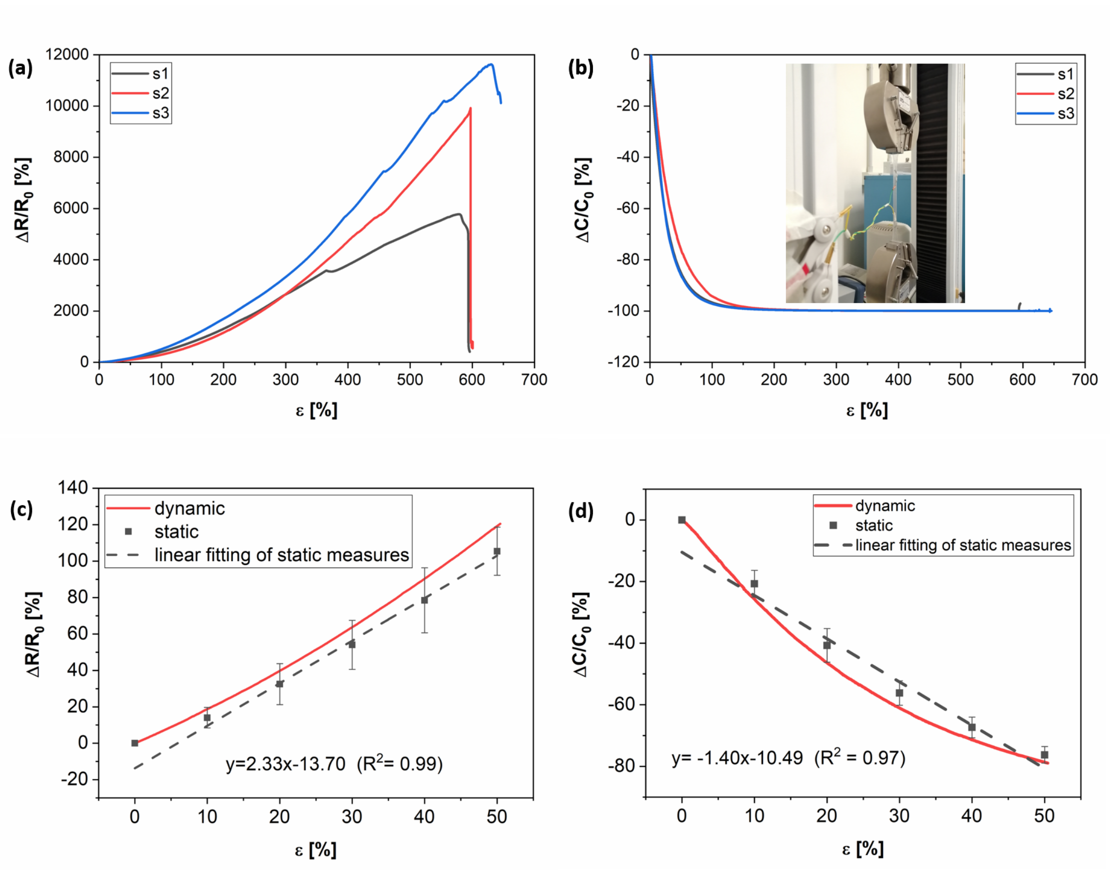

Figure 4.20: Tensile machine test of 3 samples: relative variation of resistance (a) and capacitance (b). In the inset the sensor subjected to the tensile test. Comparison of averaged transfer curves obtained through the tensile machine (dynamic) and the home made tensile instrument (by step) and its linear fitting: piezoresistance (c) and piezocapacitive (d) modes; the ideal linear transfer curves are also reported

was interesting to evaluate the electrical characteristics of the 4%_NC sensors on their entire range of deformation in a dynamic way. Hence, the tensile machine (Instron) and the LCR meter (BK Precision 894) were used and three samples were tested (s1, s2, s3). The values at rest of resistance and capacitance (R_0, C_0) were computed by averaging the initial data of the impedance acquisition, before the starting of the tensile test. In this way transfer curves ($\Delta R/R_0$ or $\Delta C/C_0$ VS strain) were computed (figure 4.20a and b). Since the mechanical properties especially depends on the VHB tape, two sensors (s1, s3) slipped away from the clamps due to its high deformability: thus the transfer curves (figure 4.20)a shows some instabilities for high strains. Therefore, the most reliable curve is that of the second sample (s2), which is the only subjected to rupture. The resistance has a linear behavior after 400% of strain and sensitivity is approximately constant ($GF \approx 24$);

for lower deformations the sensor is slightly not-linear. On the other hand, the capacitance transfer curve is similar to a exponential decay: hence, in the high deformation range (over than 100%) the value of capacitance does not change anymore and the sensor is thus unresponsive to strains. Piezoresistance mode is consequently preferable.

In figure 4.20c and d are shown two enlargement, in the range of strains 0-50%, of the averaged curves obtained from the specimens tested dynamically through the tensile machine (in this range sensors have not slipped) and those derived from samples stretched by the home-made instrument (static measurements). Since static measurements were made point by point a linear fitting is performed for these data. The transfer curves are almost the same, demonstrating that analyses performed through the home-made instrument were reliable. Moreover, in piezoresistance mode the sensor behaviour can be approximated as linear because the black dashed fitting line and the red solid one are very close: in fact, for almost all the point considered in the static acquisition, all the curves are comprised in the error bars. According to the fitted linear curves, the gauge factor is approximately 2.3. On the other hand, the capacitive behaviour shows an higher non-linear error: the experimental dynamic curve and the points relative to the static measurements, are slightly different with respect to the fitted ones. In fact, the R squared coefficient is smaller than that of the previous fitting, indicating that the linear model works worse in this case. In addition, the gauge factor, which measures about 1.4 for the fitted line, is lower compared to that of piezoresistance mode.

Tensile test machine was also employed to perform cyclic analyses: sensors were repeatedly stretched controlling the strain. In this case two sensors with 4% and 4%_NC hydrogels were examined for comparing their repeatability property. Owing to the mechanical features mainly depends on the encapsulation and VHB tape is a viscoelastic material, in the $\sigma - \epsilon$ graph an hysteresis loop is evident (figure 4.21). In these plots four consecutive cycle of stretching are shown; after the first one, the others are similar and they highlight a constant residual strain of about 10% for both the specimens. The energy dissipated in form of heat is almost the same for the two sensors, since the hysteresis cycle areas are similar.

Electrical parameters were also measured during the cyclic test. Values of resistance and

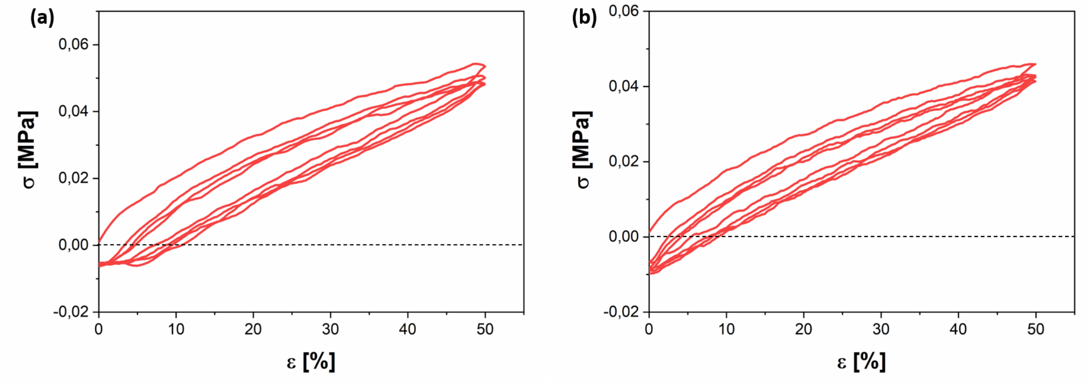

Figure 4.21: Hysteresis cycles of 4%_NC (a) and 4% (b) samples

capacitance at rest were computed as done before in the tensile test. Therefore, in figures 4.22 and 4.23, the evolution in time of the strain (ϵ), the stress (σ), the relative variations of resistance and capacitance ($\Delta R/R_0$ and $\Delta C/C_0$) are reported. Observing the graphs of the 4%_NC sample (figure 4.22), both resistance and capacitance vary in a repeatable way during the cycles. Moreover, resistance signal holds a shape similar to that of the tension applied (σ). Only the first two cycles are slightly different from the others, because the system need to reach stability condition. Rather, the sample with the 4% cured hydrogel (figure 4.23) holds unstable electrical properties in the different cycles. This can be seen more accurately in figure 4.24, in which the relative variations of electrical parameters with respect to the strain applied are reported for subsequent cycles. As regards the sensor with the not-cured hydrogel (figure 4.24a), the cycles following the first one show an optimal repeatability of both resistance and capacitance variation except for the small deformations. In fact, the resistance and capacitance do not perfectly return to their initial values: the former tends to increase (up to 10%) as the number of cycles grows, while the latter decreases (up to -30%), as it is shown by the curved arrows. However, after several cycles, the offset seems to become more similar to that of the previous cycles, indicating that sensor has reached a more stable state. On the other hand, for the sample based on cured hydrogel (figure 4.24b) it is clear that there is no repeatability of measures. These studies confirm again that stiffer hydrogels are irreversibly damaged if they are subjected to excessive deformations.

From these results, it is clear that the hydrogel composed of CMC not cured is the best solution for flexible sensors because ensure the greater reproducibility between measures and, in addition, it remains homogeneous also after water evaporation, resulting in a increased durability. Higher electrical frequencies (such as 1000 Hz) and piezoresistance mode ensure the best performances in a whole range of strains (up to 600%). However, for little deformation, also piezocapacitive mode could be exploited, since the sensitivity does not change drastically compared to the other transduction method.

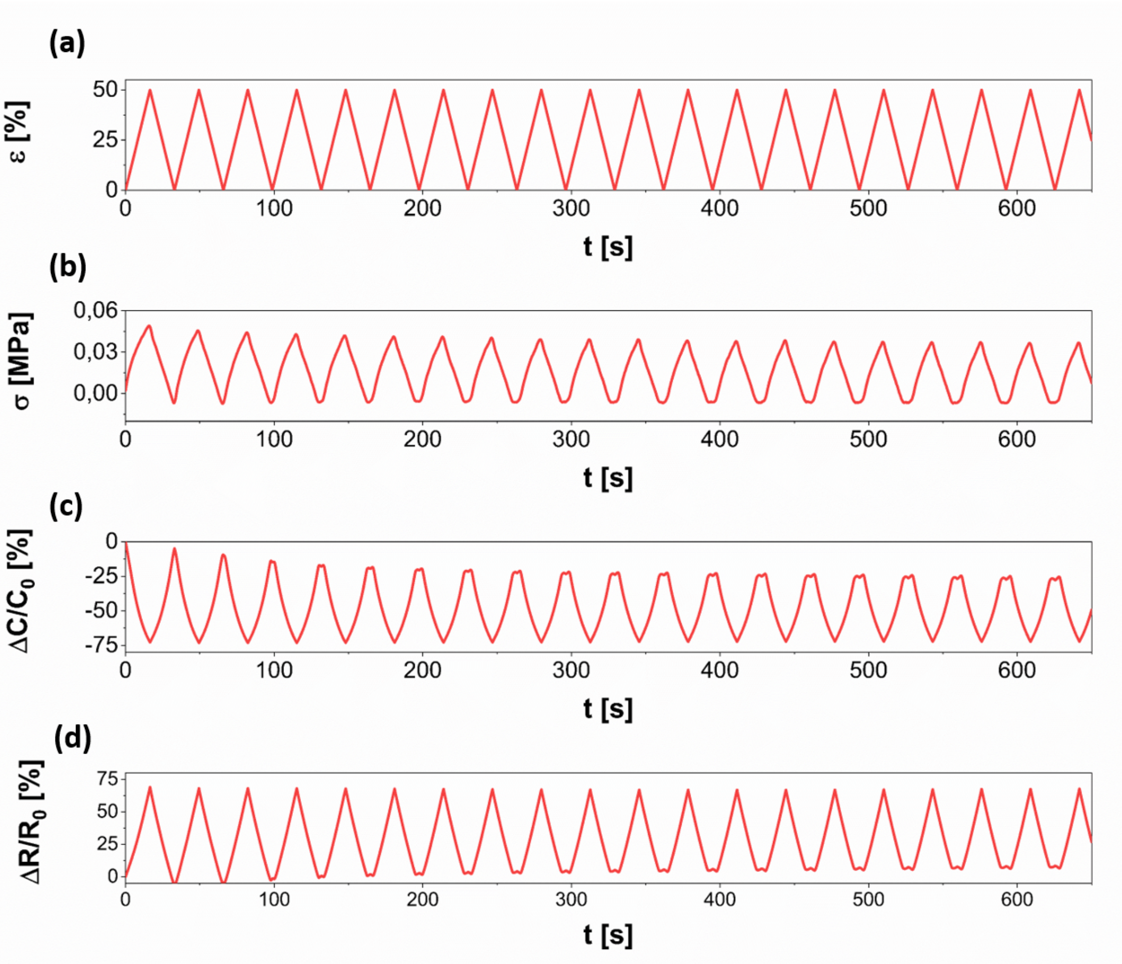

Figure 4.22: Electrical behavior under cyclic strain stimuli for 4%_NC: strain (a), stress (b), capacitance (c) and resistance (d) relative variations with respect to time.

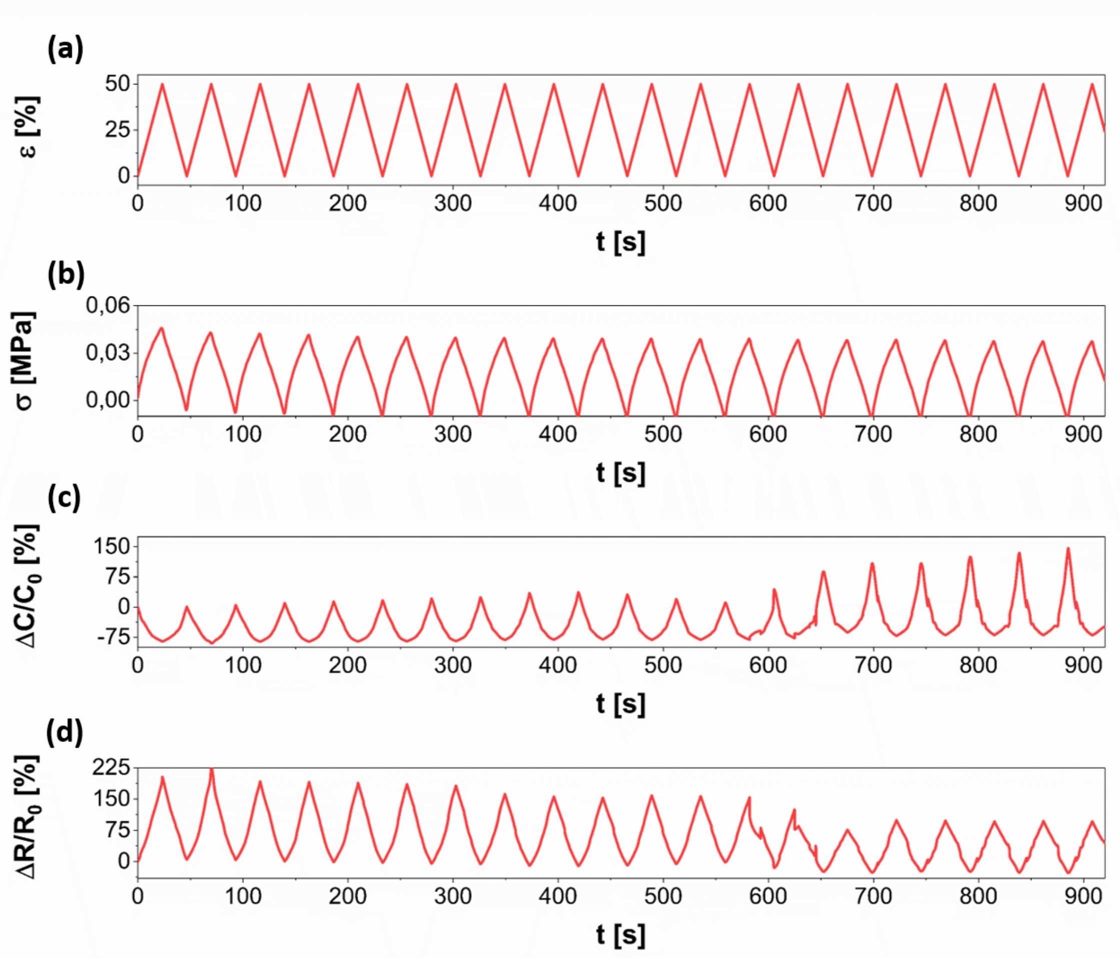

Figure 4.23: Electrical behavior under cyclic strain stimuli for 4%: strain (a), stress (b), capacitance (c) and resistance (d) relative variations with respect to time.

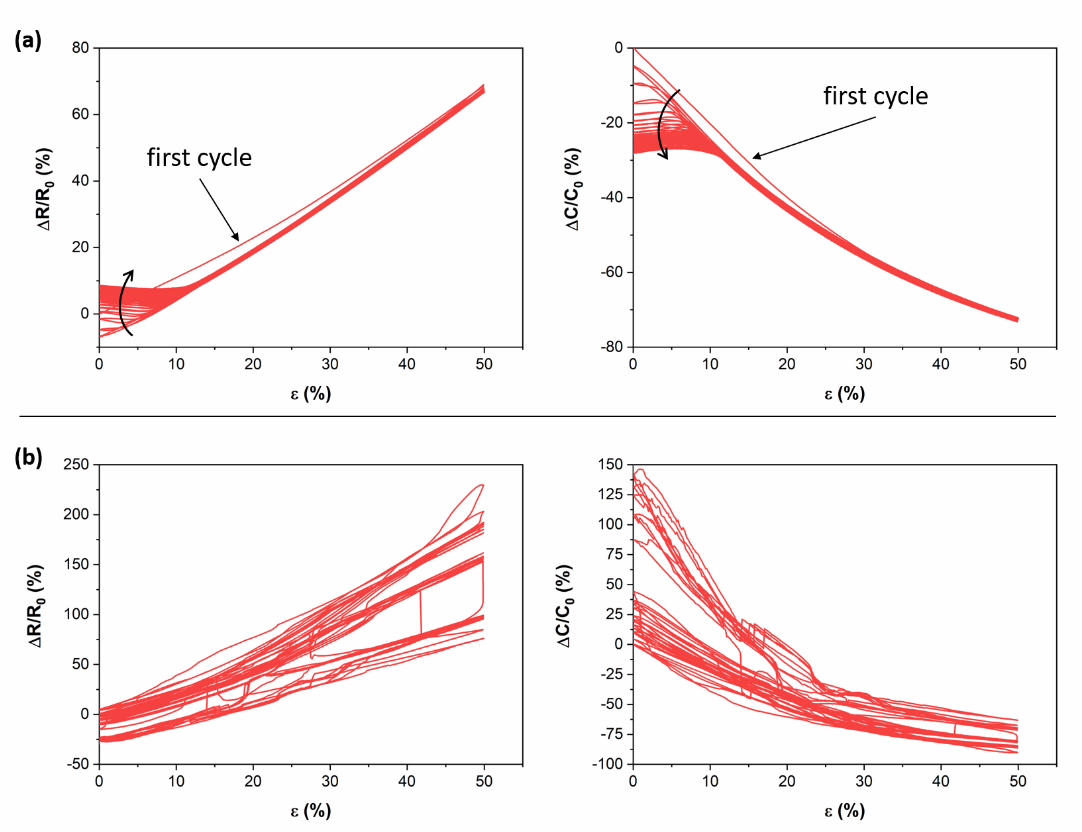

Figure 4.24: Relative variation of resistance (on the left) and capacitance (on the right) with respect to strain for 4%_NC (a) and 4% (b) sensors

4.4.2 Comparison between EIS and LCR data

Therefore, these outcomes confirm what has been achieved through the EIS analyses. In fact, the real and imaginary part of impedance can be derived from R_p and C_p according to these formulae:

$$Re(Z) = \frac{R_p}{1 + (\omega R_p C_p)^2};\ Im(Z) = \frac{R_p^2 C_p}{1 + (\omega R_p C_p)^2}; \tag{4.1}$$

where ω is the pulse ($\omega = 2\pi f$). Therefore, for each point of the average transfer curve shown in figure 4.16 the real and imaginary part of impedance are computed. Then, from EIS data (section 4.3), for each strain step, the value of Re(Z) and Im(Z) were extracted at 20 Hz and 1000 Hz. In both case the relative variations of the real and imaginary part with respect to their values at rest are derived. In figures 4.25 and 4.26 are plotted the curves obtained through the potentiostat and the LCR meter for the four kinds of sensor.

Considering that the potentiostat data are relative to a single sample, there is a good similarity between the two set of data. In fact, it is evident that the variations of the real part are strongly greater than those of the imaginary one. This confirms that the EIS analysis can represent another tool to investigate ionic conductivity sensors.

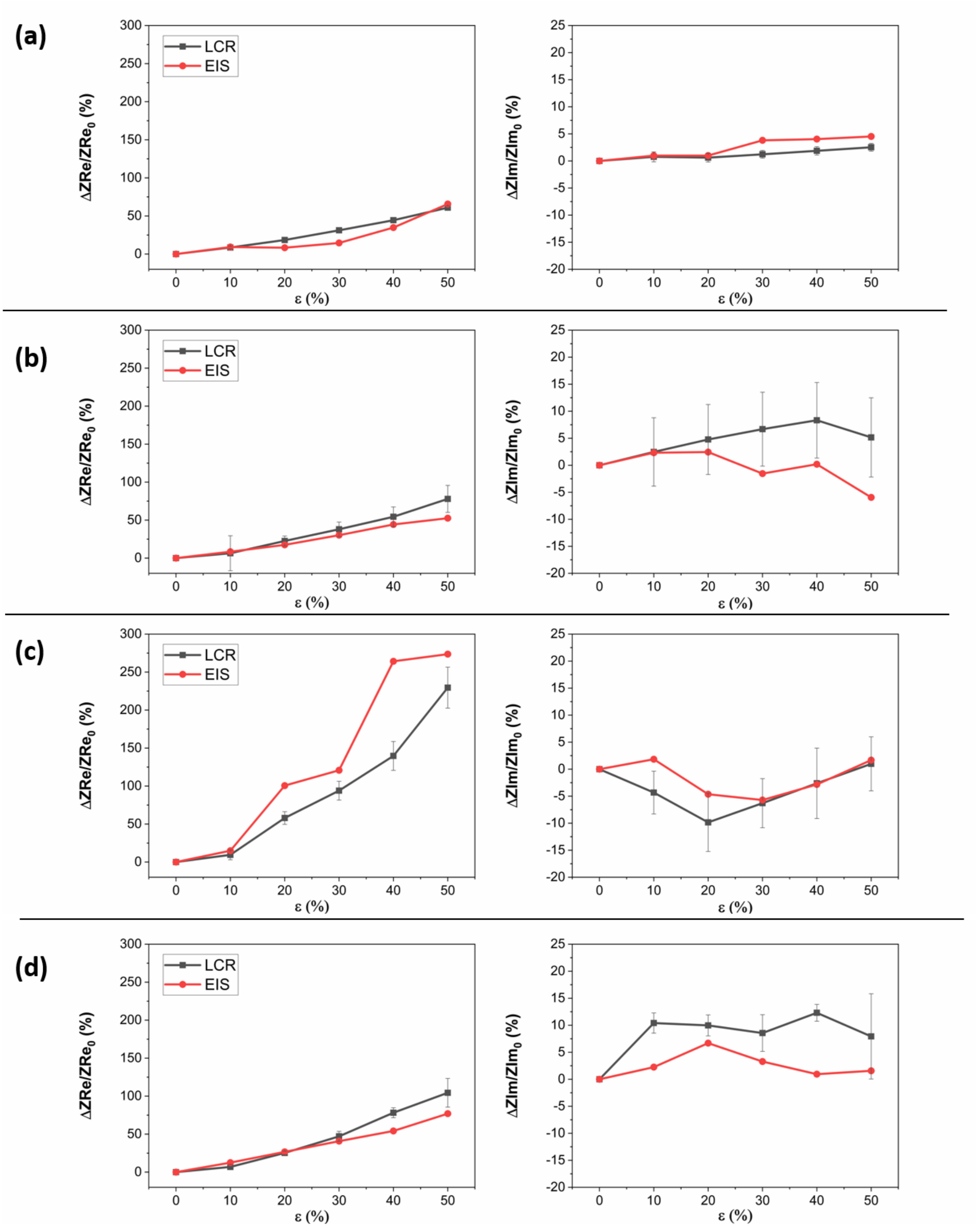

Figure 4.25: Comparison between LCR and EIS acquisitions at 20 Hz: relative variation of the real (on the left) and the imaginary (on the right) part of impedance for 2% (a) 3% (b) 4% (c) and 4%_NC (d) sensors

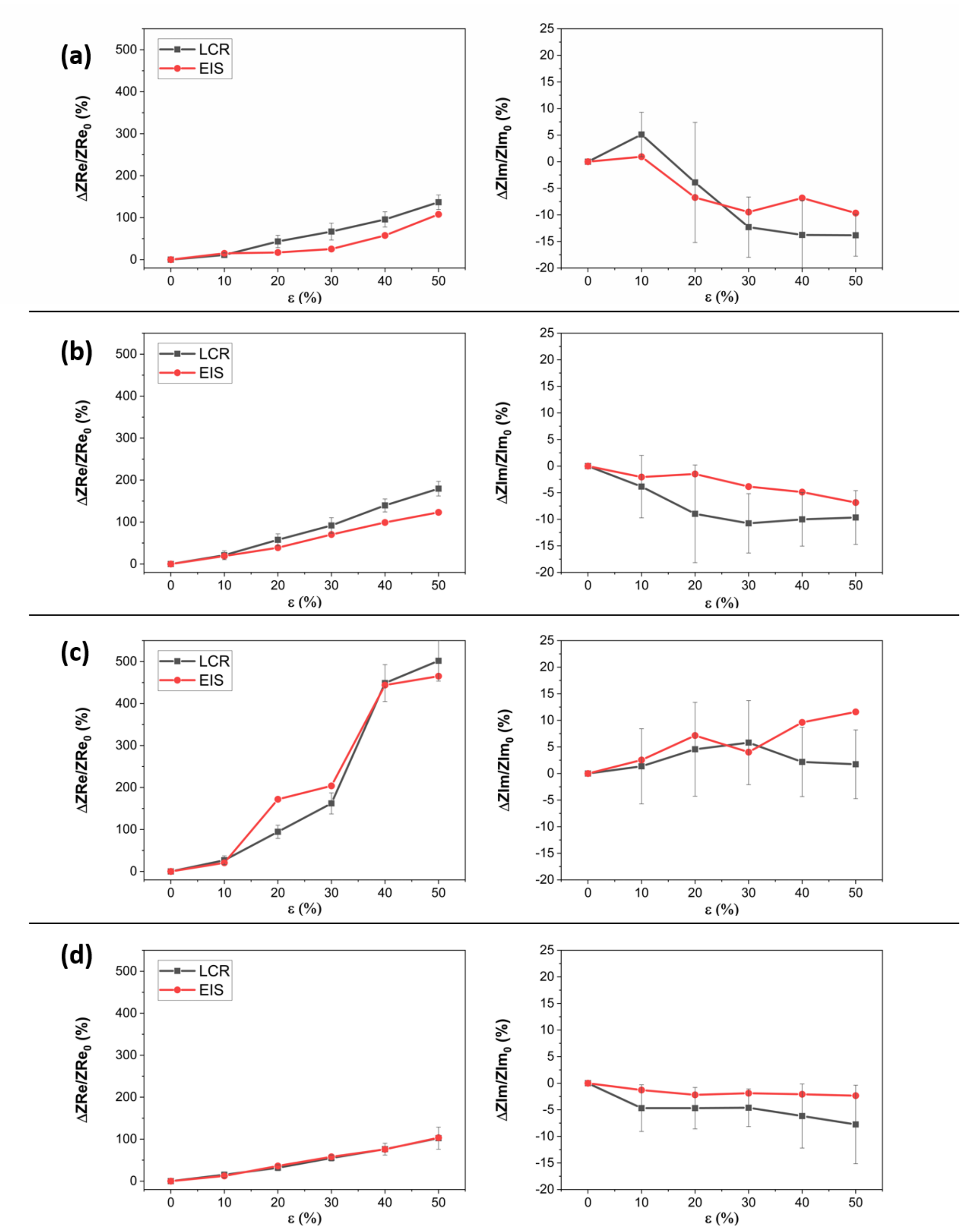

Figure 4.26: Comparison between LCR and EIS acquisitions at 1000 Hz: relative variation of the real (on the left) and the imaginary (on the right) part of impedance for 2% (a) 3% (b) 4% (c) and 4%_NC (d) sensors

4.4.3 Bending test

Similarly to the stretching test, bending analyses were performed through the home-made bending instrument presented in section 3.2.5. Since, from the previous evaluations, higher electrical frequencies ensure greater sensitivity, the frequency of 1000 Hz was used for all the following analyses. Static acquisition of 1 minute (voltage amplitude of 0.5 V) for different curvature radii (15 cm, 9 cm, 5 cm, 3 cm and 2,5 cm) were done. Then average values on acquisition time of Rp and Cp were derived. Since these values were rather stable for each acquisition, the standard deviations were neglected. After the loading part (in which the radii was diminished gradually), unloading acquisitions were also carried out. For each type of hydrogel (2%, 3%, 4% and 4%_NC) three specimens were tested. Figures 4.27 and 4.28 show the loading (up) and unloading (down) curves of single samples (s1, s2, s3). On the x-axis the reciprocal of the curvature radii is reported, for convenience. The relative variation of resistance or capacitance compared to their values at rest, are

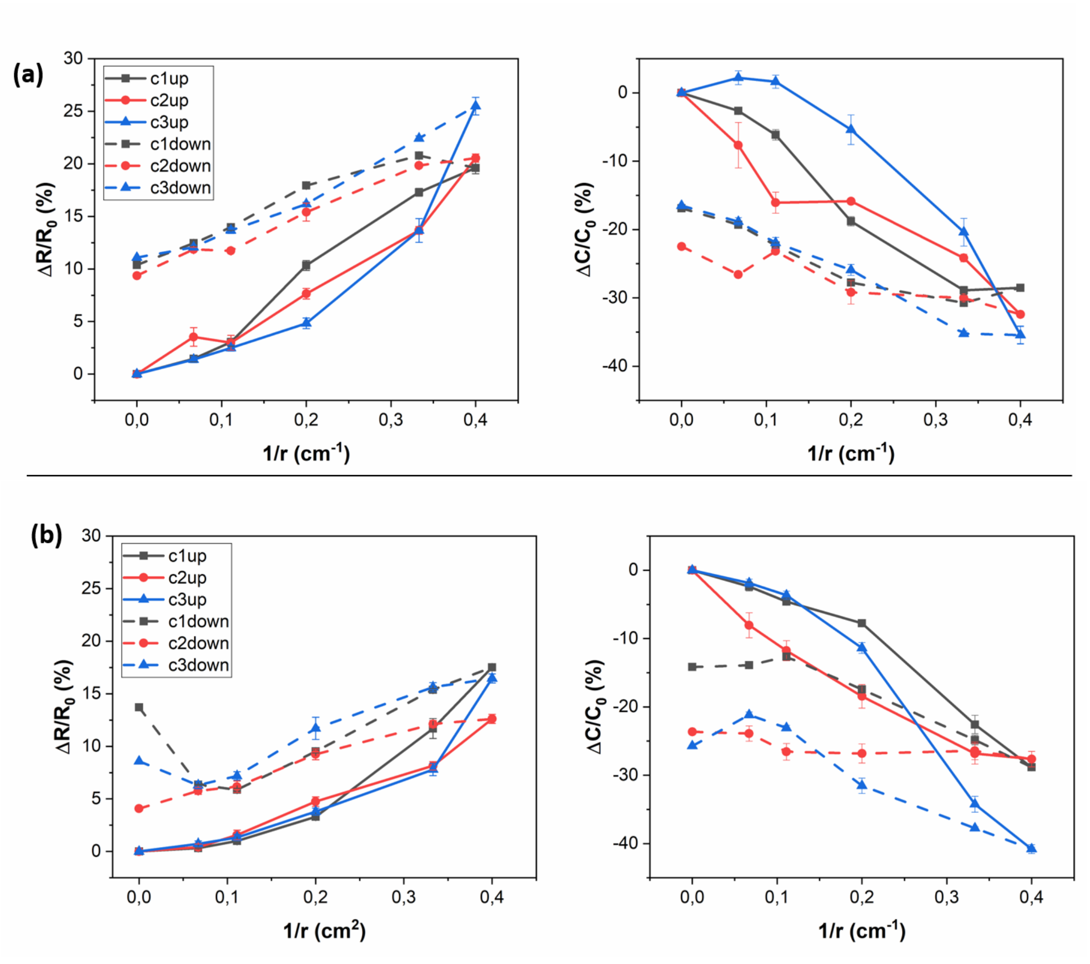

Figure 4.27: Bending test of devices with 2% (a) and 3% (b) hydrogels: loading and unloading of single specimens

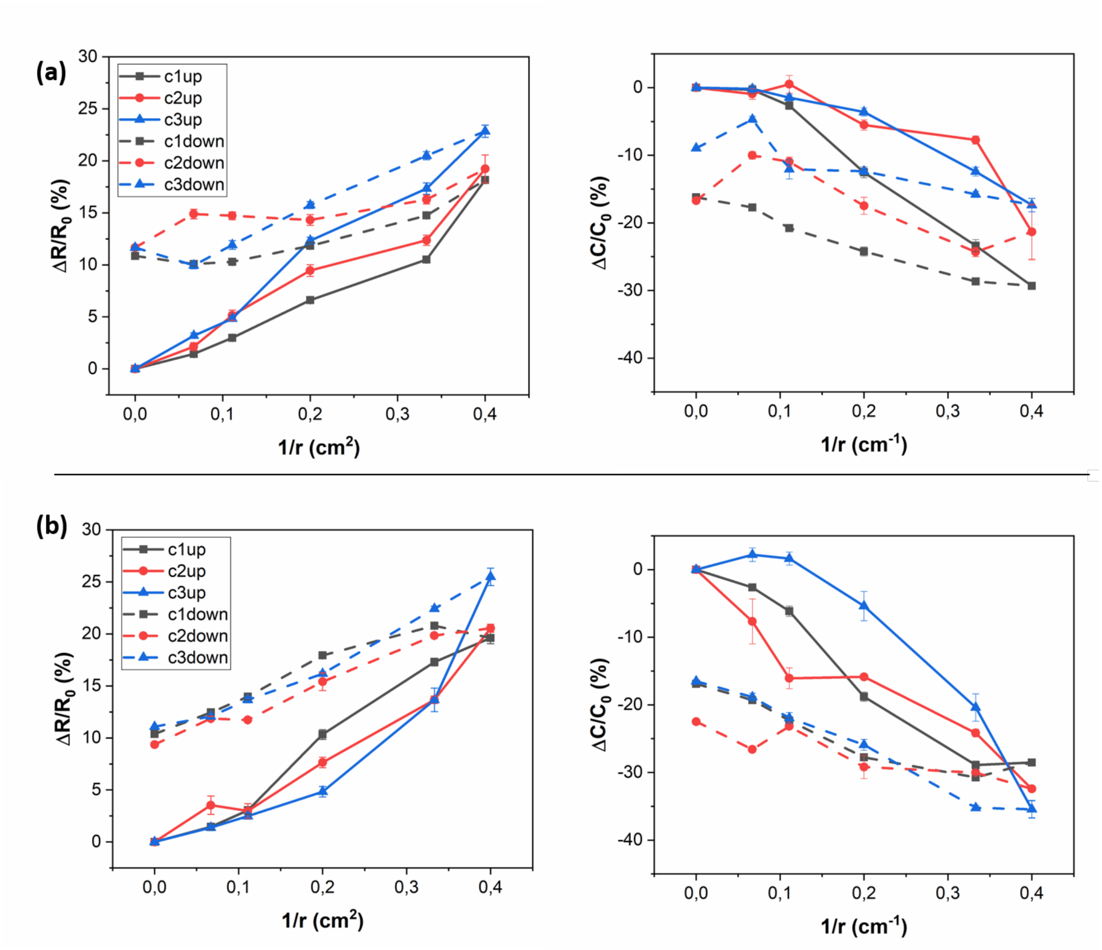

Figure 4.28: Bending test of devices with 4% (a) and 4%_NC (b) hydrogels: loading and un-loading of single specimens

set out on the ordinate axis. It is evident that no sample of any kind holds a perfect recoverability of electrical properties. In contrast to tensile test, 4%_NC hydrogel also does not recover its initial resistance and capacitance (figure 4.27d). This is mainly due to the rubber stripes in which the sensor is held: after the bending they do not return to the initial shapes resulting in a residual bending of the sensor. Therefore, this instrument is not the best solution to test the recoverability after bending stimuli.
However, observing the ascent curves, it is possible to derive an average transfer curve considering the three samples of each cellulose concentration considered (figure 4.29). First of all, both the resistance ad the capacitance shows a non-linear behavior. The resistance increases and the capacitance decreases as the bending becomes greater. This behavior is similar to that found with stretching stimuli. As regards the piezoresistance, the more rigid is the hydrogel, the higher are the variations of resistance. This attitude is not reflected by the capacitance, in which the 4% hydrogel is the least sensitive (in absolute value): in fact, also in this case, the electrical parameters changes strongly depends on the places in

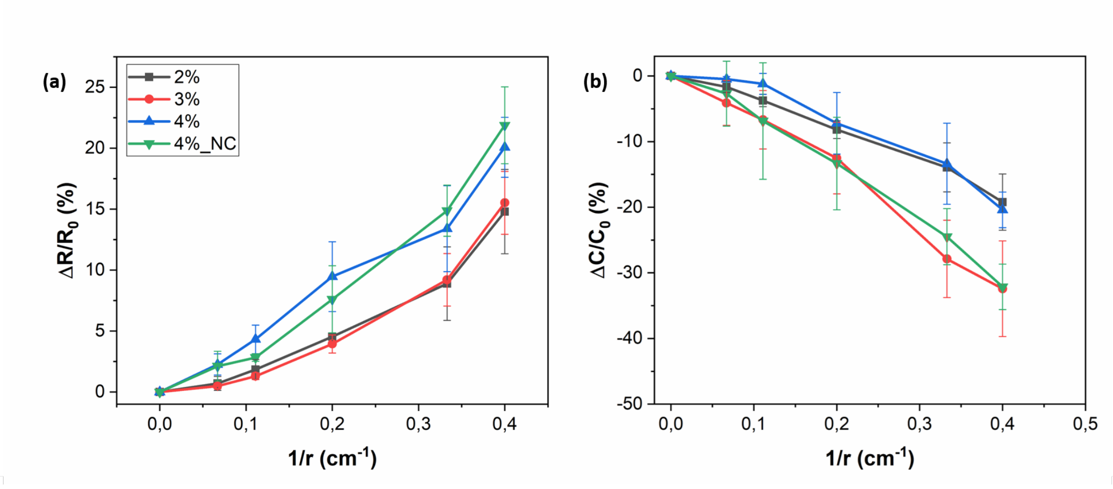

Figure 4.29: Transfer curves of sensors subjected to bending stimuli: piezoresistance (a) and piezocapacitive (b) mode

which the polymeric network breaks down.
The hydrogel not cured (4%_NC) seems to have the best performances in both the transduction methods. Owing to its superior softness, it is slightly pressed between the two rubber stripes while the bending stimuli are applied, resulting in higher variations of resistance and capacitance. Hence, the curves of the 4%_NC hydrogel mainly reflect the bending stimuli, but, in part, also the pressure. This effect is reduced in the other types of sample, due to the crosslinked hydrogels that are more rigid and thus oppose to pressure until they get damaged.
Moreover, while in the stretching analyses the piezoresistance mode was preferable, in this case the sensitivity to external bending stimuli is slightly greater if piezocapacitive transduction method is exploited. However there is no consistent differences between the two modes in this range of curvature radii. Therefore, piezoresistance mode could be equally used. These analyses show that, under bending stimuli, sensors with different hydrogels holds similar behaviors. Nevertheless the solution with 4%_NC is always the best, because it ensures repeatability of measures since the hydrogel remains homogeneous also after external deformations.

4.4.4 Temperature dependency

Since was demonstrated that the 4%_NC hydrogel based sensor owned the best overall performances, the temperature dependency was analyzed only for this kind of device. LCR meter acquisition for each step of temperature lasted about 1 minutes and so average values of Rp and Cp were derived neglecting the standard deviations, since the measures were quite stable. Then transfer curves for the piezoresistance and piezocapacitive modes are computed averaging those of the three samples tested. The points of the static acquisition and their linear fittings are reported in figure 4.30. The resistance Rp exhibits a negative quasi-linear relationships with respect to the temperature rise. In fact, when temperature increases, ions mobility becomes higher and thus ionic conductivity is boosted. In parallel, the VHB encapsulation dilates causing changes of geometry of the devices. These effects result in a decreasing of the resistance. The sensitivity of the fitted curve is about 1 %°C^{-1}. On the other hand, capacitance own a positive stronger linear temperature dependency ($R^2 = 0.999$) compared to that of the resistance ($R^2 = 0.979$): it increases when temperature rises mainly due to geometric effect. In this case, sensitivity measures about 3 % °C^{-1} , resulting higher than that found for the piezoresistive mode.

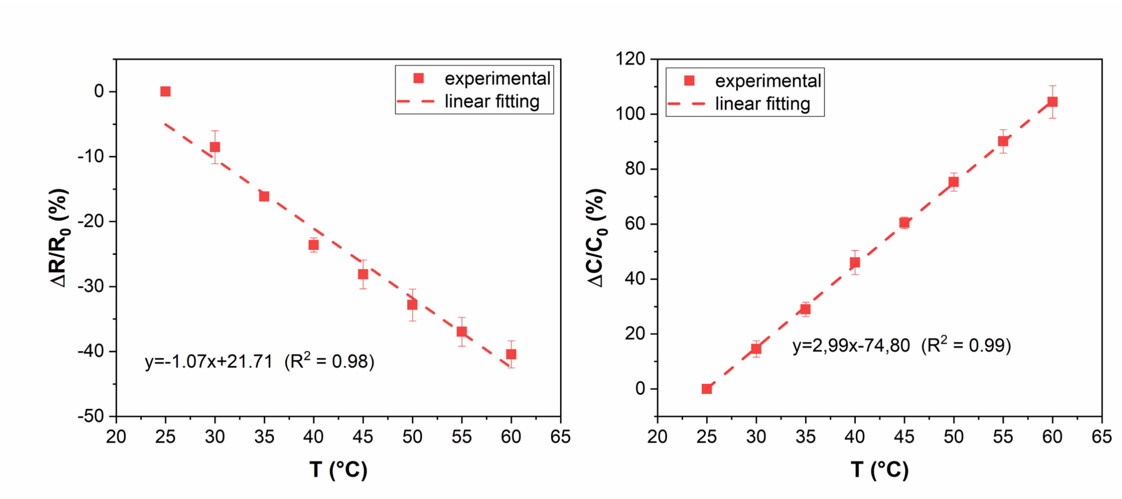

Figure 4.30: Temperature dependency of electrical parameters: piezoresistance (a) and piezocapacitive (b) mode

Therefore, the piezocapacitive transduction method is preferable to use owing to its excellent linearity and superior sensitivity. This analysis suggests that the cellulose based devices presented in this work could be also employed in temperature sensing. Applications in high temperature environments must be certainly avoided because the hydrogel water evaporates more quickly and thus sensors durability drastically decreases. Strain-temperature flexible devices find applications in a wider number of fields. However, it is not possible to sense strain applied and temperature in the same time, since both the stimuli affect electrical parameters (Rp and Cp) and thus, if both temperature and strain are unknown, their contributes cannot be separated. Therefore, these devices, if are used for strains sensing, need to be applied at a fixed temperature and vice versa.

4.4.5 Applications

VHB sensors with 4%_NC hydrogel were finally employed as wearable devices to detect physiological signals. Piezoresistance transduction mode was exploited to convert the mechanical deformations of the human body into electrical signals. Resistance variations were detected by the BK precision 894 LCR meter (1000 Hz of electrical frequency).

First of all, ionic conductivity was verified through the implementation of a sensor in series to a light emitting diode (LED): this series was connected to a voltage source, as it is shown in figure 4.31a. When the device is twisted or stretched its electrical resistance increase

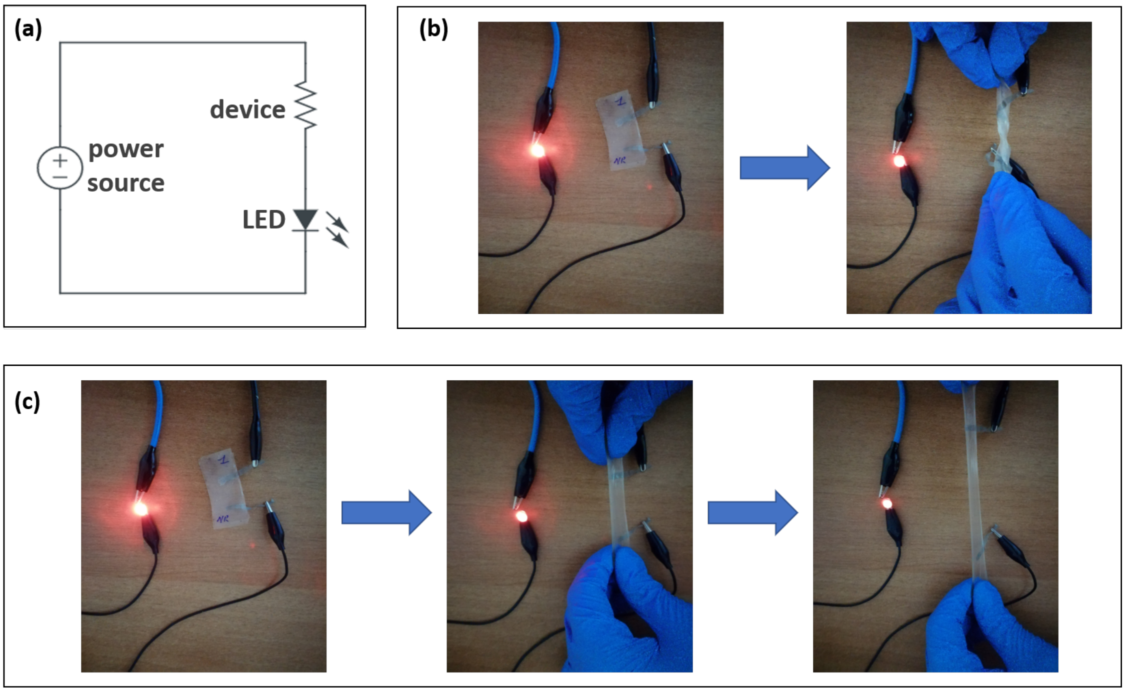

Figure 4.31: (a) Presentation of the circuit in which the sensor (device) is used as conductor; LED brightness changes when the sensor is subjected to twisting (b) and to different strains (c)

and the LED brightness consequently decrease (figures 4.31b and c).
Then, in order to assess the potential applicability to monitoring human signals, the sensor was stuck on the wrist for sensing the peripheral pulse wave. This pressure signal derives from the arterial vessels wall dilatation, caused by the blood ejected from the left ventricle during the systole. A first acquisition was done with the patient at rest (figure 4.32a). Then, another trial was performed after mild physical activity (figure 4.32b). The sensor was left stuck in the same position. From these data, it is easy to derive the heart rate by counting the peaks of the pulse wave: in fact, comparing the frequency before and after the exercise, the beats per minutes increased from 60 to 84. Moreover, it is possible to find similarities with the typical shape of the pulse wave in the radial artery presented in figure 4.32c. In almost all the waves the dichrotic notch, which corresponds to the semilunar valves closure at the end of the systolic phase, is distinguishable. Rather, the inflection point is barely visible. However it appears in some pressure waves, like the one presented in figure 4.32c. Thus, in this case, a more rigid ionogel, which holds an higher sensitivity, or a geometry that promotes the piezocapacitive effect, could be useful. However, these trials shows that the sensor is applicable as a non-invasive method to continuously monitor the pulse rate. Moreover, from the analyses of pulse wave shape several cardiovascular parameters, which are helpful in diagnosis and prognostic, can be extracted [5].
Another field of possible applications is the detection of human joint movement. The sensor was applied on a finger (inset in figure 4.33a) to record its bending. From graph 4.33a, it is evident that the sensor holds an optimal repeatability in successive bending cycles.

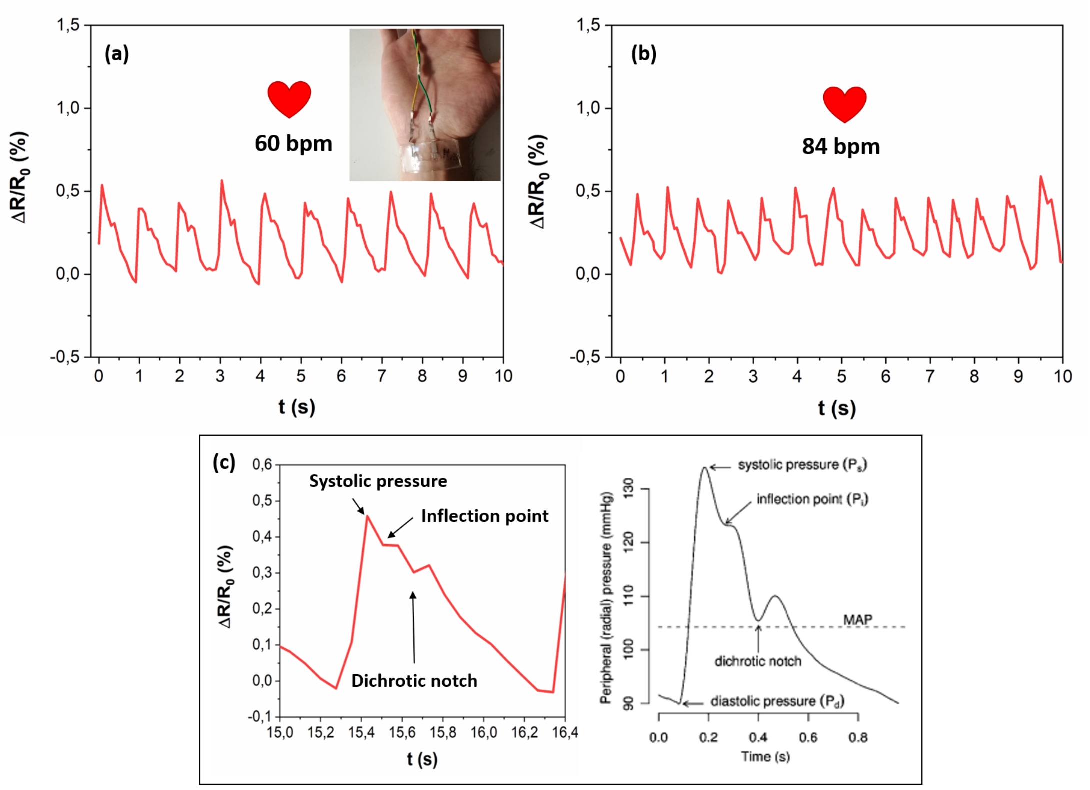

Figure 4.32: Pulse rate monitoring at rest (a) and after physical activity (b); in the inset the positioning of the sensor; (c) on the left, the shape of the radial pressure measured; on the right, the typical radial pressure shape [116]

The finger was also bent step by step, as can be seen from the insets in figure 4.33b. As a consequence, the resistance increase gradually and, when the finger is held at a certain angle, it is quite stable (figure 4.33). Since the finger movement is detected, the sensor is certainly applicable for sensing motion of other joints, such as the elbow or the knee. Therefore, it could constitute a minimally invasive and aesthetic solution for ensuring a continuous monitoring in rehabilitation field.

The sensor, stuck on the throat of the patient (inset of figure 4.34a) can also measure the vibration of vocal chords while speaking. In figure 4.34 laugh of different duration are recognized: whenever "ah" is pronounced, a peak in the resistance signal is recorded. These findings suggest that the tactile sensor could be employed in real-time speech detection instead of microphones, that are unreliable in overcrowded environments [117].

VHB sensor good sensitivity makes it applicable also for muscular activity identification for those muscles which are closer to the skin surface. In fact it was applied on the muscular flexors of the fingers, located in the forearm, and the hand was repeatedly closed as shown in the inset of figure 4.34b. The resistance pattern show in figure 4.34b demonstrates that the device is able to sense deformations caused by the muscles contraction. Also in this

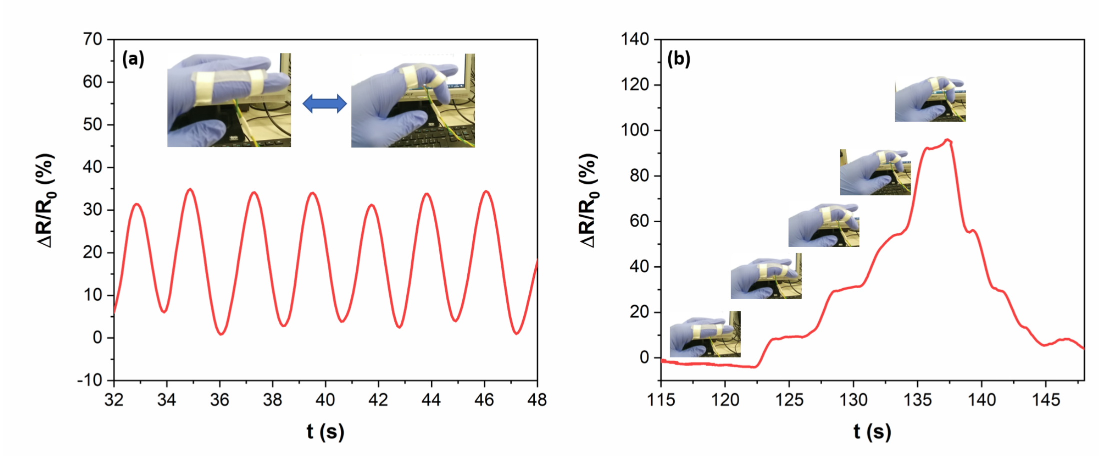

Figure 4.33: Finger bending monitoring: (a) repeatability of measures when different cycles of bending are performed (b) resistance signal in reaction to different bending angles (shown in the insets)

case a quite good repeatability of resistance variation is achieved, considering that the patient is unable to perfectly replicate the same movement. As a consequence, for instance, these flexible sensors could be also employed in amputee prosthetic controlled by extrinsic muscles.

These examples proves that the VHB strain sensors based on cellulose hydrogels could find employment in various biomedical fields such as continuous health monitoring, detection of muscular activities and joint motions. They show a good versatility, because they are able to perceive both large and subtle deformations, indeed. Therefore, they represent ideal devices for bridging the human world with the robotic one, since they could be integrated into textiles, used as e-skin for soft robots or employed in prosthetic to reproduce haptic sensation, for instance.

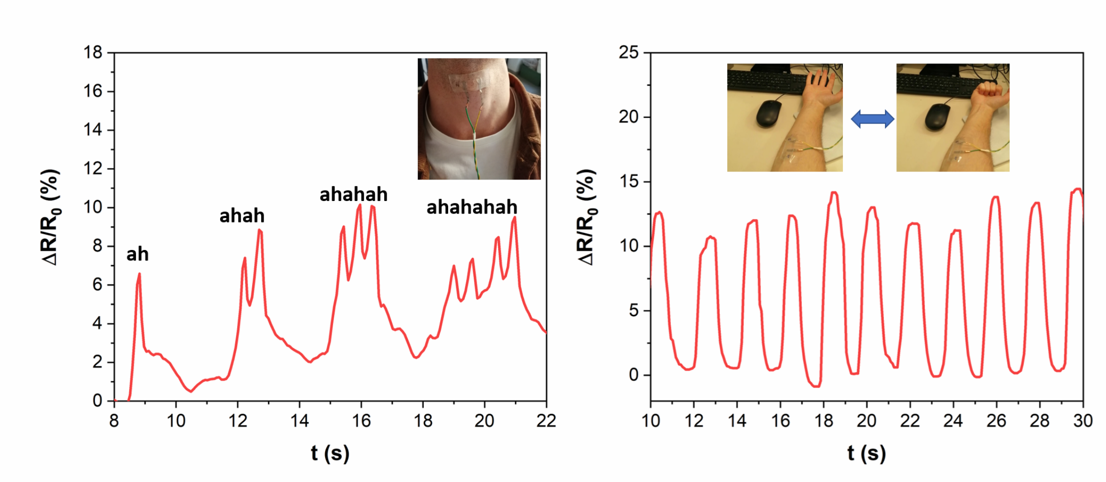

Figure 4.34: (a) Vocal cord vibrations detection when "ah", "ahah", "ahahah", "ahahahah" are pronounced; (b) Detection of fingers muscular flexors activity when the hand is closed

Conclusion

In summary, here, a flexible transparent tactile sensor based on green hydrogel is investigated. A sandwich-like configuration was chosen to build it: the sensitive part, namely the hydrogel, was enclosed between two shells of an elastic material, indeed. Two flat electrodes were placed in contact with the hydrogel to provide the connection with the external environment. The electrical conductivity was given by the ions of a salt (NaCl) dispersed in the precursor solution of the hydrogel, which, for this reason, is also called "ionogel". Methacrylated carboxymethylcellulose (M-CMC), a widely available cellulose derivative, was employed for the sensitive part, because it is reactive to UV light, making simpler the hydrogel preparation.

Three materials were investigated for the shells: polydimethylsiloxane (PDMS), TRAD (an acrylic UV curable elastomer) and the commercial VHB tape. PDMS showed a good stretchability but its too long curing process (24h at room temperature) was a problem because hydrogel water drastically evaporates during this time. As regards the TRAD encapsulations production, three solutions with different concentrations of photoinitiators were examined: no differences were found about the reactivity and the mechanical performances. However the solution with lower concentration of photoinitiators was selected owing to its superior transparency. TRAD shells could be cured rapidly through UV light avoiding long production time. Moreover, they could be 3D printed through DLP method, allowing an excellent repeatability between samples. TRAD unfortunately held the lowest flexibility and transparency and thus was discarded. Therefore, VHB tape was selected for the further test, due to its outstanding stretchability (up to $\sim 600\%$), optimal transparency, adhesiveness and sensor manufacturing easiness and quickness.

In parallel, the influence of salt molarity (0.5 M, 1 M, 2 M) on reactivity and mechanical behavior of M-CMC hydrogel was assessed through photoreology. No discrepancies were found and thus 1 M was chosen as salt molarity for the subsequent analyses. In the same way, different concentrations (2%, 3%, 4%) of M-CMC were tested, showing that the higher is the M-CMC content, the greater are the stiffness and brittleness of hydrogel. An additional hydrogel (4%_NC) made of commercial carboxymethylcellulose (CMC) was also taken into account due to its softness.

Electrochemical impedance spectroscopy (EIS) were carried out to find a equivalent electrical model of the sensors. These test, performed while the sensors were stretched, were also useful to find the best material for electrodes, among stainless steel, titanium, copper-kapton and copper-kapton-copper. Stainless steel sensors proved to be the optimal solution due to the electrodes resistance to corrosion and their good sensitivity to external deformations.

EIS results showed also that higher electrical frequencies (such as 1000Hz) ensured greater electrical parameter changes when external strains were applied, with respect to lower ones (like 20Hz).
To validate this results and to choose the best concentration of M-CMC for hydrogels, an impedance meter was applied to measure the electrical properties of sensor while they were stretched or bent. Both parallel resistance and capacitance were measured to assess the best working mode. Devices with higher cellulose content held the highest sensitivity to the external deformation. However, this is due to the irreversibly rupture of the hydrogel network after external stimuli application, resulting in poor repeatability of measures. Therefore, it was found that the softest hydrogel (4%_NC) represents the best trade-off between good sensitivity, durability and repeatability. Moreover piezoresistance working mode had the best performances and linearity (gauge factor of $\sim$ 24) especially for higher strains (400%-600%). Whereas, for lower deformations, the resistance shows a behaviour closer to the linear one, with a greater gauge factor (2.3) with respect to that of the piezocapacitance mode (1.4).
Temperature dependency of the sensors based on the not cured hydrogel was further investigated. A positive linear relationship between the capacitance variation and the temperature was found. Moreover the sensitivity ($3\ ^{\circ}\mathrm{C}^{-1}$) was higher than that of the piezoresistance mode, which showed a slightly non-linear behaviour. These studies demonstrates the possible application of this hydrogel based devices both for strain and temperature: however they are not able to sense simultaneously both the kinds of stimuli due to the mutual action that strain and temperature play on the electrical properties of the devices. VHB based sensors with 4%_NC hydrogel were then applied to the human body to monitor physiological signals and motions. It was demonstrated their applicability for both large deformations (like joint motion) and tiny ones (radial artery pulse wave, vocal chord vibrations and muscle contractions) detection.
Therefore, this sandwich-like sensor could represent a good starting point to achieve a transparent and easy manufacturable tactile device usable in various field, like wearables, soft robotics, artificial intelligence and health monitoring. However, further studies involving these kind of devices could be carried on:

- increase the number of samples for mechanical, electrical and electrochemical characterization analyses;
- a deeper investigation on the encapsulation materials, such as water permeability analyses and skin-compatibility test;
- multi-material 3D printing of TRAD and M-CMC hydrogel, to increment reproducibility and make easier the manufacturing processes;
- examine the effect of salt molarity on devices performances;
- finding a way to fix electrodes to the sensor in a more stable manner;
- maintaining adhesive the VHB tape after several applications;
- trying to change sensors configuration for promoting pressure sensing;
- conditioning circuitry for elaborating signals;

- portable and lightweight power supplies;

In this way, a comprehensive characterization of this kind of devices would be performed, overcoming the current limitations, in order that their effective applicability, scalability and large scale manufacturing can be assessed.

Bibliography

[1] H. B. Helbig and M. O. Ernst, "Optimal integration of shape information from vision and touch," *Experimental Brain Research*, vol. 179, no. 4, pp. 595–606, 2007.

[2] M. O. Ernst and M. S. Banks, "Humans integrate visual and haptic information in a," *Nature*, vol. 415, no. January, pp. 429–433, 2002.

[3] Z. Wang, Y. Cong, and J. Fu, "Stretchable and tough conductive hydrogels for flexible pressure and strain sensors," *Journal of Materials Chemistry B*, vol. 8, no. 16, pp. 3437–3459, 2020.

[4] M. Park, B. G. Bok, J. H. Ahn, and M. S. Kim, "Recent advances in tactile sensing technology," *Micromachines*, vol. 9, no. 7, 2018.

[5] V. Suresh Kumar and C. Krishnamoorthi, "Development of electrical transduction based wearable tactile sensors for human vital signs monitor: Fundamentals, methodologies and applications," *Sensors and Actuators, A: Physical*, vol. 321, 2021.

[6] S. Xia, S. Song, F. Jia, and G. Gao, "A flexible, adhesive and self-healable hydrogel-based wearable strain sensor for human motion and physiological signal monitoring," *Journal of Materials Chemistry B*, vol. 7, no. 30, pp. 4638–4648, 2019.

[7] Z. Lei, Q. Wang, S. Sun, W. Zhu, and P. Wu, "A Bioinspired Mineral Hydrogel as a Self-Healable, Mechanically Adaptable Ionic Skin for Highly Sensitive Pressure Sensing," *Advanced Materials*, vol. 29, no. 22, pp. 1–6, 2017.

[8] C. Pang, G. Y. Lee, T. I. Kim, S. M. Kim, H. N. Kim, S. H. Ahn, and K. Y. Suh, "A flexible and highly sensitive strain-gauge sensor using reversible interlocking of nanofibres," *Nature Materials*, vol. 11, no. 9, pp. 795–801, 2012.

[9] J. Wang, F. Tang, Y. Wang, Q. Lu, S. Liu, and L. Li, "Self-Healing and Highly Stretchable Gelatin Hydrogel for Self-Powered Strain Sensor," *ACS Applied Materials and Interfaces*, vol. 12, no. 1, pp. 1558–1566, 2020.

[10] H. Liu, M. Li, C. Ouyang, T. J. Lu, F. Li, and F. Xu, "Biofriendly, Stretchable, and Reusable Hydrogel Electronics as Wearable Force Sensors," *Small*, vol. 14, no. 36, pp. 1–9, 2018.

[11] E. Marin, F. Boschetto, and G. Pezzotti, "Biomaterials and biocompatibility: An historical overview," *Journal of Biomedical Materials Research - Part A*, vol. 108, no. 8, pp. 1617–1633, 2020.

[12] E. Roh, B.-u. Hwang, D. Kim, B.-y. Kim, and N.-e. Lee, "Sensor for Human À Machine Interfaces Comprising a Nanohybrid of Carbon," *ACS Nano*, no. 6, pp. 6252–6261, 2015.

[13] L. Han, L. Yan, M. Wang, K. Wang, L. Fang, J. Zhou, J. Fang, F. Ren, and X. Lu, "Transparent, Adhesive, and Conductive Hydrogel for Soft Bioelectronics Based on

Light-Transmitting Polydopamine-Doped Polypyrrole Nanofibrils," *Chemistry of Materials*, vol. 30, no. 16, pp. 5561–5572, 2018.

[14] Y. Liang, X. Sun, Q. Lv, Y. Shen, and H. Liang, "Fully physically cross-linked hydrogel as highly stretchable, tough, self-healing and sensitive strain sensors," *Polymer*, vol. 210, no. July, p. 123039, 2020.

[15] D. Jones, L. Wang, A. Ghanbari, V. Vardakastani, A. E. Kedgley, M. D. Gardiner, T. L. Vincent, P. R. Culmer, and A. Alazmani, "Design and evaluation of magnetic hall effect tactile sensors for use in sensorized splints," *Sensors (Switzerland)*, vol. 20, no. 4, pp. 1–13, 2020.

[16] B. Ward-Cherrier, N. Pestell, L. Cramphorn, B. Winstone, M. E. Giannaccini, J. Rossiter, and N. F. Lepora, "The TacTip Family: Soft Optical Tactile Sensors with 3D-Printed Biomimetic Morphologies," *Soft Robotics*, vol. 5, no. 2, pp. 216–227, 2018.

[17] J. Konstantinova, A. Stilli, and K. Althoefer, "Fingertip fiber optical tactile array with two-level spring structure," *Sensors (Switzerland)*, vol. 17, no. 10, pp. 1–13, 2017.

[18] C. H. Chuang, H. K. Weng, J. W. Chen, and M. O. Shaikh, "Ultrasonic tactile sensor integrated with TFT array for force feedback and shape recognition," *Sensors and Actuators, A: Physical*, vol. 271, pp. 348–355, 2018.

[19] Y. Lin, S. Liu, S. Chen, Y. Wei, X. Dong, and L. Liu, "A highly stretchable and sensitive strain sensor based on graphene-elastomer composites with a novel double-interconnected network," *Journal of Materials Chemistry C*, vol. 4, no. 26, pp. 6345–6352, 2016.

[20] M. L. Hammock, A. Chortos, B. C. Tee, J. B. Tok, and Z. Bao, "25th anniversary article: The evolution of electronic skin (E-Skin): A brief history, design considerations, and recent progress," *Advanced Materials*, vol. 25, no. 42, pp. 5997–6038, 2013.

[21] C. Shao, M. Wang, L. Meng, H. Chang, B. Wang, F. Xu, J. Yang, and P. Wan, "Mussel-Inspired Cellulose Nanocomposite Tough Hydrogels with Synergistic Self-Healing, Adhesive, and Strain-Sensitive Properties," *Chemistry of Materials*, vol. 30, no. 9, pp. 3110–3121, 2018.

[22] Y. Al-Handarish, O. M. Omisore, T. Igbe, S. Han, H. Li, W. Du, J. Zhang, and L. Wang, "A Survey of Tactile-Sensing Systems and Their Applications in Biomedical Engineering," *Advances in Materials Science and Engineering*, vol. 2020, 2020.

[23] C. Metzger, E. Fleisch, J. Meyer, M. Dansachmüller, I. Graz, M. Kaltenbrunner, C. Keplinger, R. Schwödiauer, and S. Bauer, "Flexible-foam-based capacitive sensor arrays for object detection at low cost," *Applied Physics Letters*, vol. 92, no. 1, pp. 1–4, 2008.

[24] H. K. Lee, J. Chung, S. I. Chang, and E. Yoon, "Normal and shear force measurement using a flexible polymer tactile sensor with embedded multiple capacitors," *Journal of Microelectromechanical Systems*, vol. 17, no. 4, pp. 934–942, 2008.

[25] J. Heikenfeld, A. Jajack, J. Rogers, P. Gutruf, L. Tian, T. Pan, R. Li, M. Khine, J. Kim, J. Wang, and J. Kim, "Wearable sensors: Modalities, challenges, and prospects," *Lab on a Chip*, vol. 18, no. 2, pp. 217–248, 2018.

[26] D. J. Lipomi, M. Vosgueritchian, B. C. Tee, S. L. Hellstrom, J. A. Lee, C. H. Fox, and Z. Bao, "Skin-like pressure and strain sensors based on transparent elastic films

of carbon nanotubes," *Nature Nanotechnology*, vol. 6, no. 12, pp. 788–792, 2011.

[27] J. A. Dobrzynska and M. A. Gijs, "Polymer-based flexible capacitive sensor for three-axial force measurements," *Journal of Micromechanics and Microengineering*, vol. 23, no. 1, 2013.

[28] J. Y. Sun, C. Keplinger, G. M. Whitesides, and Z. Suo, "Ionic skin," *Advanced Materials*, vol. 26, no. 45, pp. 7608–7614, 2014.

[29] R. Puers, "Capacitive sensors: When and how to use them," *Sensors and Actuators: A. Physical*, vol. 37-38, no. C, pp. 93–105, 1993.

[30] M. Y. Cheng, C. L. Lin, Y. T. Lai, and Y. J. Yang, "A polymer-based capacitive sensing array for normal and shear force measurement," *Sensors (Switzerland)*, vol. 10, no. 11, pp. 10211–10225, 2010.

[31] A. Ballato, "Piezoelectricity: History and new thrusts," *Proceedings of the IEEE Ultrasonics Symposium*, vol. 1, pp. 575–583, 1996.

[32] D. Damjanovic, "Ferroelectric, dielectric and piezoelectric properties of ferroelectric thin films and ceramics - Abstract - Reports on Progress in Physics," *Reports on Progress in Physics*, vol. 61, no. dc, p. 1267, 1998.

[33] R. Delmdahl, C. L. Gmbh, and C. Kg, "Laser lift-off : reducing device heights in micro electronics by means of substrate transfer," *Photonik international*, pp. 2–4, 2013.

[34] K. I. Park, J. H. Son, G. T. Hwang, C. K. Jeong, J. Ryu, M. Koo, I. Choi, S. H. Lee, M. Byun, Z. L. Wang, and K. J. Lee, "Highly-efficient, flexible piezoelectric PZT thin film nanogenerator on plastic substrates," *Advanced Materials*, vol. 26, no. 16, pp. 2514–2520, 2014.

[35] G. T. Davis, "Piezoelectric polymer transducers.," *Advances in dental research*, vol. 1, no. 1, pp. 45–49, 1987.

[36] C. Chang, V. H. Tran, J. Wang, Y. K. Fuh, and L. Lin, "Direct-write piezoelectric polymeric nanogenerator with high energy conversion efficiency," *Nano Letters*, vol. 10, no. 2, pp. 726–731, 2010.

[37] J. B. Park, M. S. Song, R. Ghosh, R. K. Saroj, Y. Hwang, Y. Tchoe, H. Oh, H. Baek, Y. Lim, B. Kim, S.-W. Kim, and G.-C. Yi, "Highly sensitive and flexible pressure sensors using position- and dimension-controlled ZnO nanotube arrays grown on graphene films," *NPG Asia Materials*, vol. 13, no. 1, pp. 1–9, 2021.

[38] D. P. Cotton, P. H. Chappell, A. Cranny, N. M. White, and S. P. Beeby, "A novel thick-film piezoelectric slip sensor for a prosthetic hand," *IEEE Sensors Journal*, vol. 7, no. 5, pp. 752–761, 2007.

[39] J. Tao, R. Bao, X. Wang, Y. Peng, J. Li, S. Fu, C. Pan, and Z. L. Wang, "Self-Powered Tactile Sensor Array Systems Based on the Triboelectric Effect," *Advanced Functional Materials*, vol. 29, no. 41, pp. 1–23, 2019.

[40] H. Zou, Y. Zhang, L. Guo, P. Wang, X. He, G. Dai, H. Zheng, C. Chen, A. C. Wang, C. Xu, and Z. L. Wang, "Quantifying the triboelectric series," *Nature Communications*, vol. 10, no. 1, pp. 1–9, 2019.

[41] S. Wang, L. Lin, Y. Xie, Q. Jing, S. Niu, and Z. L. Wang, "Sliding-triboelectric nanogenerators based on in-plane charge-separation mechanism," *Nano Letters*, vol. 13, no. 5, pp. 2226–2233, 2013.

[42] S. Wang, Y. Xie, S. Niu, L. Lin, and Z. L. Wang, "Freestanding triboelectric-layer-based nanogenerators for harvesting energy from a moving object or human motion in

contact and non-contact modes," *Advanced Materials*, vol. 26, no. 18, pp. 2818–2824, 2014.

[43] Y. Han, Y. Han, X. Zhang, L. Li, C. Zhang, J. Liu, G. Lu, H. D. Yu, and W. Huang, "Fish Gelatin Based Triboelectric Nanogenerator for Harvesting Biomechanical Energy and Self-Powered Sensing of Human Physiological Signals," *ACS Applied Materials and Interfaces*, vol. 12, no. 14, pp. 16442–16450, 2020.

[44] E. M. Ahmed, "Hydrogel: Preparation, characterization, and applications: A review," *Journal of Advanced Research*, vol. 6, no. 2, pp. 105–121, 2015.

[45] M. Bahram, N. Mohseni, and M. Moghtader, "An Introduction to Hydrogels and Some Recent Applications," *Emerging Concepts in Analysis and Applications of Hydrogels*, 2016.

[46] M. Hamidi, A. Azadi, and P. Rafiei, "Hydrogel nanoparticles in drug delivery," *Advanced Drug Delivery Reviews*, vol. 60, no. 15, pp. 1638–1649, 2008.

[47] L. Zhang, K. Li, W. Xiao, L. Zheng, Y. Xiao, H. Fan, and X. Zhang, "Preparation of collagen – chondroitin sulfate – hyaluronic acid hybrid hydrogel scaffolds and cell compatibility in vitro," *Carbohydrate Polymers*, vol. 84, no. 1, pp. 118–125, 2011.

[48] T. Ogata, K. Nagayoshi, T. Nagasako, S. Kurihara, and T. Nonaka, "Synthesis of hydrogel beads having phosphinic acid groups and its adsorption ability for lanthanide ions," *Reactive and Functional Polymers*, vol. 66, no. 6, pp. 625–633, 2006.

[49] W. Zhang, P. Feng, J. Chen, Z. Sun, and B. Zhao, "Electrically conductive hydrogels for flexible energy storage systems," *Progress in Polymer Science*, vol. 88, pp. 220–240, 2019.

[50] K. Mohana Raju and M. Padmanabha Raju, "Synthesis of novel superabsorbing copolymers for agricultural and horticultural applications," *Polymer International*, vol. 50, no. 8, pp. 946–951, 2001.

[51] D. A. Gyles, L. D. Castro, J. O. C. Silva, and R. M. Ribeiro-Costa, "A review of the designs and prominent biomedical advances of natural and synthetic hydrogel formulations," *European Polymer Journal*, vol. 88, no. 01, pp. 373–392, 2017.

[52] J. Sun, Y. Wang, S. Dou, C. Ruan, and C. Hu, "PEG derived hydrogel: A novel synthesis route under mild condition," *Materials Letters*, vol. 67, no. 1, pp. 215–218, 2012.

[53] N. A. Peppas, J. Z. Hilt, A. Khademhosseini, and R. Langer, "Hydrogels in biology and medicine: From molecular principles to bionanotechnology," *Advanced Materials*, vol. 18, no. 11, pp. 1345–1360, 2006.

[54] J. J. Sperinde and L. G. Griffith, "Synthesis and characterization of enzymatically-cross-linked poly(ethylene glycol) hydrogels," *Macromolecules*, vol. 30, no. 18, pp. 5255–5264, 1997.

[55] K. Varaprasad, G. M. Raghavendra, T. Jayaramudu, M. M. Yallapu, and R. Sadiku, "A mini review on hydrogels classification and recent developments in miscellaneous applications," *Materials Science and Engineering C*, vol. 79, pp. 958–971, 2017.

[56] A. S. Hoffman, "Hydrogels for biomedical applications," *Advanced Drug Delivery Reviews*, vol. 64, no. SUPPL., pp. 18–23, 2012.

[57] H. Yuk, B. Lu, and X. Zhao, "Hydrogel bioelectronics," *Chemical Society Reviews*, vol. 48, no. 6, pp. 1642–1667, 2019.

[58] S. Adhikari and P. Banerji, "Polyaniline composite by in situ polymerization on a swollen PVA gel," *Synthetic Metals*, vol. 159, no. 23-24, pp. 2519–2524, 2009.

[59] W. Zhang, P. Feng, J. Chen, Z. Sun, and B. Zhao, “Electrically conductive hydrogels for flexible energy storage systems,” *Progress in Polymer Science*, vol. 88, pp. 220–240, 2019.

[60] L. Pan, G. Yu, D. Zhai, H. R. Lee, W. Zhao, N. Liu, H. Wang, B. C. Tee, Y. Shi, Y. Cui, and Z. Bao, “Hierarchical nanostructured conducting polymer hydrogel with high electrochemical activity,” *Proceedings of the National Academy of Sciences of the United States of America*, vol. 109, no. 24, pp. 9287–9292, 2012.

[61] Y. Wang, Y. Shi, L. Pan, Y. Ding, Y. Zhao, Y. Li, Y. Shi, and G. Yu, “Dopant-Enabled Supramolecular Approach for Controlled Synthesis of Nanostructured Conductive Polymer Hydrogels,” *Nano Letters*, vol. 15, no. 11, pp. 7736–7741, 2015.

[62] L. Tang, S. Wu, J. Qu, L. Gong, and J. Tang, “A review of conductive hydrogel used in flexible strain sensor,” *Materials*, vol. 13, no. 18, pp. 1–17, 2020.

[63] J. Xu, Y. L. Tsai, and S. H. Hsu, “Design Strategies of Conductive Hydrogel for Biomedical Applications,” *Molecules (Basel, Switzerland)*, vol. 25, no. 22, pp. 1–17, 2020.

[64] K. Chen, Y. Hu, M. Liu, F. Wang, P. Liu, Y. Yu, Q. Feng, and X. Xiao, “Highly Stretchable, Tough, and Conductive Ag@Cu Nanocomposite Hydrogels for Flexible Wearable Sensors and Bionic Electronic Skins,” *Macromolecular Materials and Engineering*, vol. 2100341, pp. 1–11, 2021.

[65] T. Dvir, B. P. Timko, M. D. Brigham, S. R. Naik, S. S. Karajanagi, O. Levy, H. Jin, K. K. Parker, R. Langer, and D. S. Kohane, “Nanowired three-dimensional cardiac patches,” *Nature Nanotechnology*, vol. 6, no. 11, pp. 720–725, 2011.

[66] Y. Y. Choi, D. H. Ho, and J. H. Cho, “Self-Healable Hydrogel-Liquid Metal Composite Platform Enabled by a 3D Printed Stamp for a Multimodular Sensor System,” *ACS Applied Materials and Interfaces*, vol. 12, no. 8, pp. 9824–9832, 2020.

[67] H. Sun, K. Zhou, Y. Yu, X. Yue, K. Dai, G. Zheng, C. Liu, and C. Shen, “Highly Stretchable, Transparent, and Bio-Friendly Strain Sensor Based on Self-Recovery Ionic-Covalent Hydrogels for Human Motion Monitoring,” *Macromolecular Materials and Engineering*, vol. 304, no. 10, pp. 1–10, 2019.

[68] S. Liu and L. Li, “Ultrastretchable and Self-Healing Double-Network Hydrogel for 3D Printing and Strain Sensor,” *ACS Applied Materials and Interfaces*, vol. 9, no. 31, pp. 26429–26437, 2017.

[69] B. Yang and W. Yuan, “Highly Stretchable and Transparent Double-Network Hydrogel Ionic Conductors as Flexible Thermal-Mechanical Dual Sensors and Electroluminescent Devices,” *ACS Applied Materials and Interfaces*, vol. 11, no. 18, pp. 16765–16775, 2019.

[70] R. Tong, G. Chen, D. Pan, J. Tian, H. Qi, R. Li, F. Lu, and M. He, “Ultrastretchable and Antifreezing Double-Cross-Linked Cellulose Ionic Hydrogels with High Strain Sensitivity under a Broad Range of Temperature,” *ACS Sustainable Chemistry and Engineering*, vol. 7, no. 16, pp. 14256–14265, 2019.

[71] C. I. Idumah, I. C. Nwuzor, and R. S. Odera, “Recent advances in polymer hydrogel nanoarchitectures and applications,” *Current Research in Green and Sustainable Chemistry*, vol. 4, no. June, 2021.

[72] T. Hattori, K. Ishii, T. Tominaga, Y. Osada, and T. Tahara, “A fluorescence study on the local environment of hydrogels: Double-network hydrogels having extraordinarily high mechanical strength and its constituent single-network hydrogels,” *Chemical*

Physics, vol. 419, pp. 172–177, 2013.

[73] Y. Xu, M. Patino Gaillez, R. Rothe, S. Hauser, D. Voigt, J. Pietzsch, and Y. Zhang, "Conductive Hydrogels with Dynamic Reversible Networks for Biomedical Applications," *Advanced Healthcare Materials*, vol. 10, no. 11, 2021.

[74] T. Wang, X. Ren, Y. Bai, L. Liu, and G. Wu, "Adhesive and tough hydrogels promoted by quaternary chitosan for strain sensor," Adhesive and tough hydrogels promoted by quaternary chitosan for strain sensor. Carbohydrate Polymers, 254(October 2020), 117298. https://doi.org/10.1016/j.carbpol.2020.117298, vol. 254, no. October 2020, p. 117298, 2021.

[75] Q. Chen, L. Zhu, C. Zhao, Q. Wang, and J. Zheng, "A robust, one-pot synthesis of highly mechanical and recoverable double network hydrogels using thermoreversible sol-gel polysaccharide," *Advanced Materials*, vol. 25, no. 30, pp. 4171–4176, 2013.

[76] Y. J. Liu, W. T. Cao, M. G. Ma, and P. Wan, "Ultrasensitive Wearable Soft Strain Sensors of Conductive, Self-healing, and Elastic Hydrogels with Synergistic "soft and Hard" Hybrid Networks," *ACS Applied Materials and Interfaces*, vol. 9, no. 30, pp. 25559–25570, 2017.

[77] C. Keplinger, J. Y. Sun, C. C. Foo, P. Rothemund, G. M. Whitesides, and Z. Suo, "Stretchable, transparent, ionic conductors," *Science*, vol. 341, no. 6149, pp. 984–987, 2013.

[78] L. Wang and W. A. Daoud, "Hybrid conductive hydrogels for washable human motion energy harvester and self-powered temperature-stress dual sensor," *Nano Energy*, vol. 66, no. July, p. 104080, 2019.

[79] G. Rong, Y. Zheng, and M. Sawan, "Energy solutions for wearable sensors: A review," *Sensors*, vol. 21, no. 11, pp. 1–23, 2021.

[80] Q. Guan, G. Lin, Y. Gong, J. Wang, W. Tan, D. Bao, Y. Liu, Z. You, X. Sun, Z. Wen, and Y. Pan, "Highly efficient self-healable and dual responsive hydrogel-based deformable triboelectric nanogenerators for wearable electronics," *Journal of Materials Chemistry A*, vol. 7, no. 23, pp. 13948–13955, 2019.

[81] X. Wang, L. Dong, H. Zhang, R. Yu, C. Pan, and Z. L. Wang, "Recent Progress in Electronic Skin," *Advanced Science*, vol. 2, no. 10, pp. 1–21, 2015.

[82] J. Wang, F. Tang, Y. Wang, Q. Lu, S. Liu, and L. Li, "Self-Healing and Highly Stretchable Gelatin Hydrogel for Self-Powered Strain Sensor," *ACS Applied Materials and Interfaces*, vol. 12, no. 1, pp. 1558–1566, 2020.

[83] M. Roccetti, G. Marfia, and A. Semeraro, "Playing into the wild: A gesture-based interface for gaming in public spaces," *Journal of Visual Communication and Image Representation*, vol. 23, no. 3, pp. 426–440, 2012.

[84] Y. Wan, Y. Wang, and C. F. Guo, "Recent progresses on flexible tactile sensors," *Materials Today Physics*, vol. 1, pp. 61–73, 2017.

[85] M. L. Hammock, A. Chortos, B. C. Tee, J. B. Tok, and Z. Bao, "25th anniversary article: The evolution of electronic skin (E-Skin): A brief history, design considerations, and recent progress," *Advanced Materials*, vol. 25, no. 42, pp. 5997–6038, 2013.

[86] E. D. Engeberg and S. G. Meek, "Adaptive sliding mode control for prosthetic hands to simultaneously prevent slip and minimize deformation of grasped objects," *IEEE/ASME Transactions on Mechatronics*, vol. 18, no. 1, pp. 376–385, 2013.

[87] J. Kim, M. Lee, H. J. Shim, R. Ghaffari, H. R. Cho, D. Son, Y. H. Jung, M. Soh, C. Choi, S. Jung, K. Chu, D. Jeon, S. T. Lee, J. H. Kim, S. H. Choi, T. Hyeon, and D. H. Kim, “Stretchable silicon nanoribbon electronics for skin prosthesis,” *Nature Communications*, vol. 5, 2014.

[88] M. A. Abd, R. Paul, A. Aravelli, O. Bai, L. Lagos, M. Lin, and E. D. Engeberg, “Hierarchical tactile sensation integration from prosthetic fingertips enables multi-texture surface recognition†,” *Sensors*, vol. 21, no. 13, 2021.

[89] A. Mahmoudi Khomami and F. Najafi, “A survey on soft lower limb cable-driven wearable robots without rigid links and joints,” *Robotics and Autonomous Systems*, vol. 144, 2021.

[90] John Miller, “Inventing the Apollo Spaceflight Biomedical Sensors.”

[91] T. A. Baldo, L. F. De Lima, L. F. Mendes, W. R. De Araujo, T. R. Paixão, and W. K. Coltro, “Wearable and Biodegradable Sensors for Clinical and Environmental Applications,” *ACS Applied Electronic Materials*, vol. 3, no. 1, pp. 68–100, 2021.

[92] Y. J. Liu, W. T. Cao, M. G. Ma, and P. Wan, “Ultrasensitive Wearable Soft Strain Sensors of Conductive, Self-healing, and Elastic Hydrogels with Synergistic "soft and Hard" Hybrid Networks,” *ACS Applied Materials and Interfaces*, vol. 9, no. 30, pp. 25559–25570, 2017.

[93] X. Li, L. Sun, and C. A. Rochester, “Embedded system and smart embedded wearable devices promote youth sports health,” *Microprocessors and Microsystems*, vol. 83, no. January, p. 104019, 2021.

[94] Intuitive, “Da Vinci surgical system,”

[95] N. Enayati, E. De Momi, and G. Ferrigno, “Haptics in robot-assisted surgery: Challenges and benefits,” *IEEE Reviews in Biomedical Engineering*, vol. 9, no. March, pp. 49–65, 2016.

[96] C.-h. King, M. O. Culjat, M. L. Franco, C. E. Lewis, E. P. Dutson, W. S. Grundfest, and J. W. Bisley, “Force in Robot-Assisted Surgery,” vol. 2, no. 2, pp. 103–110, 2009.

[97] S. McKinley, A. Garg, S. Sen, R. Kapadia, A. Murali, K. Nichols, S. Lim, S. Patil, P. Abbeel, A. M. Okamura, and K. Goldberg, “A single-use haptic palpation probe for locating subcutaneous blood vessels in robot-assisted minimally invasive surgery,” *IEEE International Conference on Automation Science and Engineering*, vol. 2015-October, pp. 1151–1158, 2015.

[98] C. Cui, Q. Fu, L. Meng, S. Hao, R. Dai, and J. Yang, “Recent Progress in Natural Biopolymers Conductive Hydrogels for Flexible Wearable Sensors and Energy Devices: Materials, Structures, and Performance,” *ACS Applied Bio Materials*, vol. 4, no. 1, pp. 85–121, 2021.

[99] P. K. Annamalai, A. K. Nanjundan, D. P. Dubal, and J. B. Baek, “An Overview of Cellulose-Based Nanogenerators,” *Advanced Materials Technologies*, vol. 6, no. 3, pp. 1–20, 2021.

[100] C. Campano, A. Balea, A. Blanco, and C. Negro, “Enhancement of the fermentation process and properties of bacterial cellulose: a review,” *Cellulose*, vol. 23, no. 1, pp. 57–91, 2016.

[101] G. Melilli, I. Carmagnola, C. Tonda-Turo, F. Pirri, G. Ciardelli, M. Sangermano, M. Hakkarainen, and A. Chiappone, “DLP 3D printing meets lignocellulosic biopolymers: Carboxymethyl cellulose inks for 3D biocompatible hydrogels,” *Polymers*, vol. 12, no. 8, pp. 1–11, 2020.

[102] E. Bellotti, G. Casaluce, A. Casiraghi, M. Morone, G. Norcini, and S. R. Postle, "Beyond BAPO: Liquid BAPO derivatives for use as photoinitiators in 100

[103] C. Diana, *DLP-3D printable cellulose-based hydrogels*. PhD thesis, 2020.

[104] J. R. Tumbleston, D. Shirvanyants, N. Ermoshkin, R. Janusziewicz, A. R. Johnson, D. Kelly, K. Chen, R. Pinschmidt, J. P. Rolland, A. Ermoshkin, E. T. Samulski, and J. M. Desimone, "Continuous liquid interface of 3D objects," *Science*, vol. 347, no. 6228, pp. 1349–1352, 2015.

[105] A. Al Rashid, W. Ahmed, M. Y. Khalid, and M. Koç, "Vat photopolymerization of polymers and polymer composites: Processes and applications," *Additive Manufacturing*, vol. 47, no. July, p. 102279, 2021.

[106] W. Leo Greguric, "Digital Light Processing 3D printing explained," 2021.

[107] G. Gonzalez, A. Chiappone, K. Dietliker, C. F. Pirri, and I. Roppolo, "Fabrication and Functionalization of 3D Printed Polydimethylsiloxane-Based Microfluidic Devices Obtained through Digital Light Processing," *Advanced Materials Technologies*, vol. 5, no. 9, pp. 1–10, 2020.

[108] L. Pezzana, G. Riccucci, S. Spriano, D. Battegazzore, M. Sangermano, and A. Chiappone, "3d printing of pdms-like polymer nanocomposites with enhanced thermal conductivity: Boron nitride based photocuring system," *Nanomaterials*, vol. 11, no. 2, pp. 1–17, 2021.

[109] Z. Liao, M. Hossain, X. Yao, M. Mehnert, and P. Steinmann, "On thermo-viscoelastic experimental characterization and numerical modelling of VHB polymer," *International Journal of Non-Linear Mechanics*, vol. 118, no. September 2019, p. 103263, 2020.

[110] T. F. Scientific, "FTIR Sample Handling Techniques."

[111] A. Ausili, M. Sánchez, and J. C. Gómez-Fernández, "Attenuated total reflectance infrared spectroscopy: A powerful method for the simultaneous study of structure and spatial orientation of lipids and membrane proteins," *Biomedical Spectroscopy and Imaging*, vol. 4, no. 2, pp. 159–170, 2015.

[112] H. T. Banks, S. Hu, and Z. R. Kenz, "A brief review of elasticity and viscoelasticity for solids," *Advances in Applied Mathematics and Mechanics*, vol. 3, no. 1, pp. 1–51, 2011.

[113] J. R. Macdonald, "Impedance spectroscopy," 1992.

[114] A. Sacco, "Electrochemical impedance spectroscopy: Fundamentals and application in dye-sensitized solar cells," 2017.

[115] A. S. Bondarenko and G. A. Ragoisha, "Eis spectrum analyser."

[116] A. P. Avolio, M. Butlin, and A. Walsh, "Arterial blood pressure measurement and pulse wave analysis-their role in enhancing cardiovascular assessment," *Physiological Measurement*, vol. 31, no. 1, 2010.

[117] D. Saurav, A. Mahnan, and J. Konczak, "Real time voice activity detection using neck mounted accelerometers for controlling a wearable vibration device to treat speech impairment.," pp. 7–9, 2020.